



Wave generation and propagation at tribological interfaces

Mariano Di Bartolomeo

► To cite this version:

Mariano Di Bartolomeo. Wave generation and propagation at tribological interfaces. Other. INSA de Lyon, 2011. English. NNT : 2011ISAL0144 . tel-00715732

HAL Id: tel-00715732

<https://theses.hal.science/tel-00715732>

Submitted on 9 Jul 2012

HAL is a multi-disciplinary open access archive for the deposit and dissemination of scientific research documents, whether they are published or not. The documents may come from teaching and research institutions in France or abroad, or from public or private research centers.

L'archive ouverte pluridisciplinaire **HAL**, est destinée au dépôt et à la diffusion de documents scientifiques de niveau recherche, publiés ou non, émanant des établissements d'enseignement et de recherche français ou étrangers, des laboratoires publics ou privés.



SAPIENZA
UNIVERSITÀ DI ROMA

N° order 2011ISAL0144



Year 2011

Ph.D. Thesis

Wave generation and propagation at tribological interfaces

Jointly awarded at the

La Sapienza University of Rome

Dottorato di ricerca in Meccanica Teorica e Applicata XXIV ciclo

and at the

Institut National des Sciences Appliquées of Lyon

Ecole doctorale: Mécanique, Energétique, Génie Civil, Acoustique (MEGA)

Spécialité: Mécanique

by

Mariano DI BARTOLOMEO

On December 19, 2011

PhD Committee:

Examiner/Tutor	Y. BERTHIER	Research director CNRS	(LaMCoS, INSA de Lyon)
Examiner/Tutor	F. MASSI	Maître de Conférence	(LaMCoS, INSA de Lyon)
Examiner/Tutor	A. FREGOLENT	Associated professor (DIMA,"Sapienza" University of Rome)	
Examiner	A. CULLA	Assistant Professor (DIMA,"Sapienza" University of Rome)	
Examiner	L. BAILLET	Professor (ISTerre, Université Joseph Fourier, Grenoble)	
Examiner/Reviewer	A. AKAY	Professor (ME, Bilkent University, Ankara)	
Examiner/Reviewer	F. LEBON	Professor CNRS (LMA, Université de Provence, Marseille)	

Research Laboratories:

Dipartimento Ingegneria Meccanica e Aerospaziale (DIMA)

Laboratoire de Mécanique des Contacts et des Structures (LaMCoS)

Thesis supported by the:



SIGLE	ECOLE DOCTORALE	NOM ET COORDONNEES DU RESPONSABLE
CHIMIE	CHIMIE DE LYON http://www.edchimie-lyon.fr Insa : R. GOURDON	M. Jean Marc LANCELIN Université de Lyon – Collège Doctoral Bât ESCPE 43 bd du 11 novembre 1918 69622 VILLEURBANNE Cedex Tél : 04.72.43 13 95 directeur@edchimie-lyon.fr
E.E.A.	ELECTRONIQUE, ELECTROTECHNIQUE, AUTOMATIQUE http://edeea.ec-lyon.fr Secrétariat : M.C. HAVGOUDOUKIAN eea@ec-lyon.fr	M. Gérard SCORLETTI Ecole Centrale de Lyon 36 avenue Guy de Collongue 69134 ECULLY Tél : 04.72.18 60 97 Fax : 04 78 43 37 17 Gerard.scorletti@ec-lyon.fr
E2M2	EVOLUTION, ECOSYSTEME, MICROBIOLOGIE, MODELISATION http://e2m2.universite-lyon.fr Insa : H. CHARLES	Mme Gudrun BORNETTE CNRS UMR 5023 LEHNA Université Claude Bernard Lyon 1 Bât Forel 43 bd du 11 novembre 1918 69622 VILLEURBANNE Cédex Tél : 04.72.43.12.94 e2m2@biomserv.univ-lyon1.fr
EDISS	INTERDISCIPLINAIRE SCIENCES-SANTE http://ww2.ibcp.fr/ediss Sec : Safia AIT CHALAL Insa : M. LAGARDE	M. Didier REVEL Hôpital Louis Pradel Bâtiment Central 28 Avenue Doyen Lépine 69677 BRON Tél : 04.72.68 49 09 Fax :04 72 35 49 16 Didier.revel@creatis.uni-lyon1.fr
INFOMATHS	INFORMATIQUE ET MATHEMATIQUES http://infomaths.univ-lyon1.fr	M. Johannes KELLENDONK Université Claude Bernard Lyon 1 LIRIS - INFOMATHS Bâtiment Nautibus 43 bd du 11 novembre 1918 69622 VILLEURBANNE Cedex Tél : 04.72. 43.19.05 Fax 04 72 43 13 10 infomaths@bat710.univ-lyon1.fr
Matériaux	MATERIAUX DE LYON	M. Jean-Yves BUFFIERE Secrétaire : Mériem LABOUNE INSA de Lyon École Doctorale Matériaux Mérim LABOUNE Bâtiment Antoine de Saint-Exupéry 25bis Avenue Jean Capelle 69621 VILLEURBANNE Tel : 04 72 43 71 70 Fax : 04 72 43 72 37 ed.materiaux@insa-lyon.fr
MEGA	MECANIQUE, ENERGETIQUE, GENIE CIVIL, ACOUSTIQUE (ED n°162)	M. Philippe BOISSE Secrétaire : Mériem LABOUNE INSA de Lyon École Doctorale MEGA Mérim LABOUNE Bâtiment Antoine de Saint-Exupéry 25bis Avenue Jean Capelle 69621 VILLEURBANNE Tel : 04 72 43 71 70 Fax : 04 72 43 72 37 mega@insa-lyon.fr Site web : http://www.ed-mega.com
ScSo	Histoire, Géographie, Aménagement, Urbanisme, Archéologie, Science politique, Sociologie, Anthropologie M. OBADIA Lionel Sec : Viviane POLSINELLI Insa : J.Y. TOUSSAINT	M. OBADIA Lionel Université Lyon 2 86 rue Pasteur 69365 LYON Cedex 07 Tél : 04.78.69.72.76 Fax : 04.37.28.04.48 Lionel.Obadia@univ-lyon2.fr

ACCORD DE COOPERATION POUR LA MISE EN ŒUVRE D'UNE COTUTELLE DE THESE

L'Université de Rome "La Sapienza" ayant son siège à Rome (Italie), Piazzale Aldo Moro 5, représentée par son Recteur Professeur Luigi FRATI agissant en-qualité et en vertu des pouvoirs qui lui sont conférés d'une part

ET

L'INSA de LYON, représenté par le Professeur Daniel BARBIER, Directeur Adjoint de la Recherche, agissant en-qualités et en vertu des pouvoirs qui lui sont conférés, d'autre part

Pour la partie italienne :

- Vue la Loi n. 210 du 3 juillet 1998 art. 4 – doctorat de recherche ;
- Vu le D.M. 224/99 relatif aux normes en matière de doctorat de recherche ;
- Vu le D.M. 509/99 relatif aux normes en matière d'autonomie didactique des Universités ;
- Vu le Règlement de l'Université en matière de doctorat de recherche ;
- Vue la délibération du Sénat Académique du 2 octobre 2003 ;

ET

Vu pour la part française :

- L'arrêté du 6 janvier 2005 relatif à la procédure de cotutelle internationale de thèse (France);
- L'arrêté du 7 août 2006 relatif aux études doctorales (France);
- La convention cadre franco-italienne entre la Conférence des Présidents d'Université (CPU) et la Conferenza dei Rettori delle Università Italiane (CRUI) sur la reconnaissance des diplômes et validation des titres universitaires signée en date 18 janvier 1996;
- La convention cadre franco-italienne entre la Conférence des Présidents d'Université (CPU) e la Conferenza dei Rettori delle Università Italiane (CRUI) sur la co-tutelle de thèse signée le 13 février 1998;

désireux (désireuses) de contribuer à l'instauration et/ou au développement de la coopération scientifique entre équipes de recherche italiennes et étrangères en favorisant la mobilité des doctorants

sont convenu(e)s des dispositions suivantes

Titre I – Modalités administratives

Art. 1 – L'Université de Rome "La Sapienza" et L'INSA de Lyon désignées ci-après "les établissements", décident dans le respect des lois et des règlements en vigueur dans chacun des pays et/ou établissements, d'organiser conjointement une cotutelle de thèse au bénéfice de l'étudiant désigné ci-après :

Prénom et nom : Mariano DI BARTOLOMEO

spécialité : ingénieur Mécanique – Doctorat en Meccanica Teorica ed Applicata

sujet de thèse : Conséquences tribologiques des vibrations des contacts induites par le frottement.

Au fil des années les exigences industrielles sont devenues de plus en plus sévères en ce qui concerne les conditions de fonctionnement et la durée de vie utile des mécanismes qui pour réduire les coûts et les risques de pollution contiennent de plus en plus de pièces en contact « direct » c'est-à-dire en « frottement sec ou solide »

Le frottement sec entre des surfaces en contact, que ce soit quasi statique ou de grande amplitude, engendre des vibrations qui sont liées à la fois aux caractéristiques locales des surfaces et à la dynamique des structures qui contiennent ces surfaces. Dans ce contexte, cette thèse porte sur la compréhension des différents phénomènes inhérents aux vibrations qui sont générées par les contacts frottants. Ces vibrations peuvent aussi bien être la cause d'instabilités vibratoires dommageables (bruit de crissement, usure...), que nécessaire pour permettre le mouvement relatif entre les surfaces (réduction du coefficient de frottement global...). Par conséquent la compréhension de la génération de ces vibrations s'impose pour comprendre l'influence de la dynamique locale de contact sur le frottement.

Le sujet de cette thèse est donc l'analyse de la propagation d'ondes générées par le contact frottant, en fonction des caractéristiques locales (mécaniques et physico-chimiques), des surfaces et de la dynamique des systèmes. L'objectif du projet de recherche est le contrôle de la génération et la propagation des ondes superficielles tant pour éviter les instabilités que pour en contrôler les effets sur le frottement.

Dans un premier temps, une simulation numérique comprenant à la fois une analyse fréquentielle et une analyse temporelle d'un problème modèle, permettra de comprendre les phénomènes à la base de la génération des ondes superficielles et de leur propagation. Les paramètres d'influence seront recherchés et leur influence sur le coefficient de frottement global sera analysée. La plateforme ANSYS et le code PLAST, dédié aux problèmes de contact, serviront de cadre de travail pour l'analyse numérique.

En fonction des résultats numériques obtenus, une analyse expérimentale sera proposée afin de valider la séparation des variables locales des variables structurelles obtenue par la modélisation aux éléments finis.

Ce travail se démarque des travaux antérieurs sur le stick-slip, notamment par le fait que le frottement n'est plus un paramètre de calage, mais est un paramètre à part entière, déterminé par calculs (tribologie numérique).

Les principes et les modalités administratives et pédagogiques de cette cotutelle sont définis par le présent accord.

Art. 2 - La durée prévue pour la préparation de la thèse en cotutelle est de 3 ans, à partir de l'année scolaire 2008/2009.

En cas de nécessité, cette durée peut être prolongée en conformité avec la réglementation en vigueur dans les deux établissements.

Art. 3 - La préparation de la thèse s'effectue par périodes alternées, à peu près équivalentes, dans chacun des deux établissements partenaires. La durée de ces périodes sera déterminée de commun accord par les deux directeurs de thèse.

Art. 4 – L'étudiant Mariano DI BARTOLOMEO

est tenu à s'inscrire régulièrement dans les deux établissements. L'étudiant paiera les droits d'inscriptions à l'Université La Sapienza de Rome et en sera dispensé près l'INSA de Lyon.

Art. 5 – Pour les périodes d'études effectuées en France et pour la soutenance, le doctorant bénéficie de l'ensemble des dispositions de l'arrêté du 7 août 2006 susvisé, et de la charte des thèses de l'INSA de Lyon.

Art.6 –Lors de son inscription, le doctorant devra fournir les justificatifs relatifs à ses ressources, à sa couverture sociale ainsi qu'à son assurance relative aux accidents du travail, dans chacun des pays.

Titre II – Modalités pédagogiques

Art. 1 – Le travail de thèse de l'étudiante sera réalisé sous la supervision commune de deux directeurs de thèse :

- Annalisa FREGOLENT (Professeur du Département de Meccanica e Aeronautica), directeur de thèse à l'Université "La Sapienza" ;
- Yves BERTHIER (Professeur au Laboratoire de Mécanique des Contacts et des Structures), directeur de thèse à l' INSA de Lyon ;

qui s'engagent à exercer pleinement la fonction de tuteurs de la candidate ainsi qu'à formuler chacun un avis écrit sur la thèse de Doctorat.

L'avis favorable des deux Directeurs de Thèse est une condition nécessaire à l'admission à l'examen final.

Art. 2- La thèse donnera lieu à une soutenance unique, reconnue par les deux établissements concernés. La soutenance aura lieu à l'INSA de Lyon. Le jury de soutenance est composé sur la base d'une proportion équilibrée de membres de chaque établissement désignés conjointement par les établissements contractants et comprend, en outre, des personnalités extérieures à ces établissements.

Il comprendra au moins quatre membres et au maximum huit membres, dont, sauf dérogation, les deux directeurs de thèse.

Art. 3-La thèse sera rédigée et discutée en Anglais. Elle comportera un résumé substantiel rédigé en français.

Art. 4 – En cas de rapport favorable du Jury, chacun des deux établissements s'engage à conférer le titre de docteur de recherche pour la même thèse.

L'Université de Rome "La Sapienza" s'engage à conférer le grade de docteur de recherche en Meccanica Teorica e Applicata.

L'INSA de Lyon s'engage à conférer le grade de docteur de recherche en Mécanique.

Art. 5-Lorsque le doctorant doit valider des formations complémentaires (scientifiques ou visant à son insertion professionnelle), les établissements (l'Ecole Doctorale MEGA pour l'INSA) préciseront les modalités de reconnaissance mutuelle de ces formations, en accord avec les directeurs de thèse et le doctorant.

Titre III – Conclusions

Art. 1 – L'étudiant est tenu de respecter les règlements et les usages de l'établissement d'accueil.

Art. 2 – Par l'intermédiaire de leurs directeurs de thèses respectifs, les établissements signataires s'engagent à se communiquer toutes les informations et la documentation utiles à l'organisation de la cotutelle de thèse faisant l'objet du présent accord.

Art. 3 – Les modalités de présentation, de dépôt et de reproduction de la thèse seront établies dans chaque pays dans le respect de la réglementation en vigueur.

La protection du sujet de thèse, ainsi que la publication, l'exploitation et la protection des résultats issus des travaux de recherche du doctorant dans les deux établissements signataires seront assujetties à la réglementation en vigueur et assurées conformément aux procédures spécifiques à chacun des pays impliqués dans la cotutelle.

Sur demande, les dispositions concernant la protection des droits de propriété intellectuelle pourront faire l'objet de protocoles ou de documents spécifiques.

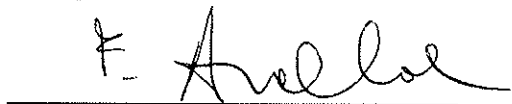
Art. 4 – Le présent accord entre en vigueur à partir de la date de signature du représentant légal de chaque établissement signataire et le reste jusqu'à la fin de l'année universitaire au cours de laquelle la thèse ou les travaux seront soutenus.

Dans le cas où l'étudiant ne serait pas inscrit dans l'un et/ou l'autre des établissements signataires, ou bien renoncerait par écrit à poursuivre, ou bien n'est pas autorisé à poursuivre la préparation de sa thèse en vertu de la décision de l'un au moins des deux directeurs de thèse, les deux établissements signataires mettront fin conjointement et sans délai, aux dispositions du présent accord.

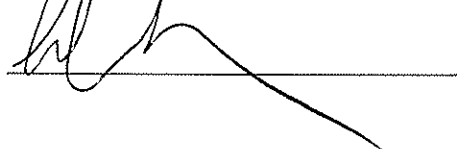
Art. 5 – Le présent accord est rédigé en quatre exemplaires originaux, dont deux en italien et deux en française, faisant également foi.

Roma, li 10/12/2008

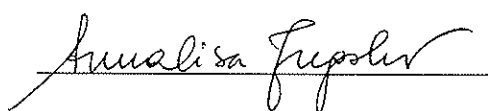
P Pour le Recteur de l'Université
La Sapienza de Rome



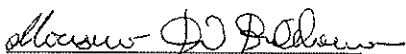
Il Coordinatore del Dottorato di Ricerca
Carlo Massimo CASCIOLA

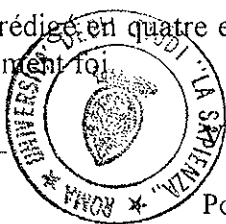


Il Co-direttore di tesi
Annalisa FREGOLENT



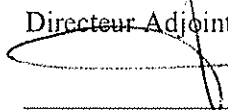

Le Doctorant
Mariano DI BARTOLOMEO



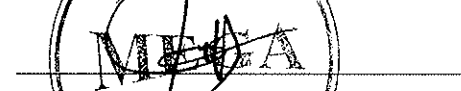


Lilleurbanne, li 15/12/2008

P Pour le directeur de l'INSA de Lyon
Professeur Daniel BARBIER
Directeur Adjoint de la Recherche

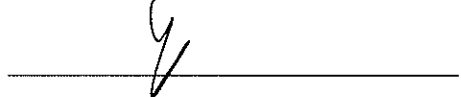
Le Responsable de l'Ecole Doctorale
Jean-Louis GUYADER



Le Directeur du laboratoire
Alain COMBESCURE



Co-directeur (s) de thèse
Yves BERTHIER



Francesco MASSI



CONVENZIONE PER UNA CO-TUTELA DI TESI DI DOTTORATO DI RICERCA

L'Università degli Studi di Roma "La Sapienza" con sede in Roma (Italia), Piazzale Aldo Moro, 5 rappresentata dal Rettore Prof. Luigi FRATI, che opera in virtù dei poteri che gli sono conferiti, da una parte

e

L'INSA di Lione rappresentata dal Professore Daniel BARBIER, Addetto alla Direzione della Ricerca, che opera in virtù dei poteri che gli sono conferiti, dall'altra parte

Per la parte italiana:

- VISTA la Legge 210 del 3 luglio 1998 art. 4 – dottorato di ricerca;
- VISTO il D.M. 224/99 recante norme in materia di dottorato di ricerca
- VISTO il D.M. 509/99 recante norme concernenti l'autonomia didattica degli Atenei;
- VISTO il Regolamento di Ateneo in materia di dottorato di ricerca;
- VISTA la delibera del Senato Accademico del 2 ottobre 2003;

e

Visti, per la parte francese,

- La delibera del 6 gennaio 2005 relativo alla procedura internazionale per la cotutela di tesi (Francia);
- La delibera del 7 agosto 2006 relativo al dottorato (Francia);
- La convenzione franco-italiana tra la Conférence des Présidents d'Université (CPU) e la Conferenza dei Rettori delle Università Italiane (CRUI) sul riconoscimento dei diplomi e della validità dei titoli universitari siglata in data 18 gennaio 1996;
- La convenzione franco-italiana tra la Conférence des Présidents d'Université (CPU) e la Conferenza dei Rettori delle Università Italiane (CRUI) sulla cotutela di tesi siglata li 13 febbraio 1998;

nell'intento di contribuire ad instaurare e/o sviluppare la cooperazione scientifica tra équipe di ricerca italiana e straniera attraverso la mobilità dei dottorandi

convengono e stipulano quanto segue

Parte prima – Modalità amministrative

Art. 1 – L'Università degli Studi di Roma "La Sapienza" e L'INSA di Lione denominati qui di seguito "Istituzioni" concordano, nel rispetto delle leggi e dei regolamenti in vigore in ciascun Paese e/o Istituzione, di organizzare congiuntamente una co-tutela di tesi di dottorato a beneficio del dottorando sottoindicato:

nome e cognome: Mariano Di Bartolomeo

iscritto al corso di Dottorato di Ricerca in Meccanica Teorica e Applicata presso l'Università La Sapienza di Roma e in "Mecanique" presso l' "ecole doctoral MEGA".

Soggetto di tesi: Conseguenze tribologiche delle vibrazioni indotte dall'attrito di contatto

Nel corso degli anni le richieste industriali sono divenute sempre più esigenti per quanto riguarda le condizioni di funzionamento e la vita utile dei sistemi meccanici che, per ridurre i

costi e contenere i rischi di inquinamento, sono costituiti di più parti in contatto diretto, vale a dire in condizioni di attrito secco o di lubrificazione con lubrificanti solidi.

L'attrito secco tra le superfici in contatto, sia in condizioni quasi-statiche che per ampi spostamenti relativi, causa vibrazioni che sono legate sia alle caratteristiche locali delle superfici in contatto che alla dinamica delle strutture che contengono tali superfici. In questo contesto, la tesi si concentra sulla comprensione dei fenomeni connessi con le vibrazioni che vengono generate al contatto. Queste vibrazioni possono essere la causa di instabilità indesiderate (emissioni acustiche come lo squeal, usura ...), che risultare necessarie per permettere il movimento relativo tra le superfici (riducendo il coefficiente di attrito globale ...). Pertanto la comprensione della generazione di queste vibrazioni è necessaria per capire l'influenza della dinamica locale al contatto sull'attrito.

Il soggetto della tesi è l'analisi della propagazione d'onde generate dall'attrito al contatto, in base alle caratteristiche locali (meccanico e chimico-fisiche) delle superfici e della dinamica dei corpi in contatto. L'obiettivo del progetto di ricerca è il controllo della generazione e propagazione delle onde di superficie sia per evitare le instabilità che per controllarne gli effetti sull'attrito.

In una prima fase, la simulazione numerica comprendente sia l'analisi in frequenza che l'analisi temporale (transient) di un problema modello permetterà di comprendere il fenomeno alla base della generazione delle onde di superficie e la loro propagazione. Saranno ricercati i parametri di influenza e sarà analizzata la loro influenza sul coefficiente di attrito. Gli strumenti utilizzati per l'analisi numerica saranno: la piattaforma numerica ANSYS ed il codice numerico PLAST, dedicato ai problemi di contatto.

In funzione dei risultati ottenuti dall'analisi numerica, sarà proposta un'analisi sperimentale per convalidare la separazione delle variabili locali e variabili globali ottenuta dalla modellazione agli elementi finiti.

Questo lavoro si distingue dai lavori precedenti sullo stick-slip per il fatto che l'attrito non è più un parametro di aggiustamento introdotto nel modello, ma è un parametro di analisi, determinato attraverso simulazioni numeriche (tribologia numerica).

I principi e le modalità amministrative e didattiche di tale co-tutela sono definiti dalla presente convenzione.

Art.2 - La durata per la preparazione della tesi è di 3 anni, a partire dall'anno accademico 2008/2009.

In caso di necessità tale durata potrà essere prorogata in conformità con la regolamentazione vigente nelle due Istituzioni.

Art.3 - La preparazione della tesi si effettuerà in periodi alterni, pressoché equivalenti, in ciascuna delle due Istituzioni. La durata di tali periodi sarà fissata in comune accordo dai due Direttori di tesi.

Art.4 - Il dott. Mariano Di Bartolomeo sarà iscritto in entrambe le Istituzioni. Corrisponderà i regolari diritti di iscrizione all'Università "La Sapienza" di Roma e ne sarà esonerato presso INSA di Lione.

Art.5 - Per tutto il periodo di preparazione della tesi il dott. Mariano Di Bartolomeo beneficerà di quanto disposto dalla delibera del 7 Agosto 2006 e della carta dei tesisti de l'INSA de Lyon.

Art.6 - Per la durata della sua iscrizione, il dott. Mariano Di Bartolomeo dovrà fornire giustificazione relativamente alle sue risorse, alla sua coperta sanitaria così come alla sua assicurazione sugli incidenti di lavoro, in ognuno dei paesi.

Parte seconda – Modalità didattiche

Art.1 – Il dott. preparerà la tesi sotto la direzione comune dei professori:

- Annalisa FREGOLENT (Docente presso il dipartimento di Meccanica e Aeronautica), direttore di tesi a l'Università di Roma "La Sapienza"
- Yves BERTHIER (Docente presso il Laboratorio di Meccanica dei Contatti e delle strutture), direttore di tesi all'INSA di Lione

che si impegnano ad esercitare pienamente la funzione di tutori del dottorando e si impegnano a valutarne, ciascuno con propria relazione scritta, la tesi di Dottorato.

Il giudizio positivo di entrambi i Direttori di Tesi è condizione necessaria per l'ammissione all'esame finale.

Art. 2 - La discussione della tesi, unica e riconosciuta dalle due istituzioni, avrà luogo presso l'Università di Roma "La Sapienza". La Commissione giudicatrice, nominata dai Rettori delle due Università, sarà composta da un numero pari di studiosi appartenenti alle due Istituzioni e designati congiuntamente da esse, oltre a membri esterni alle due Istituzioni. Essa dovrà essere composta da un minimo di quattro membri ed un massimo di otto, appartenenti ai settori scientifico-disciplinari del Dottorato, tra cui, a meno di derogazioni, i due direttori di tesi.

Art. 3 – La tesi sarà redatta e discussa in inglese; un riassunto sostanziale sarà redatto in lingua francese.

Art. 4 – Ognuna delle due Istituzioni si impegna a conferire il titolo di dottore di ricerca per la stessa tesi, in seguito ad una relazione favorevole della Commissione giudicatrice.

L'Università degli Studi di Roma "La Sapienza" conferirà il titolo di dottore di ricerca in Meccanica Teorica e Applicata.

L'INSA di Lione conferirà il titolo di dottore di ricerca in Meccanica.

Art. 5- In caso il dottorando dovesse convalidare le formazioni complementari (scientifiche o mirate alla sua inserzione professionale), le Istituzioni (l'Ecole Doctorale MEGA pour l'INSA) specificheranno le modalità di riconoscimento reciproco di queste formazioni, in accordo con i direttori di tesi ed la dottoranda.

Parte terza – Conclusione

Art. 1 – Il dottorando dovrà rispettare i regolamenti e le consuetudini dell'Istituzione ospitante.

Art. 2 – Le Istituzioni contraenti, attraverso l'intermediazione dei rispettivi direttori di tesi, si impegnano a comunicarsi rispettivamente tutte le informazioni e la documentazione utile per l'organizzazione della co-tutela di tesi oggetto della presente convenzione.

Art. 3 – Le modalità di presentazione, di deposito e riproduzione della tesi saranno effettuati in ogni paese secondo i regolamenti in vigore.

La protezione dell'oggetto della tesi, così come la pubblicazione, lo sfruttamento e la protezione dei risultati ottenuti con lo studio di ricerca del dottorando nelle Istituzioni contraenti saranno assoggettati alla normativa in vigore e assicurati conformemente alle procedure specifiche di ciascun Paese coinvolto nella co-tutela.

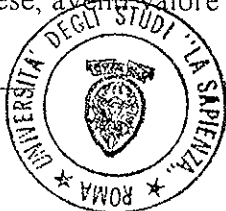
Qualora richiesto, le disposizioni relative alla protezione dei diritti di proprietà intellettuale potranno costituire oggetto di protocolli o documenti specifici.

Art. 4 – La presente convenzione entra in vigore dalla data di firma del rappresentante legale di ciascuna Istituzione contraente e sarà valida fino alla fine dell'anno accademico nel corso del quale la tesi o lo studio saranno discussi.

Nel caso in cui il dottorando non fosse iscritto in una e/o l'altra delle Istituzioni contraenti, oppure rinunciasse per iscritto a proseguire, oppure, in virtù della decisione di almeno uno dei due direttori di tesi, non fosse autorizzato a proseguire la preparazione della tesi in co-tutela, le Istituzioni contraenti porranno fine, congiuntamente e senza ritardo, alle disposizioni del presente accordo.

Art. 5 – La presente convenzione è redatta in quattro esemplari originali, di cui due in lingua italiana e due in lingua francese, aventi valore legale.

Roma, li 10/12/2008
Per il Rettore dell'Università
di Roma "La Sapienza"



F. Anella

Il Responsabile del Dottorato di Ricerca
Carlo Massimo CASCIOLA

[Signature]

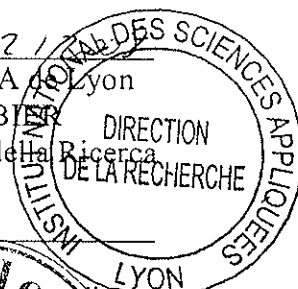
Co-direttore di tesi
Annalisa FREGOLENT

Annalisa Fregolent

Il Dottorando
Mariano DI BARTOLOMEO

Mariano Di Bartolomeo

Villeurbanne, li 15/12/2008
Per il Direttore dell'INSA di Lyon
Professore Daniel BARBIER
Addetto alla Direzione della Ricerca



[Signature]

Il Responsabile del Dottorato di Ricerca
Jean-Louis GUYADER

[Signature]

Il Direttore del Laboratorio
Alain COMBESCURE

[Signature]

Co-direttori di tesi
Yves BERTHIER

[Signature]

Francesco MASSI

Francesco Massi

To Barbara and Matteo

"Among the innumerable mortifications that way-lay human arrogance on every side may well be reckoned our ignorance of the most common objects and effects, a defect of which we become more sensible by every attempt to supply it. Vulgar and inactive minds confound familiarity with knowledge, and conceive themselves informed of the whole nature of things when they are shown their form or told their use; but the speculatist, who is not content with superficial views, harasses himself with fruitless curiosity, and still as he enquires more perceives only that he knows less."

[Samuel Johnson](#)

'The Idler' no. 32, Saturday, 25th November 1758

Acknowledgements

This thesis has been developed in the framework of a joint French-Italian doctoral course between La Sapienza of Rome and the INSA of Lyon, so the first tanks goes to the institutions that have supported this research and made it possible: the two doctoral schools (Theoretical and Applied Mechanics of the University of Rome "La Sapienza" and Mécanique, Energetique, Génie Civil, Acoustique, MEGA of the INSA of Lyon) and the French-Italian University for his very helpful research grant.

I would like to continue by thanking my Italian and French supervisors and co-supervisors of thesis the Professors Annalisa Fregolent, Antonio Culla, Francesco Massi, Yves Berthier for their professional guidance and constant support during the development of this research work, with a special thanks to Francesco Massi for his encouragement and the valuable help he has given me during these years.

I would also to express my gratitude to the Professor Laurent Baillet for his collaboration and contribution to the comprehension of the phenomena and for have given me always stimulating cues for the continuation of the research.

A sincere thanks goes also to the reviewers, Professor Adnan Akay and Professor Frédéric Lebon for their comments and suggestions which allowed me to improve this work.

I would like to finish extending my greeting to all the friends, colleagues, professors, people that I have had the opportunity and the pleasure to met during these years, at the LaMCoS as well at the DIMA or somewhere else. Among them Cyril, Fabrizio, Ramona, Cosimo, Fangfang, Coumba, Matthieu, Alexandra, Jing, Pavel, Guillaume, Mathieu, Viet-hung, Hong-Phong, Livia, Hiromi, Soumia. I want to wish them sincerely a very good luck for their personal and professional future. It has been a very unique experience to discuss about the history and the culture of so different countries and to understand what has been happening in so different places in the world, even in opposite part of it, directly with somebody who came from there. A sort of library in the flesh!

Concluding a last but certainly not least thanks to my family Luigi, Lorenza, Paolo and Nunzio and to Barbara and Matteo to whom this thesis and my life are dedicated.

Wave generation and propagation at tribological interfaces

Abstract

Wave generation and propagation at contact interfaces is a relevant issue in mechanics because they affect directly a large number of mechanical systems involving either static or sliding frictional parts. Contact dynamics is at the origin of friction induced vibrations, acoustical instabilities, surface damage, wear and fatigue failures [IBRA 94][AKAY 02] Propagating waves at the interface can be exploited for controlling the global friction features of the contact.

Beside classical experiments, numerical analysis on dry contacts in sliding state has been one of the mayor topic in recent literature to which a relevant number of important papers have been dedicated ([RENO 11] and reference therein), due also to the fact that it is a substantial subject of interest for researchers working on many different domains, from dynamics to tribology and geophysics.

At the origin of the phenomena cited above there is the wave generation and propagation at the frictional contact interface. Moreover when the two materials in contact are different, the dynamics of the phenomenon increases in complexity due to the so-called "bimaterial" effect ([WEER 80][ADA 95][BEN 01] and reference therein).

This thesis is addressed to the understanding of the mechanisms at the origin of the contact wave fields and its relationship with the local characteristics of the surfaces in contact, as well as with the global dynamics and macroscopic frictional behaviour of the system. The aim of this work is to provide insights on the generation and propagation of the waves through the contact both to avoid instabilities and to control their effect on friction. The work is organized in two main parts.

The first part presents the development of a non-linear finite element analysis in large transformations of the dynamic rupture at the interface with contact friction separating two bodies (isotropic and elastic) without relative motion. A rupture is considered when an initially sticking zone shifts in sliding state. The properties of the obtained ruptures are analyzed for a flat interface between dissimilar materials in function of the nucleation energy; then the effect of the interface roughness is analyzed. The differentiated rupture inside the asperities and the conditions for coupling and uncoupling between the waves radiating in the two bodies have been also investigated.

In the second part, the analysis deals with the sliding onset between two bodies in contact. The sliding between two bodies made of different isotropic elastic materials and separated by a frictional interface is simulated. The

evolution along the time of the global normal and tangential forces is analyzed, relating it to the local phenomena occurring at the interface. This part tries to investigate how micro-slips at the interface, acting as distributed ruptures, trigger the macro-slips between the two bodies. The interaction between local and global dynamics is also studied. Finally a numerical parameter space study is carried out, as a function of several system parameters (contact law, friction coefficient, material damping, normal load, translational velocity and regularization time).

The results show the key role of the micro-slips and precursors (detectable wave propagations that occur at tangential global force well below the critical value expected by the friction law) in triggering the macro-slip between the two bodies. Depending on their distribution and magnitude the evolution of the contact forces passes from stick-slip-like behaviour to continuous sliding. The local dynamics at the contact (wave and rupture propagation) is linked to the global behaviour of the system (stick-slip, continuous sliding, induced vibrations); the effect of the contact and system parameters on the transfer of vibrational energy between the sliding contact and the system is investigated.

The numerical results obtained by the two parts of the work show a good agreement with experimental results in literature.

Keywords: : Dry friction - Wave propagation - Dynamic rupture - Numerical analysis - Friction instabilities - Roughness - Precursors - Dissimilar materials - Stick-slip

Wave generation and propagation at tribological interfaces

Résumé

La génération et la propagation d'ondes aux interfaces de contact est un problème fondamental en mécanique car il a une incidence directe sur un grand nombre de systèmes mécaniques qui sont constitués aussi bien de zones de contact statiques ou en glissement relatif.

La dynamique de contact est à l'origine des vibrations induites par le frottement, des instabilités acoustiques, de l'endommagement des surfaces, de l'usure et de la rupture par fatigue [IBRA 94][AKAY 02]; de plus, les ondes qui se propagent à l'interface peuvent être exploitées pour contrôler les caractéristiques du frottement global entre les corps en contact.

En parallèle des expériences classiques, l'analyse numérique du contact sec entre corps en déplacement relatif a été un des plus importants sujets de la littérature scientifique récente, et un nombre considérable de publications s'y intéressent (voir [RENO 11] et sa bibliographie); ceci est aussi dû au fait que ce sujet intéresse des chercheurs impliqués dans de nombreux domaines allant de la dynamique des systèmes à la tribologie en passant par la géophysique.

A l'origine de ces phénomènes se trouvent la génération et la propagation d'ondes à l'interface du contact frottant. En outre, quand les deux matériaux en contact sont différents, la dynamique du phénomène augmente en complexité, à cause de l'«effet bi-matériau» ([WEER 80][ADA 80][BEN 01]).

Dans ce contexte cette thèse s'intéresse à la compréhension des mécanismes à l'origine de la dynamique locale au contact et à sa relation avec les caractéristiques locales de la surface de contact, ainsi qu'à sa relation avec la dynamique globale et le comportement macroscopique du système. L'objectif de ce travail est d'approfondir la connaissance sur la génération et la propagation des ondes à travers l'interface de contact à la fois pour contrôler leurs effets sur le frottement, contrôler les instabilités et réduire les phénomènes d'usure.

Le travail est organisé en deux parties principales.

La première partie est axée sur une analyse non-linéaire par éléments finis en grandes transformations; la rupture dynamique à l'interface de contact avec frottement, qui sépare deux corps (isotropes et élastiques) en condition de pré-charge statique, est simulée. On définit comme étant une rupture une zone, initialement en adhérence, qui change son état en devenant glissante. Les propriétés des ruptures sont analysées pour une surface plane entre deux matériaux différents en fonction de l'énergie de nucléation; l'effet de la rugosité de surface est ensuite analysée. En outre, la rupture "cumulative" dans les aspérités et les conditions pour le couplage ou le non-couplage entre les ondes qui se propagent dans les deux corps sont étudiées.

Dans la deuxième partie, l'analyse focalise sur le glissement entre deux corps en contact. L'amorçage du glissement entre deux corps constitués de matériaux différents (élastiques et isotropes), et séparés par une interface avec frottement, est simulée. L'évolution, en fonction du temps, des forces globales (normale et tangentielle) a été mise en relation avec les phénomènes locaux qui se déroulent à l'interface. L'analyse montre comment les micro-slips à l'interface, en agissant comme ruptures localisées, déclenchent les macro-slips entre les deux corps. L'interaction entre les dynamiques locale du contact et globale du système a été aussi étudiée. Enfin, une analyse paramétrique est menée en fonction de plusieurs paramètres (loi de contact, coefficient de frottement, amortissement matériau, charge normale, vitesse de translation, temps de régularisation).

Les résultats mettent en avant le rôle-clé des micro-slips et des précurseurs (propagations d'ondes détectables qui ont lieu pour des valeurs de la force tangentielle globale inférieures à la valeur prévue par la loi de frottement) dans l'amorçage du macro-slip entre les deux corps. En fonction de leur distribution et de leur intensité, l'évolution des forces de contact change en passant d'un comportement de type stick-slip à un glissement continu. La dynamique locale au contact (propagation des ondes et ruptures) a été reliée au comportement global du système (stick-slip, glissement continu, vibrations induites); l'effet des paramètres du contact et du système sur le transfert d'énergie vibrationnelle entre le contact glissant et le système a également été examinée: en fonction de leurs valeurs, on peut avoir différentes modalités d'excitation du système (par une distribution de micro-slips ou par des macro-slips) et différents processus de propagation et dissipation d'énergie (en passant par la réponse dynamique des corps en contact).

Les résultats numériques obtenus dans les deux parties de la thèse sont cohérents avec les résultats expérimentaux de la littérature.

Mots-clés: Frottement sec - Propagation d'onde – Rupture dynamique – Analyse numérique - Instabilités frottement - Rugosité – Précurseurs – Bi-matériaux - Stick-slip

Summary

Abstract	14
Nomenclature, list of symbols	18
Introduction	20
1 Contact Friction: an always current issue	28
1.1 Introduction	28
1.2 Wave propagation at contact interfaces	30
1.2.1 Analytical studies	30
1.2.2 Numerical works	35
1.2.3 Experimental works	37
1.3 Dynamic Rupture in mode II	40
1.4 Friction instabilities	41
2 Dynamic rupture at frictional contact interface	44
2.1 Introduction	44
2.1.1 Effect of the roughness	44
2.2 Numerical tool:Plast2D	47
2.3 Description of the model	49
2.4 Rupture between smooth contact surfaces	51
2.4.1 Results for a nucleation length of 0.125mm	52
2.4.2 Influence of the length of nucleation	55
2.5 Rupture at contact surfaces with asperities	56
2.5.1 Introduction of the roughness	56
2.5.2 Effect of roughness on wave propagation	58
2.5.2.1 Coupled/uncoupled on wave propagation	58
2.5.2.2 Stress distribution and rupture profile	61
2.5.3 Effect of roughness patterns	63
2.6 Conclusions	64

3	Wave propagation during sliding initiation	66
3.1	Introduction	68
3.2	Description of the model	68
3.3	Sliding initiation	70
3.3.1	Study of the contact force	70
3.3.2	Wave propagation analysis	72
3.3.3	From local to global dynamics	76
3.4	Comparison with experimental works	82
3.5	Conclusions	83
4	Parameter space analysis	84
4.1	Introduction	84
4.2	Effect of the damping coefficients	84
4.3	Effect of the numerical parameters	86
4.4	Effect of the regularisation parameter	87
4.5	Influence of the pre-load	88
4.6	Influence of the friction coefficient	89
4.7	Effect of the translation velocity	90
4.8	Analysis of the local dynamics	92
4.9	Comparison with experimental works	95
4.10	Conclusions	96
5	Conclusions	97

5.1	Original contributions	97
5.1.1	Effect of roughness	97
5.1.2	Sliding initiation: global and local phenomena	98
5.1.3	Parametrical analysis	99
5.2	Perspectives	100
5.2.1	Further numerical analysis	100
5.2.2	Experimental analysis	101
6	References	103

Nomenclature and list of symbols

α	Mass matrix damping coefficient
β	Stiffness matrix damping coefficient
β_2	Numerical damping parameter
δ	Density
γ	Degree of material contrast
λ	Spatial wavelength of the sinusoidal roughness
$\boldsymbol{\lambda}$	Vector of the normal and tangential contact forces
μ	Friction coefficient
σ_∞	Remote normal stress
τ_∞	Remote tangential stress
σ	Local (interface) normal stress
σ_R	Standard deviation of the distribution of the asperities heights
τ	Local (interface) tangential stress
$\hat{\tau}$	Time of regularisation of the <i>Prakash-Clifton</i> law
A	Amplitude of the sinusoidal roughness
\mathbf{C}	System damping matrix
c_c	Crack propagation speed
c_E	Eshelby velocity
c_{GR}	Generalized Rayleigh wave speed
c_P	Longitudinal wave speed
c_R	Rayleigh wave speed
c_{RUP}	Rupture front speed
c_s	Shear wave speed
d	Normalized parameter of regularization $d = \hat{\tau} / \Delta t$
Δt	Integration time step
Δx	Size of the mesh element side
E	Young modulus
\mathbf{F}	Vector of nodal external forces
GR	Generalized Rayleigh wave
\mathbf{G}	Global matrix of the displacement conditions
H	Head wave
\mathbf{K}	System stiffness matrix
\hat{L}	Characteristic slip distance of the <i>Prakash-Clifton</i> law
l	Precursor distance of propagation
L_{nuc}	Length of the nucleation zone
\mathbf{M}	System mass matrix
N	Remote normal force

R_a	Roughness arithmetical average
RW	Reflected wave
SST	Superficial Tribological Transformations
T	Remote tangential force
TLS	Seismic Tremor Like Signals
$\mathbf{u}, \dot{\mathbf{u}}, \ddot{\mathbf{u}}$	vectors of nodal displacements, velocities and accelerations
V	Global translational velocity

Introduction

Wave generation and propagation at contact frictional interfaces is a relevant issue in mechanics because they affect directly a plurality of mechanical systems involving either static or sliding frictional parts. They are among the causes of the friction induced vibrations that can cause either dynamic instabilities as squeal, chatter squeeze, or surface damages, wear and fatigue failures [IBRA 94][AKAY 02]. At the meantime, wave propagation at the interface can be exploited for controlling the global friction features of sliding contacts.

Nevertheless, the prediction and control of the local dynamics at a contact surface result quite difficult because of the interaction between the structural (global) and contact (local) phenomena. Moreover when the two materials in contact are different, which is the most common case in mechanics, the dynamics of the phenomenon increases in complexity due to the so-called "bimaterial" effect ([WEER 80][ADA 95][BEN 01] and reference therein).

Beside classical experiments, numerical analysis on dry contacts in sliding state has been one of the mayor topic in recent literature to which a relevant number of important papers have been dedicated ([RENO 11] and reference therein); this is due also to the fact that it is a substantial subject of interest for researchers involved on several domains such as dynamics, tribology, geophysics etc. This justify this joint PhD between the DIMA (Dipartimento Ingegneria Meccanica e Aerospaziale of the Sapienza University of Rome), and in particular his research group in structural dynamics, and the research laboratory LaMCoS (Laboratoires de Mécanique des Contacts et des Solides of the INSA of Lyon) with his competences in tribology.

In the matter of the justification of the classic Amontons-Coulomb friction law, the friction force, this so common effect of the daily life, is intrinsically related to the concept of the real area of contact [BOWD 50] and to the role of the interactions between the surface asperities. More precisely the friction, in the frame of the adhesion model, results from the intermolecular adhesion between the plastic deformed asperities in contact [VARO 04 and reference therein]. Alternatively, the dynamic friction has been also explained by the dissipation mechanism due to the collision between the asperities. Other models consider both the aspects [BENG 97]. Anyway the friction force appears to be affected by a long list of factors: surface texture, presence of wear particles and the consequent role of the third-body [BERT 95], environmental conditions, thermal effects etc.

Several friction laws have been formulated to try to fit better the real behaviour of the frictional interface for different materials in contact (slip-weakening, rate-and-state, laws including adhesion terms etc.). However these

models cannot fully account for some observed particularities [MART 90], as the nonuniformity of the rupture on the same interface [e.g. RUBI 04], the observed slip at tangential stress values well below the required one [e.g. ADAM 98], or the unexpected dependence [e.g. ODED 11] of the friction coefficient by other parameters as the normal load. All these clues suggest that an important role is played by the contact dynamics (wave generation and propagation) at the interface. More generally certain friction behaviours could be interpreted as a consequence of the dynamic of the system (local and global) rather than as strictly an interface property [MART 90]. In this context, the concept of the tribological triplet [GODE 84] [BERT 95] allows accounting for the interaction between the system dynamics (mechanism), the solid dynamics (first bodies) and the role of the third body layer.

Generally the study of friction induced vibration and their related instabilities are focused to the study of the relationship between the macroscopic dynamic behaviour of the component part of the systems, like for example their modal coupling, using the friction as macroscopic simplified parameter. On the other hand the studies dealing with wave propagation at the interface focus their attention on how the waves are related to the microscopic process happening at the frictional interface; indeed in the theoretical works generally they use "half-spaces" as hypothesis of work, without accounting for the "global" dynamics of the solids in contact. So, in the literature, the relationship between "global" and "local" dynamics it is not fully investigated. The understanding of this interaction could, for instance, allow for generating and controlling suitable wave fields with the aim of modifying the local dynamics and consequently the global behaviour of the system. On the other hand, the knowledge of the wave generation and propagation at contact interfaces would be of major interest when information are recovered from the generated acoustic signals, like in geophysics for the preventions of earthquakes or in structural diagnostics.

In the literature a whole branch of research deals with waves, usually in the ultrasonic range, which are sent, through the bodies, to the frictional interface and with the aim of modifying the contact conditions; allowing, for instance, for an easier relative motion [GRIG 72][SKAR 92][POPO 10] at the sliding interface. Nevertheless their approach is finely different from that which would be used in this thesis. The cited works, in fact, are based on inducing propagating elastic surface or body waves, which affect the relative motion between the bodies reducing the global friction coefficient thanks to, for example, the bouncing of the two surfaces in contact.

The aim of the project, framework of this thesis, is the understanding of the mechanisms at the base of the contact wave field (generation and propagation) and his relationship with both the local characteristics of the

surfaces in contact and the global dynamic features of the system. In fact, the understanding of this mechanisms, which are at the bases of several issues of contact and structural dynamics is basilar for the solving of nowadays problems in several field of application: surface machining issues, fretting, surface degradation phenomena (e.g. false Brinelling), dynamic instabilities, earthquakes prediction, structural diagnostic of complex structures, etc.

In literature, several numerical works deal with dynamic contact instabilities, simulating contacts in well established sliding state and investigating the dynamics response of the system (e.g. [BAIL 05b][LINC 04][MEZ 07]). On the other hand several works, mainly in geophysics, investigate the rupture (and consequently the wave) propagation in static preloaded interfaces (e.g. [BEN 01][ANDR 97]). The numerical work presented in this thesis wants to be a point of conjunction, starting from the analysis of a single rupture propagation in a preloaded static interface up to the investigation of the wave generation and propagation during the sliding initiation between the two solids. The relationship between the macroscopic behaviour of the system (stick-slip, continuous sliding, dynamic instabilities, etc.) and the local dynamics at the contact (wave propagation, ruptures and local sliding generation) is investigated.

The work is organized in three parts.

In the first part (chapter 2) a non-linear finite element analysis in large transformations of the dynamic rupture at the interface with contact friction, separating two bodies (isotropic and elastic) without relative motion, is developed. A rupture is considered when an initially sticking zone is becoming in sliding state. The properties of the obtained ruptures are analyzed for a flat interface between dissimilar materials in function of the nucleation energy; then the effect of the interface roughness is presented. The differentiated rupture inside the asperity and the conditions for coupling or uncoupling between the waves radiating in the two bodies have been also investigated.

The second part (chapter 3) of the thesis deals with the sliding initiation between the two contact surfaces. The sliding initiation between two bodies made of different isotropic elastic material and separated by a frictional interface is simulated. The evolution along the time of the global normal and tangential forces is analyzed, relating it to the local phenomena occurring at the interface. This part wants to investigate how micro-slips at the interface, acting as distributed ruptures, trigger the macro-slips between the two bodies in contact. The interaction between local and global dynamics is approached.

The third part (chapter 4) is closely related to the second one and contains a numerical parameter space study, which is performed as a function, among others, of the friction coefficient, material damping and regularization time of the contact law. The parametric analysis highlights the role of the system

and contact parameters both on the local wave and rupture propagation and on the related behaviour of the system, regulating the transfer of vibration energy from the contact to the system.

The results show the key role of the micro-slips and of the precursors, which are detectable wave propagations occurring at values of the tangential force well below the critical value expected by the friction law, in triggering the macro-slip between the two bodies. Depending on their distribution and magnitude the evolution of the contact forces passes from stick-slip-like behaviour to continuous sliding

The obtained numerical results have been compared for validation to experimental results in literature.

1 Contact dynamics: an always current issue

Introduction

Urbakh et al. [URBA 04] in a review work enumerated a part of the fundamental open questions about the dynamics of friction. This list showed that, despite of centuries of studies and countless dedicated papers, there are many aspects not yet fully understood in this so common and daily phenomenon.

The list stated:

- (1) Why is 'static friction' so universally observed between solid objects?*
- (2) How are friction and wear related? And why does surface damage often occur at the start of motion?*
- (3) How are the static and kinetic friction forces, and the characteristic transition velocities between smooth and stick-slip sliding, determined by the molecule-molecule and molecule-surface interactions and, in macroscopic systems, asperity-asperity or grain-grain interactions?*
- (4) Are the stick and slip regimes indicative of different phase states (liquid, solid, glassy) of the confined films or interfaces?*
- (5) What 'hidden' information is contained in chaotic as opposed to periodic motion? This is particularly important for predicting earth quakes.*
- (6) And finally, how can we control friction in practice, most often to reduce it or eliminate stick-slip at all pressures and velocities? But there are also situations when one wants high friction, as in clutches and brakes, or stick-slip, to enrich the sound of a violin and improve the feel or 'texture' of processed food as sensed during biting and chewing.*

Nowadays, some years later, further advances have been made and new directions (an extensive review is presented in [RENO 11]) have been undertaken to get more insight in these issues; nevertheless the most part of the aforementioned questions still remain unanswered. The "onset of frictional motion", which crosses transversally the most part of the aforementioned questions, is one of the oldest and, perhaps, more fascinating issue about friction and, beside the related wave propagation, is the main subject of these thesis.

How the solids in contact start to slide each other was, likely, one of the first questions wondered since the begin of the formulization of the friction concept: from the "*Confregazione*" of Leonardo Da Vinci, five century ago, passing by the "*Frottement*" of Amontons and Coulomb [AMON 699][COUL 785] to arrive to the "*Friction*" of Bowden and Tabor [BOWD 50][BOWD 54]. However some historian [RUSS 01] argues that this concept was not so unknown in the antiquity and that Erone (10-70 A.D), the Greek mathematician and engineer, in his "*Mechanica*", seems to use it knowledgeably; thus, "*Τριβος*" should be added at the head of the list.

There are different points of view by means of which to approach this issue: dynamic rupture, wave propagation, frictional instabilities, friction modelling, superficial transformations etc; each of them outlines broadly the field of provenience of the researcher who uses it: geophysics, fracture mechanics, non-linear dynamics, computational mechanics, contact mechanics, tribology, etc. Therefore it results not easy to resume entirely the works on sliding friction dynamics because of its intrinsic multidisciplinary nature. It is needed to select a guideline to develop a state of art with the intent of illustrating what this subject involves. Due to the continuum mechanics and vibrational approach of this thesis, it has been chosen to follow the papers mainly dedicated to the wave propagation at contact interface between elastic bodies, deferring the deeper discussion on the types of rupture (where rupture is considered when an initially sticking zone is becoming in sliding state) to a following section and treating specifically the frictional instabilities in a separated section.

1.2 Wave propagation at contact interfaces

1.2.1 Analytical works

Every statement about waves on a boundary cannot neglect the fundamental work of Lord Rayleigh [RAYL 900]; Rayleigh showed that along a free surface of an elastic half-space, a wave, whose amplitude decreases exponentially with the distance from the surface, can propagate at velocity slightly (subsequently calculated by Victorov [VICT 67]) lower than the shear wave (S) velocity of the body.

When two dissimilar elastic half-spaces are put in frictionless contact and constrained avoiding the formation of opening gaps, first Weertman [WEER 63] and then Achenbach et al. [ACHE 67] and Murty [MURT 75] showed that an interfacial wave solution can exist if the material mismatch is not too high (up to 30 % contrast in the shear waves velocity); this wave is called slip wave or generalized Rayleigh wave (GR). Without loss of generality, it could be considered as an interaction between the two Rayleigh waves of the two bodies in contact. In effect when the mismatch between the materials turns to zero, the slip wave reduces to a pair of Rayleigh waves, one in each body, propagating at the interface with the same speed, amplitude and wavelength, i.e. without interaction. The generalized Rayleigh wave speed lies between the individual Rayleigh wave speed of each material and it is slower than the slower S speed. A similar wave, called Stoneley wave, exists between two bonded elastic half-spaces [STON 24], and its range of existence has been founded by Scholte [SCHO 46].

In a following study Weertman [WEER 80] considered two dissimilar elastic half-spaces in frictional contact and argued that, in the range of existence of the generalized Rayleigh wave (in frictionless contact), a self-healing slip pulse can propagate along the frictional interface even when the remote shear stress is less than the frictional strength of the interface.

Adams [ADAM 95] studied the dry frictional sliding of two dissimilar elastic half-spaces pressed together with a constant (Amontons-Coulomb friction law) coefficient of friction at the interface and subjected to a constant remote applied tangential speed.

He found that although a nominally steady state solution exists, it can be dynamically unstable due to eigenvalues with positive real part that give rise to self-excited oscillations; these oscillations exist for a wide range of material combination, friction coefficient and sliding speed, leading to an ill-posedness of the problem (see section 3). These oscillations are due to the destabilization (hereafter referred as "Adams instability") of the interfacial (slip) wave and can cause either partial separation or regions of stick-slip. As a consequence, the *in-*

terface coefficient of friction (ratio of shear and normal stress at the interface) can be greater than the *apparent* coefficient of friction (ratio of remote shear and normal stress); thus the measured coefficient of friction, usually referred to the remote stress, does not represent the exact behaviour of the sliding interface. Adams investigated further this topic [ADAM 98]. He found that "his" instability may generate a stick-slip wave propagating along the interface in the direction of sliding of the more compliant solid, which is the body with the lower shear speed. The apparent coefficient of friction can decrease with sliding speed even though the interface coefficient of friction is constant. In other words there can be relative sliding in spite of the fact the remote shear stress is less than the required one by the frictional law and theoretically "*...the presence of slip waves may be possible for two frictional bodies to slide without a resisting shear stress and without an interface separation*" [ADAM 98], i.e. a sort of "wrinkle-like" motion.

The results of Adams seem to be in close relationship with those of Weertman; in fact Ranjith and Rice [RANJ 01] demonstrated that when the generalized wave exists (in frictionless contact), the stability problem with Coulomb friction law is ill-posed for arbitrary small values of friction. They also re-derived in a simpler manner the ill-posedness results of Adams. The approach of Adams was by a periodic solution, while Ranijith, like Weertmann, used a moving dislocation formulation. Referring to figure 1.1, which shows two half-spaces subjected to a remote normal and shear stress σ_∞ and $\tau_\infty = \mu \sigma_\infty$, where μ is

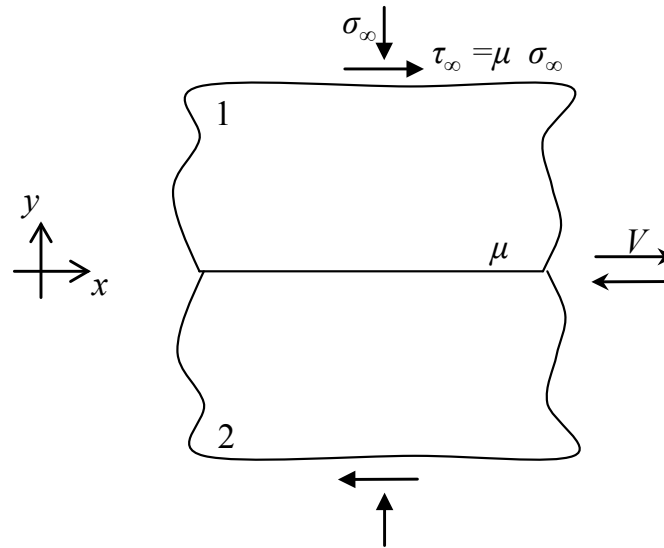


Figure 1.1 The 2-D model of [RANJ 01].

the Coulomb coefficient, when the shear stress τ at the interface is perturbed in a single spatial mode of wavenumber k :

$$\Delta\tau = \mathbf{Q}(t)e^{ikx} \quad (1.1)$$

where $Q(t)$ is an arbitrary function of time, propagating slip-rate modes are found:

$$\Delta V = A(k)e^{ik(x-ct)}e^{a|k|t} \quad (1.2)$$

Where $A(k)$ is the amplitude of the mode and a and c are independent of the wavelength. For $a>0$ (that happens for a broad range of material and pairs) wavelengths in the slip response are unstable and the growth rate of the instability is inversely proportional to the wavelength. Thus, there is a flow of energy toward the smaller wavelengths. The response to a shear stress perturbation with general spatial dependency is

$$\Delta V = \frac{1}{\sqrt{2\pi}} \int_{-\infty}^{\infty} A(k)e^{ik(x-ct)}e^{a|k|t} dk \quad (1.3)$$

This integral diverges for all cases (if $A(k)$ doesn't decay faster than the divergence of the exponential term), and makes the response of the elastic system to a generic perturbation mathematically ill-posed and grid-size depending (see below). The results of Ranjith and Rice can be conveniently resumed by their stability diagram (Figure 1.2).

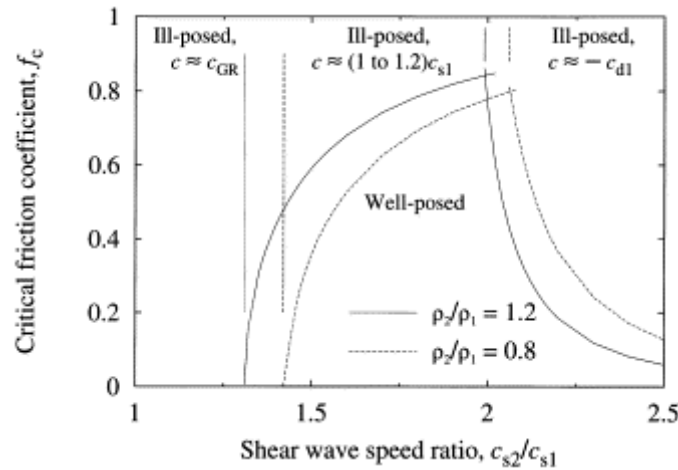


Figure 1.2 Stability diagram for two families of bi-material pairs as a function of the shear wave speed ratio. For one pair, the density ratio is $\rho_2/\rho_1=1.2$ and for the other is $\rho_2/\rho_1=0.8$. For both families of material pairs, $v_1=v_2=0.25$. c_s is the shear wave speed. It is assumed that $c_{s2} > c_{s1}$. c is the phase velocity of the instability (From [RANJ 01]).

It can be seen that when the generalized Rayleigh wave speed (c_{GR}) exists the problem is ill-posed for all values of the coefficient of friction, whereas when the c_{GR} does not exist the problem is well-posed up to a critical value of f_c .

Finally they proposed a simplified version (see section 3) of a constitutive friction law experimentally obtained [PRAK 93] and demonstrated how this type of law, with no instantaneous dependence of the shear stress τ on the normal stress σ , makes the problem well-posed, acting as a "regularizing" law.

Figure 1.3 and expression (1.4) show schematically, the behaviour of this law:

$$\dot{\tau} = -\left(\frac{V}{\hat{L}}\right)(\tau + \mu\sigma) \quad (1.4)$$

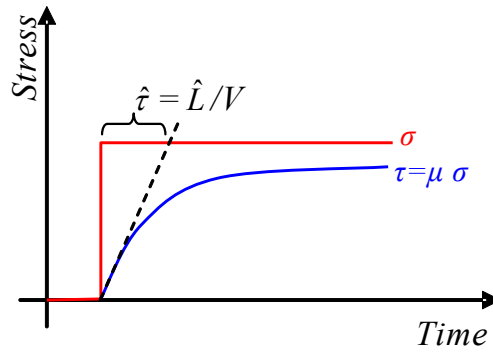


Figure 1.3 A simplified Prakash-Clifton law. It can be noted the delayed response of the shear stress (blue line) to abrupt change in the normal stress (red line).

where V is the sliding velocity, \hat{L} is a characteristic slip length over which the changes in the tangential stress occur and $\hat{\tau}$ is the time of regularisation.

Interface stick-slip waves with separation have been investigated by Comninou and Dundurs both between dissimilar frictionless [COMN 77] and identical with friction [COMN 78a] half-spaces. Their conclusion is that such waves could exist, but there are also singularities at the tips of the slip zones; in the opinion of Freund [FREU 78] these singularities are not realistic because they should require energy sources and sink. It can be noted as Comninou has not encountered the Adams instability. They also investigated [COMN 78b] the possibility of sliding motion between two identical bodies without interface slipping (i.e. the points of the interface assume only stick or detachment status) by only interface wave separation, which is the so-called "carpet-fold" motion (to distinguish it from the aforementioned "wrinkle-like" motion here used for a motion without separation); although they demonstrated that, when such motion exists, singularity were also encountered. This type of motions were also inves-

tigated by Adams [ADAM 99], but in the case of dissimilar materials. He found that a separation wave pulse can exist and it causes the two bodies to slide without slipping. He also encountered a singularity at the trailing edge of the separation zone, but its order is small enough to not produce an energy sink.

Both Adams in [ADAM 01] and Weertman in [WEER 02], with their different approaches, deal with the propagation of an intersonic (i.e. with velocity between the shear wave speed and the longitudinal wave speed) slip pulse at the interface between dissimilar materials. Adams showed that an intersonic slip pulse exists for sufficient friction and for modest mismatches in the material combinations. This slip-pulse travels in the opposite direction of the sliding of the more compliant material, i.e. in the opposite direction of the generalized Rayleigh wave, and at a speed just below the slower dilatational wave speed (in this work it is referred indifferently to dilatational, primary P (Push) or longitudinal wave, as well as to rotational, secondary S (Shake) or shear wave [GRAF 91]. Weertman demonstrated the existence of a dislocation moving at velocity closed to the Eshelby velocity c_E ($c_E = \sqrt{2} c_s$, with c_s shear wave velocity in the case of identical material) in the direction of sliding of the most compliant solid. Their results show that there is a normal stress reduction in the slip process originated by the different elastic properties, namely a coupling between slip and normal stress, similarly to what happens in the sub-Rayleigh case. It is useful to remark that in the case of identical materials, there cannot be, in any case, coupling between slip and normal stress.

Miller [MILL 79] [MILL 81], Comninou and Dundurs [DUND 79] [COMN 82] and Nosonovsky [NOSO 01] [NOSO 02] cover the interaction of a frictional interface with different types of incident waves: dilatational, shear (SV, vertically polarized shear wave or SH horizontally polarized shear wave) plane elastic pulse, and plane elastic waves of arbitrary form. These works could be specially useful in the case where there are waves interacting with the frictional interface, like in this thesis where it will be necessary to consider the waves reflected by the boundaries of the system and then interacting with the interface. Their contribution to the comprehension of the phenomena object of this work will be cited in the relative section.

All this theoretical studies, due to the intrinsic complexity of problems concerning friction (non-linearity, non-smoothness, chaos etc.) are in general greatly idealized. Many effects have been omitted (thermal effect, real contact area, plastic deformation, surface roughness), while they play an important role in the experimental works (see section 1.2.2). Nonetheless these works are an essential base upon which to lean the numerical analysis.

1.2.2 Numerical works

Friction involves phenomena at different scales, belonging to those non-linear problems for which small-scale processes and the large scale ones are strongly coupled. The numerical works dealing with this issue generally differ by their approach: continuum, discrete, atomistic [LEBO 03][RENO 11]. Passing from the former to the latter they refine the physical view of phenomena but, due to the dramatic growth of the number of degree of freedom, the analysis becomes more limited in dimensions of the sample and of the time scale.

As already mentioned this thesis uses a finite element model in the framework of a 2D continuum approach; consequently, the major part of the numerical works reviewed here below shares the same type of approach. A large part of the reported numerical works belong to the geophysics field, due to key role that the dynamics of frictional interface between faults plays in triggering earthquakes.

Andrews and Ben-Zion [ANDR 97] first found a numerical solution for the slip pulse. Using a classic Coulomb friction law (without regularisation) at the interface between dissimilar materials and performing the calculation by a finite difference method, they calculated a self-sustaining narrow pulse of slip velocity associated with a tensile change of the normal traction and propagating in the direction of the more compliant solid, as predicted by Weertman [WEER 80]. The slip pulse propagates at a velocity close to the slower shear wave speed and his width tends to become narrower as it propagates, while his slip velocity increases, i.e. a sort of "sharpening" effect. The solution is unstable and there is a continuous transfer of energy to shorter wavelengths (Adams instability).

Cochard and Rice [COCH 00] studied numerically the ill-posedness involving dissimilar materials, reproducing the simulations of Andrews and Ben-Zion [ANDR 97]. They highlighted the ill-posedness by showing that, in the unstable range, the numerical solutions do not converge through grid size reduction. They also showed numerically that a regularized law, which is a law that does not have an abrupt change in shear stress in response to a change in normal stress, (like the one used by Ranjith and Rice [RANJ 01]) makes the problem well-posed; the classical slip-weakening or rate-and-state constitutive laws do not regularize the problem. After regularizing the problem and making it well-posed, they obtained results in agreement with the Weertman analysis: when the c_{GR} exists a slip-pulse propagates (with a speed close to c_{GR}) in the direction of the more compliant solid; when the c_{GR} does not exists a slip-pulse propagates in the same direction but at velocity close to the slower shear speed. Cochard and Rice provided a synoptic table (Table 1.1) that resumes what just explained and shows the comparison with the result of Ranjith and Rice (modal analysis).

		20% contrast; c_{GR} defined	30% contrast; c_{GR} not defined
f		0 $f_{crit} \approx 0.22$ $+\infty$	0 $f_{crit1} \approx 0.15$ $f_{crit2} \approx 1.75$ $+\infty$
Coulomb law	Modal analysis	Unstable modes, R independent of k $V_{prop} \approx +c_{GR}$ $V_{prop} \approx +c_{GR}$ and/or $ V_{prop} \gtrsim P_{slow} (V_{prop} < 0)$	Stable modes Unstable modes, R independent of k $V_{prop} \approx +S_{slow}$ $V_{prop} \approx +S_{slow}$ and/or $ V_{prop} \gtrsim P_{slow} (V_{prop} < 0)$
	Realistic cases	Ill posed: no convergence through grid size reduction	Well posed; only dying pulses Ill posed: no convergence through grid size reduction
Modified Prakash-Clifton law	Modal analysis	Unstable modes V_{prop} (weak) function of k R function of k	Stable modes Unstable modes V_{prop} (weak) function of k for $k < k_{crit1}$ for $k < k_{crit2}$ ($k_{crit2} > k_{crit1}$)
	Realistic cases	Regularization of ill-posedness at large k Self-sustained pulses may propagate at $V_r \lesssim +c_{GR}$ $V_r \lesssim +c_{GR}$ and/or $V_r \approx -P_{slow}$	Well posed; only dying pulses Regularization of ill-posedness Self-sustained pulses may propagate at $V_r \approx +S_{slow}$ $V_r \approx +S_{slow}$ and/or $V_r \approx -P_{slow}$

Table 1.1 . Summary of results of [COCH 00], with link to [RANJ 00] modal analysis. R is the normalized growth rate (see Figure 2); k is the mode number; V_{prop} is the propagation velocity of harmonic modes; V_r is the propagation velocity of pulses in simulations like reported here. Sign of propagation velocities refers to the direction of propagation: + addresses the direction of slip in the more compliant medium; - addresses the opposite direction. f is the friction coefficient.

Cochard and Rice also studied the effect of the characteristic distance L (Figure 1.3 and expression 1.4), peculiar of the regularized friction law. L controls whether the pulse decays or is self-sustained, and there is a transition value below which the pulse becomes self-sustained.

Finally they verified the existence of the self-sustained pulse at intersonic velocity (close to the slower dilatational wave speed), propagating in the opposite direction, which is the direction of sliding of the stiffer solid.

Ben-Zion and Huang [BEN 02] studied the dynamic rupture at interfaces between dissimilar materials using a regularized Coulomb friction law. They found that the self-sharpening and divergent behaviour exists also with a regularized law, for large enough propagation distance and that "the parameters of regularized friction have to be fine tuned to produce apparent stability for a given propagation distance".

Brietzke et Ben-Zion [BRIE 06], using both regularized and not regularized friction laws, observed the remarkable tendency of ruptures, nucleated in homogeneous media, to migrate toward bimaterial (i.e. dissimilar) interfaces; they migrate to parallel boundaries where the homogeneous medium is in contact with a different material, assuming self-sustained pulse-like features for wide ranges of conditions.

SHI et al. [SHI 06] investigated the rupture along a bimaterial interface governed by a slip-weakening friction. Their results show that an in-plane rupture evolves to an unilateral pulse-like in the direction of the more compliant solid, with velocity close to c_{GR} . When the difference between the static and the dynamic friction is smaller, the evolution to unilateral pulse occurs for a smaller value of the contrast between the materials. However increasing either material contrast or initial shear stress promote the development of self-sustained pulses in the positive direction (i.e. the direction of sliding of the more compliant solid). In particular larger material contrast produces stronger dynamic reduction of normal stress at the propagating tip of the pulse; while higher initial shear stress makes it easier, for the rupture, to continue inducing failure ahead. They also observed, for enough high imposed rupture speed in the source region, a pulse-like rupture propagating in the negative direction at speed close to the slower dilatational wave speed.

1.2.3 Experimental works

Rubinstein et al. in [RUBI 04] studied the onset of dynamic friction between two blocks (of PMMA, polymethyl-methacrylate) separated by a rough interface. By their apparatus they measured the real area of contact during the propagation of the rupture. They observed that the dynamic rupture is governed by three well defined crack-like detachment fronts and after each detachment front the net contact area is reduced. The detachment process is initiated at the trailing edge where the shear stress is applied by a propagation of sub-Rayleigh front that propagates along the interface at a speed less than the Rayleigh speed (c_R), but accelerating towards c_R . When it reaches approximately the c_R speed it bifurcates into two distinct fronts: an intersonic front and a "slow" detachment front propagating at velocities an order of magnitude slower than c_R . The slow detachment front does not always reach the leading edge of the sample, undergoing toward a reverse transition back to a sub-Rayleigh front. When the sub-Rayleigh or the slow detachment front reach the leading edge a rebound wave, propagating at intersonic speed, arises from the reflection. Only after the passage of this rebound wave there is a self-organization of the contact points. In addition the displacement of the leading edge occurs only after the passage of

the sub-Rayleigh or of the slow detachment front. More precisely only the sub-Rayleigh and the slow detachment front give rise to an appreciable reduction of the contact area (in particular the area reduction due to the slow detachment is twice the sub-Rayleigh one), while the supersonic front causes only a negligible reduction of the contact area. In other words the onset of the sliding friction is strongly related to the passage of the sub-Rayleigh and mostly of the slow detachment front; although the acoustic signature of the last one is significantly weaker than the faster fronts.

Another work [RUBI 07] investigated the role of the precursors in the onset of the sliding. They found that before the arise of sliding, a series of rapid crack-like precursors propagate partially through the interface at a value of the shear stress well below the required one of the friction law. The distance of propagation l of these precursors increases (approximately linearly) as the shear force increases, up to about the value of $L/2$, where L is the entire length of the interface. During this phase the precursors have a sub-Rayleigh speed. When l exceeds $L/2$ the sub-Rayleigh front becomes a slow-front and l have a more rapid growth with the shear stress until the value of L , which means the sliding of the whole interface. Another important observation is that after each successive precursor the surface contact area becomes systematically less uniform on the interface, conversely to statically uniform distribution of microcontacts, which is usually considered.

Using a monocrystal of NaCl sliding on a glass base, Voisin et al. [VOIS 07] analyzed the evolution of different stages of the frictional response. They observed that the macroscopic stick-slip regime is progressively vanishing eventually reaching the stable sliding regime. They assumed a rate-and-state behaviour for the frictional law at the interface and consequently derived the parameters of the law by the experimental results, noting that in the case of stable sliding there is no more rate-and-state dependence. The amount of the shear stress drops as well as the slip corresponding to the single macroscopic stick-slip cycle reduces gradually along the time.

Oded and Fineberg [ODED 11] investigated the dependence of the dry friction threshold on rupture dynamics, concluding that the static friction coefficient is not a constant material property but is linked to the rupture dynamics at the interface. This provides an explanation for widely different measured values of the coefficient of friction [RUBI 04] obtained for the same materials when different loading conditions are applied.

Studying the stabilization of the stick-slip friction Capozza et al. [CAPO 11] demonstrated that applying small oscillatory perturbation to the shear force the stick-slip period can be synchronized. They further showed that this "phase locking" is related to the inhibition of slow rupture modes, which force a transition to fast rupture.

Zigone et al. [ZIGO 11] investigated experimentally the generation of the Seismic Tremor Like Signals (TLS), which is an acoustic emission of lower magnitude than the main slip events (earthquakes) that sometimes is registered before this one. They used a monocrystal of salt sliding on glass. In this work the TLS are demonstrated to be systematically correlated with the onset of the slip acceleration (as precursors). Zigone et al. identified three different behaviours with the increases of the time and the correspondent cumulative slip (Figure 1.4).

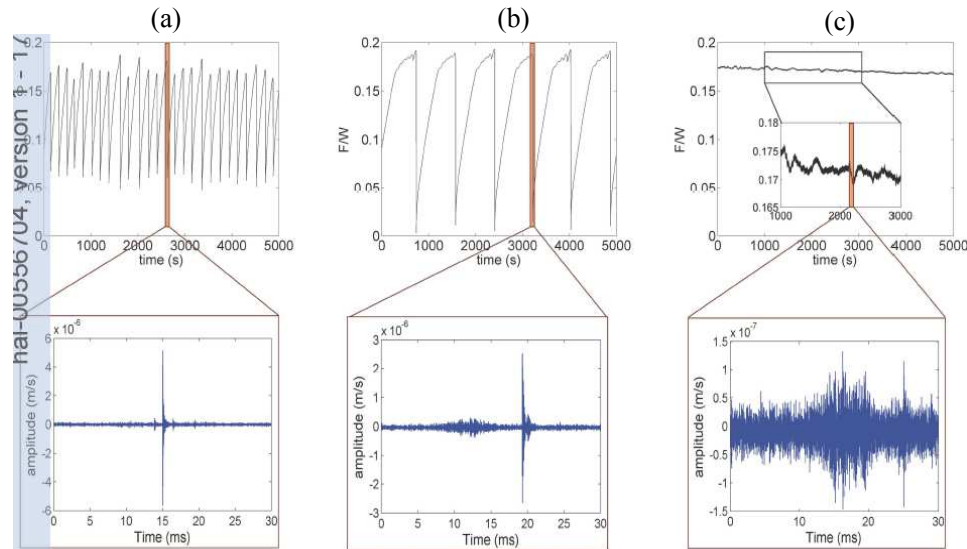


Figure 1.4 Frictional behaviour of salt/glass interface (from [ZIGO 11]). Top plots: recorded shear force divided by normal load, noted F/W . Bottom plots: acoustic emissions recorded. (a) Unstable regime; (b) Transition unstable-stable regime; (c) Stable regime.

In a first time (Figure 1.4 (a)) there is a typical stick-slip regime characterized by sudden shear stress drops separated by periods of stress accumulation. The acoustic emission is characterized by large impulsive events, sometimes preceded and followed by smaller impulsive events, not TLS is recorded. Subsequently (Figure 1.4 (b)) the frictional behaviour is more complex. If the sudden jumps still occur, they are preceded by smooth oscillations of growing amplitude. The associated acoustic emission presents a complex signal formed by a TLS with long duration (10 to 20 ms) and low amplitude followed by a strong impulsive and short duration event that represents the signature of the jump. Finally (Figure 1.4 (c)) the frictional force remains more or less constant with small variations around a mean value. The associated acoustic emission is formed of a TLS with low amplitude and long duration, emitted at each acceleration slip.

1.3 Dynamic rupture in mode II

This section provides an introductive state of art about the dynamic rupture and in particular in the case of rupture in mode II, which occurs when the slip is parallel to the direction of rupture propagation (Figure 1.5).

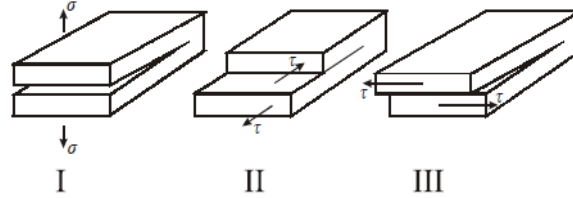


Figure 1.5 The three fracture models: opening mode (I), sliding mode (II), tearing mode (III) (from [VARO 04]).

Depending on the interface state the ruptures in mode II can be classified in : (i) Crack-like rupture: the broken part of the interface is sliding continuously. (ii) Pulse-like rupture: only a small part of the broken interface is in sliding state and there is a self-healing front at the back of the front; (iii) Train of pulse. The crack-like rupture is favoured by relatively high and smooth initial background stress, relatively weak velocity dependence of friction and low or no coupling of slip changes to normal stress; the pulse-like rupture is favoured in opposite conditions [SHI 08]. Regarding the velocity of propagation, different ranges can be identified: (j) Sub-Rayleigh if the speed is less than the Rayleigh wave speed c_R ; (jj) Supershear if the speed is greater than the shear wave speed c_S . Generally the interval between the shear wave speed and the dilatational wave speed c_P is called intersonic or transonic (in the case of bi-material interface, it is referred to the interval between the lower shear wave speed and the higher dilatational wave speed).

Initially it has been found in numerical simulations by Andrews [ANDR 76] that a growing mode II shear crack may at first rapidly accelerate toward the Rayleigh wave speed c_R and then, after a short period of readjustment, it starts running at a speed slightly greater than $\sqrt{2} c_S$. Burridge et al. [BURR 79] investigated in detail the steady motion of a semi-infinite crack. They found three types of regime of crack propagation (whose speed is indicated as c_c): for $c_c < c_R$ and $c_S < c_c < \sqrt{2} c_S$ there are unstable regimes of propagation; conversely for $\sqrt{2} c_S < c_c < c_S$ there is a stable regime. Finally the interval $c_R < c_c < c_S$ appears to be forbidden, because the propagation in this regime is associated with energy generation rather than energy dissipation. This is in agreement with, and partially explains, Andrews's results.

The presence of the forbidden interval involves the problem of how to explain the transition sub-Rayleigh/supershear velocity, experimentally observed. A possible explanation is the so-called BAM (Burridge Andrews Mechanism) [ANDR 76]: initially the rupture speed increases up to the c_R velocity. At the same time a shear stress peak ahead of the main rupture triggers a secondary rupture propagating at supershear speed, after that the rupture accelerates toward c_P .

According to the BAM theory, Xia et al [XIA 04] found experimentally that a shear rupture accelerates to a speed very close to c_R immediately after its initiation. A peak in the shear stress is found to propagate at the front rupture and the magnitude of the peak increases as the front rupture speed approaches c_R . It becomes strong enough to promote a nucleation of a secondary micro-rupture whose leading edge propagates at c_P ; then the two ruptures coalesce and propagate at c_P . Geubelle et al [GEUB 01] proposed a different mechanism to explain the transition sub-Rayleigh/supershear, against the theory of the forbidden interval, showing that the velocity can increase with continuity although very rapidly.

Festa and Villotte [FEST 06] using a non-smooth spectral method under slip-weakening friction, investigated the supershear transition of an in-plane rupture. They found, in function of the nucleation rupture, both the two types of transition, discontinuous (within the forbidden interval) and continuous. Depending on the value of the parameters related to the strength excess and to the nucleation length, they found two type of supershear propagation: pulse-like and crack-like propagation; the existence of one or the other is strongly affected by the nucleation length.

1.4 Friction instabilities

As mentioned in the introduction, friction-induced instabilities [MART 02] may be at the origin of strong oscillations or abrupt motions, which can cause undesired noise and severe wear of mechanical component. The noise arising from the friction instabilities is often classified as a function of its macroscopic mechanism (stick-slip, sprag-slip, modal coupling, etc.) or of its frequency range (*walk* (5-20 Hz), *chatter* (20-100 Hz) and *squeal* (100-20 kHz) among others). In the previous sections the name “instability” has been specifically related to the rupture mechanism due to the contrast between the materials in frictional contact. This section deals with the literature concerning instabilities caused, or related to the presence of sliding friction; because of the large amount of literature that can be found for several specific issues (brake NVH,

machining, rotating machines, etc.) it is not possible to report an extensive bibliography in this context and the reader is addressed to more specific reviews [IBRA 94][AKAY 02][MART 02].

First of all, dealing with “instabilities”, it is worth to define what is intended by “stability” [PRAT 10]. Using the definition of Adams [ADAM 95] [ADAM 98] it could be intended as stable state the one characterized by a stationary sliding contact of the two surfaces moving each other. So conversely the unstable state presents a non stationary sliding due to the propagation, for example, of stick-slip waves [ADAM 95] or stick-separation waves [COMN 78b] waves, or stick-slip-separation waves [COMN 78a]; in these works, as a reference, an example of theoretical work that deals with they propagation at the interface between half-spaces has been indicated.

The presence of these instabilities changes drastically the relation between the remote stress applied at the bodies and the stresses distribution at the interface. An example is represented by the difference between the *apparent* and the *interface* coefficient of friction (section 1.2.1). In addition the local stress can reaches extremely larger (or lower) values than the expected ones. More in general these waves define the local kinematics of the surface and therefore the distribution of the contact pressure, the shear stress, the local deformations and the tribological state of the contact zone [BAIL 05b]. Consequently they have a key role on the formation of the SSTs (Superficial Tribological Transformations) [BERT 01] as well as in the interaction with the third body [BERT 95]. In the meantime, the complex local kinematics, issue of the friction instabilities, is strongly related to the global dynamics of the bodies in contact and of the mechanical system where the contact happens. A cause-effect interaction (coupling) between local and global dynamics is at the origin of several dynamic and tribological issues [MASS 10] [MASS 08]

A consistent part of the literature dealing with friction instabilities has its origin on the analysis of NVH brake issues. Different theories have been developed to explain the onset of the friction instabilities:

i) a sliding friction coefficient decreasing with the velocity [MILL 38], with the sliding distance [RABI 58] or with sliding speed and state [RUIN 83]. In all these approaches the negative slope of the friction brings to a sort of negative damping which causes self-induced and divergent vibrations;

ii) the *sprag-slip* theory [SPUR 61], where the geometry and the actual deformation of the system assumes a more important role. In fact considering a constant friction coefficient, the instability is associated to the coupling between different degrees of freedom of the system which causes variations on the normal force at the contact and consequently on the friction force;

iii) the coalescence of eigenvalues: North [NORT 02] demonstrated as the friction instabilities could be related to the coalescence of two eigenvalues

of the system. For example, varying a parameter of the systems the two eigenvalues, initially distinct, tend to approach each other, up to the point of *lock-in* [AKAY 00] where they assume the same imaginary part (i.e. the same frequency) and opposite in sign real part. The eigenvalue with the positive real part brings to the flutter (i.e. oscillatory growth of dynamic solutions in the neighbourhood of steady sliding) instability. In particular this type of instability, when due to the asymmetry of the stiffness matrix, is named *mode lock-in* [AKAY 00].

In all these works and theories for explaining the friction induce instabilities a common aspect is the need of a coupling between the local dynamics at the contact (local stress, deformation and status) and the global dynamics of the mechanism and bodies in contact.

Although some advancement has been achieved in the analysis of the interaction between the interface and the global behaviour of the systems, a satisfactory understanding of the wave generation and propagation at the interface (which is largely affected by both the local and global dynamics) is still missing. In addition, the approach to the friction instabilities, in a large part of works, is focused rather toward their consequence (vibrations, noises, wear, etc.) than toward the local generation and propagation processes and their relationship with the global dynamics. Works that deal with local dynamics are often focused of the wave/rupture propagation (cited in the previous section). Linck et al. [Linc 04] simulated the sliding friction between two bodies with a non-negligible relative velocity. They found that stick-slip-separation waves are generated at the interface. These waves bring to a reduction of the contact area and to an increase of the contact stresses and local impacts at high velocity and high frequency. Further consequence is that the local relative sliding velocity is much higher than the macroscopic sliding velocity. They also investigated the influence of Young's modulus and Poisson's coefficient modulus of the materials in contact. They found limit values on these parameters that can change the frequency and amplitude of the instability displacement circles.

The role of the vibrations in determining the relationship between the dynamics at the interface and the steady sliding at the macroscopic level has been also highlighted in Baillet [BAIL 05].

Finally, several numerical and experimental works deal with the link between surface roughness and induced vibrations during sliding [AKAY 02] [HOFF 06]; nevertheless, in these case, the focus is often restricted to the analysis of the "global" acoustic signature (vibration spectra) of the surface roughness, rather than to the local phenomena at the interface.

2 Dynamic rupture at smooth and rough frictional interfaces

Introduction

In this chapter a non-linear finite element analysis in large transformations of the dynamic rupture at the interface with contact friction separating two bodies (isotropic and elastic) without relative motion is presented. A rupture is considered when an initially sticking zone is becoming in sliding state. The properties of the obtained ruptures are analyzed for a flat interface between dissimilar materials in function of the nucleation energy; then the effect of the interface roughness is analyzed. The differentiated rupture inside the asperity and the conditions for coupling an uncoupling between the waves radiating in the two bodies has been investigated. The aim of this part is to investigate the features of a single nucleated rupture and the parameters which affect it. The results will be used to interpret the phenomena studied in the second part. This chapter is organized as follows: first an introductory section focuses on the literature that deals with the roughness at frictional interfaces; then the numerical code used to perform all the simulations presented in this thesis is introduced; finally the results from the dynamic rupture simulations are presented.

2.1.1 Effect of roughness

The roughness of the contacting surfaces plays an important role in determining the nature of the shear stress distribution and consequently affects the rupture dynamics. Under magnification, also an apparently flatter surface shows microscopic hills and valleys called asperities. Generally the surface roughness is random and the distribution of the asperities heights usually follows a Gaussian distribution [SHEN 07]. Many statistic parameters are used to describe the roughness, among these the R_a (roughness arithmetical average), the centreline average of asperity heights over a length L and the standard deviation σ_R of the distribution of the asperities heights (Figure 2.1):

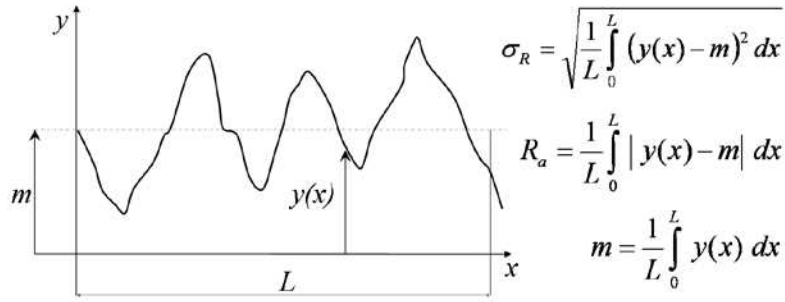


Figure 2.1 Surface roughness parameters.

When two bodies are pressed together, because surfaces are rough, the real area of contact (“fractional contact area”) is much smaller than the apparent contact area. Various models of contacting rough surfaces have been proposed; the work by Oden and Martin [ODEN 85] gives an extensive overview of these models. The fractional contact area bears the entire applied macroscopic load, such that an heterogeneous distribution of the local normal stress is produced at the interface between the bodies; if the contact is subjected to a tangential force, also the local shear stress distribution is heterogeneous. Heterogeneous stress distributions lead to complex rupture histories. The stress variability is correlated to the R_a and the σ_R roughness parameters. Flat interfaces between dissimilar materials with heterogeneous initial stress have been investigated by Ampuero and Ben-Zion [AMPU 08]. They studied ruptures on a planar interface, without roughness, with localized nucleation at the centre of the interface. They assumed a uniform initial normal stress and explored the effect of heterogeneous initial shear stress with different statistic distributions. Their analysis showed that rupture pulses are statistically sensitive to the amplitude, standard deviation and correlation of stress heterogeneities and suggested that “*the intensity of the macroscopic source asymmetry might not be a stationary property of a bi-material fault*”, i.e. the rupture style, generally asymmetric (respect to the centre of the interface) due to the difference between the materials, can become symmetric depending on the distribution of the heterogeneities.

The presence of asperities generates a complex rupture process and, because of concentrations of stresses, causes abrupt changes in slip velocity, which are the source of high frequency waves [MADR 83]. When the crack tip crosses the contact zone, it can interact with the asperity in three different ways [DAS 77]: i) the asperity is broken as the crack tip passes; ii) the crack tip proceeds beyond the barrier, leaving behind unbroken asperity; iii) the asperity is not broken at the initial passage of the crack tip but, eventually, breaks because of an increase in dynamic stresses, eventually with the passage of secondary rupture

fronts. Rubinstein et al [RUBI 07] investigated the dynamics of the incipient sliding between rough surfaces. They showed that the onset of motion is preceded by discrete sequence of crack-like precursors, which are initiated at shear level that are below the threshold of static friction. These precursors redistribute the true contact area along the interface and consequently the local stress. Dunham et al [DUNH 03] studied a 3D model of a planar fault rupture, with the presence of barriers and asperities. Barriers were investigated as region of increased fracture energy, i.e. cohesive resistance to sliding. Asperities, as pointed out earlier, are region of high initial stress concentration. Das and Kostrov [DAS 83] obtained a numerical solution to the rupture process of a single asperity. Their work examined the rupture of a single circular asperity and the resulting radiated displacement pulses on an infinite fault plane. The fault plane outside the asperity area can be frictionless or not in contact; this is interesting because it may be reasonable to assume that the interface between two bodies consists of separate asperities, and the fracture process may be visualized as the rupturing of these asperities. In fact the experience that real areas of contact are small means that relative large areas are not touching.

In the present work the analysis of the effect of the interface asperities is approached. The simulations show that, due the heterogeneous stress distribution, there is a differentiated rupture inside the asperity with different front rupture velocities for different zones of the asperity; during the process, changes of the front rupture velocity may occur. The conditions for coupling or uncoupling between the waves radiating in the two bodies have also been investigated. Their correlation to the relative dimension between the roughness and the width of the wave fronts has been suggested. The width of the wave front is correlated with the velocity field near the crack tip which depends on the instantaneous rupture velocity, on the stress intensity factor and is inversely proportional to the rigidity [MADR 83].

2.2 Numerical tool: PlastD

The explicit dynamic finite element code PLASTD (in 2D), is used to simulate the behaviour of the system (Figure 2.2) during the frictional contact. This software [BAIL 02] is designed for large deformations and non-linear contact behaviour and applies a forward Lagrange multiplier method for the contact between deformable bodies. For the dynamic study, the formulation is discretized spatially by using the finite element method and discretized temporally by using the β_2 method. The contact algorithm uses slave nodes (situated on the $P^{(1)}$ contact surface on Figure 2.2) and target surfaces (on the $P^{(2)}$ contact surface) described by a four node quadrilateral element with 2x2 Gauss quadrature rule. The elementary target segments are described by two nodes and approximated by bicubic splines [BAIL 05]. The forward Lagrange multiplier method is formulated by equations of motion at time $(t^i = i \Delta t)$ with the displacement conditions imposed on the slave node at time t^{i+1} :

$$\begin{cases} \mathbf{M}\ddot{\mathbf{u}}^i + \mathbf{C}\dot{\mathbf{u}}^i + \mathbf{K}\mathbf{u}^i + \mathbf{G}^{i+1T} \boldsymbol{\lambda}^i = \mathbf{F}^i \\ \mathbf{G}^{i+1} \{ \mathbf{X}^i + \mathbf{u}^{i+1} - \mathbf{u}^i \} \leq 0 \end{cases} \quad (2.1)$$

Where \mathbf{M} and \mathbf{K} are respectively symmetric and positively defined matrices of mass and stiffness of the system. \mathbf{C} is the Rayleigh's proportional damping matrix:

$$\mathbf{C} = (\alpha \mathbf{M} + \beta \mathbf{K}) \quad (2.2)$$

\mathbf{X}^i is the coordinate vector at time t^i . $\mathbf{u}, \dot{\mathbf{u}}, \ddot{\mathbf{u}}$ are respectively the vectors of nodal displacements, nodal velocities and accelerations. \mathbf{F} is the vector of nodal external forces.

$\boldsymbol{\lambda} = [\lambda_n \ \lambda_t]^T$ contains respectively normal and tangential contact forces acting on the nodes at the contact surface.

$\mathbf{G}^T = [\mathbf{G}_n^T \ \mathbf{G}_t^T]$ is the global matrix of the displacement conditions ensuring non-penetration and the contact law of the bodies in contact.

The equations of motion (2.1) are discretized in time by using an explicit Newmark scheme. The vectors $\ddot{\mathbf{u}}^i$ and $\dot{\mathbf{u}}^i$ are expressed at each time step using a time scheme of type β_2 ($\beta_2 \in [0.5; 1]$):

$$\begin{cases} \ddot{\mathbf{u}}^i = \frac{2}{\Delta t^2} (\mathbf{u}^{i+1} - \mathbf{u}^i - \Delta t \dot{\mathbf{u}}^i) \\ \dot{\mathbf{u}}^i = \frac{1}{1 + 2\beta_2} \left\{ \dot{\mathbf{u}}^{i+1} - \beta_2 \ddot{\mathbf{u}}^{i-1} - \frac{2\beta_2}{\Delta t} (\mathbf{u}^{i+1} - \mathbf{u}^i) \right\} \end{cases} \quad (2.3)$$

The displacements ${}^* \mathbf{u}^{i+1}$ of the nodes situated on the contact surface ($P^{(1)}$ and $P^{(2)}$) are initially computed with λ^i equal to $\mathbf{0}$. If β_2 is fixed to 0.5 (central difference method) the nodal displacements at time ${}^* t^{i+1}$ are obtained so that:

$${}^* \mathbf{u}^{i+1} \Delta t = \Delta t^2 \mathbf{M}^{-1} (\mathbf{F}^i - \mathbf{K} \mathbf{u}^i) - 2\mathbf{u}^i + \mathbf{u}^{i-1} \quad (2.4)$$

A constraint matrix \mathbf{G}^{i+1} is formulated for the slave nodes if they have penetrated through a target segment. Calculations of contact forces λ^i and nodal displacement at time t^{i+1} are then performed:

$$\begin{cases} \lambda^i = (\Delta t^2 \mathbf{G}^{i+1} \mathbf{M}^{-1} \mathbf{G}^{i+1^T})^{-1} \mathbf{G}^{i+1} ({}^* \mathbf{u}^{i+1}) \\ \mathbf{u}^{i+1} = {}^* \mathbf{u}^{i+1} - (\Delta t^2 \mathbf{M}^{-1} \mathbf{G}^{i+1^T} \lambda^i) \end{cases} \quad (2.5)$$

Equations (2.5) are solved using the Gauss-Seidel method. During each iteration the following two contact conditions for each slave node k are checked:

$$\begin{aligned} I) \quad \lambda_n^k &\leq 0 \begin{cases} \lambda_n^k < 0 & (contact) \\ \lambda_n^k = 0 & (separation) \end{cases} \\ II) \quad \|\lambda_t^k\| &\leq \mu |\lambda_n^k| \begin{cases} \text{if } \|\lambda_t^k\| < \mu |\lambda_n^k| \rightarrow \dot{\mathbf{u}}_t = 0 & (stick) \\ \text{if } \|\lambda_t^k\| = \mu |\lambda_n^k| \rightarrow \lambda_t^k \cdot \mathbf{v}_t \leq 0 & (slip) \end{cases} \end{aligned} \quad (2.6)$$

Where \mathbf{n} and \mathbf{t} are the normal and tangential vectors defining the contact, λ_n and λ_t are the normal and tangential contact force at each node k and μ is the Coulomb friction coefficient. The first condition (2.6-I) means that the contact force is a compression force (without adhesion components), while the second condition (2.6-II) is associated with the use of a Coulomb friction law. In this work, beside the classical Amontons-Coulomb friction, a regularized Coulomb friction law, built using simplified Prakash-Clifton constitutive law [PRAK 93] [COCH 00], is investigated; in this case the contact conditions are given by:

$$\begin{aligned} I) \quad \lambda_n^i &\leq 0 \begin{cases} \lambda_n^i < 0 & (contact) \\ \lambda_n^i = 0 & (separation) \end{cases} \\ II) \quad \lambda_n^i < 0, \|\lambda_t^i\| &\leq \mu |\lambda_n^i| \begin{cases} \text{if } |\lambda_t^i| < \mu |\lambda_n^i| \rightarrow \dot{\mathbf{u}}_t = 0 & (stick) \text{ and at } t^i, \lambda_t^i = \lambda_{t_c}^i \\ \text{if } |\lambda_t^i| \geq \mu |\lambda_n^i| \rightarrow \begin{cases} \dot{\lambda}_t^i = \frac{1}{\tau} (\lambda_t^i - \kappa \mu \lambda_n^i) & (slip) \text{ with } \kappa = \begin{cases} +1 & \lambda_{t_c}^i \geq 0 \\ -1 & \lambda_{t_c}^i < 0 \end{cases} \\ \exists \xi > 0 \text{ s.t. } \dot{\mathbf{u}}_t = -\xi \lambda_t^i \mathbf{t} \end{cases} \end{cases} \end{cases} \end{aligned} \quad (2.7)$$

Where $\dot{\lambda}_t^i$ is the time derivative of the tangential contact force at time t^i . The value λ_t^i is obtained from the discretization in time of the slip equation inside (2.7-II). The tangential force reaches the Coulomb tangential force $|\lambda_t^i| = \mu |\lambda_n^i|$ after a characteristic sliding time \hat{t} . $\lambda_{t_c}^i$ corresponds to the value of the tangential contact force calculated considering that the contact is in stick status. This law considers a non-null response time of the tangential force λ_t at a sudden change of the normal force $|\lambda_n|$.

2.3 Description of the model

The two-dimensional in-plane dynamic rupture model consists of two different isotropic elastic media separated by an interface governed by Coulomb friction law. Different mesh sizes have been tested. The mesh consist of quadrilateral elements (see caption figure 2.2) and the dimension has been chosen such that the deformations associated to the propagation of the waves at the interface and inside the bodies can be opportunely resolved. Table 1 and 2 show the parameters of the materials used for the simulations; they have been selected according to the literature to assure the existence of the generalized Rayleigh wave [WEER 63].

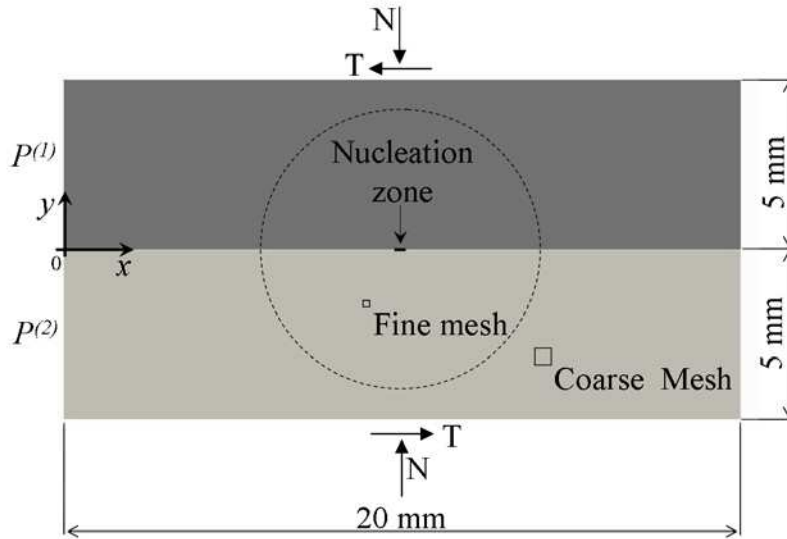


Figure 2.2 Geometry of the 2-D bi-material model. Two bodies of 5x20 mm. The mesh consists of a central circular region with fine discretization (Quadrilateral elements 0.0125x0.0125 mm) and an external region with wider mesh (Quadrilateral elements 0.1x0.1 mm). Inside the fine mesh zone 654 contact elements for each face are included. The forces are applied at the boundaries of the bodies $P^{(1)}$ and $P^{(2)}$.

	$P^{(1)}$	$P^{(2)}$
<i>Dimensions</i>		
Length	20 mm	20 mm
Width	5 mm	5 mm
<i>Materials</i>		
Young modulus (E)	5.3 GPa	3.4 GPa
Density (ρ)	1246 Kg/m ³	1246 Kg/m ³
Poisson ratio (ν)	0.25	0.25
Damping coefficient α	10 s ⁻¹	10 s ⁻¹
Damping coefficient β	0	0

Table 2.1 Input data concerning bodies in contact $P^{(1)}$ and $P^{(2)}$.

	$P^{(1)}$	$P^{(2)}$
P (longitudinal) waves	2430 m/s	1940 m/s
S (shear) waves	1270 m/s	1120 m/s
Rayleigh waves	1190 m/s	950 m/s

Table 2.2 Propagation velocities of bulk waves and Rayleigh waves in $P^{(1)}$ and $P^{(2)}$.

The two bodies are pressed together by a global normal force N applied on the external surfaces, and then subjected to a shearing force T which is calculated to be just less than the required one to produce slipping. The friction law at the interface is the classic Coulomb law, i.e. no distinction between static and kinetic friction is made; the friction coefficient is equal to 1. The rupture is initiated in the “nucleation” zone at the centre of the contact interface (Figure 2.2), by decreasing instantaneously the friction coefficient to zero on the length L_{nuc} (length of the nucleation zone) corresponding to a defined number of contact nodes (Figure 2.3); in such a way a rupture in mode II (the slip is parallel to the direction of rupture propagation) can be initiated.

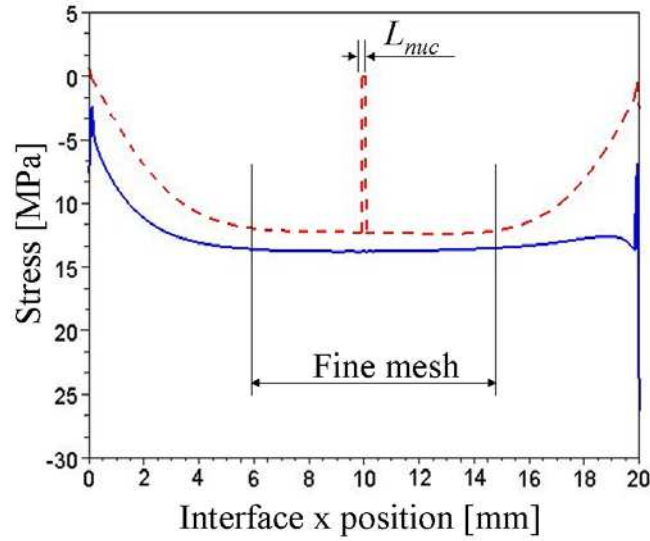


Figure 2.3 Normal (—) and tangential (---) stress at the nucleation time ($t=0$ s). The tangential stress becomes zero at the centre of the interface (nucleation nodes).

2.4 Rupture between smooth contact surfaces

This part presents the results stemming from the simulations of rupture along smooth interface separating two dissimilar materials. The data used for the simulations are given in table 2.1.

The dissymmetry induced by the difference in elastic constant cause a coupling between normal traction and tangential slip. Weertman [WEERT 80] suggested that this dynamic reduction in compressive normal traction (due to this coupling phenomenon) may allow for a slip pulse to propagate in a self-sustained manner at about the slower S (shear) wave speed.

This first part of the thesis aims to investigate the characteristics of pulse-like ruptures of a dissimilar material interface governed with constant friction coefficient, in order to validate the numerical model by comparison with the existing literature. The effect of nucleation conditions is also investigated.

2.4.1 Results for a nucleation length of 0.125mm

Figure 2.4 represents the isovalues of the velocity of the two bodies in contact. The nucleation zone centre is situated at x equal to 10 mm and measures 0.125mm ($L_{nuc}^* = L_{nuc}/\Delta x = 10$), ten times the size of the mesh element side (caption figure 2.2).

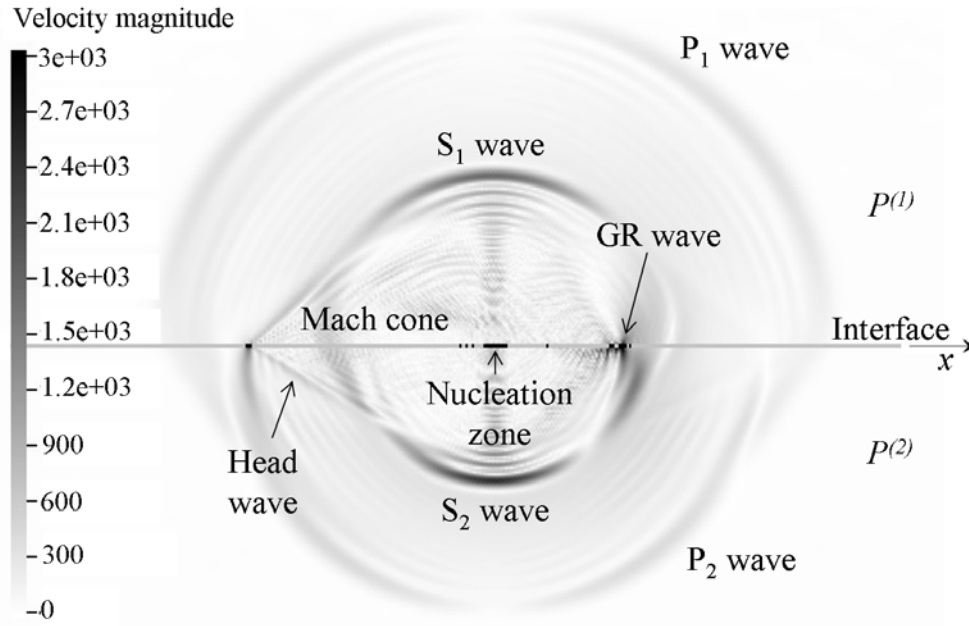


Figure 2.4 Representation of velocity isovalues [mm/s] (on the zone of fine mesh of figure 2.2). The nucleation zone is situated at the middle of the contact surface (x equal to 10 mm) and measures $L_{nuc} = 0.125$ mm. The black points at the interface are in sliding (rupture propagation in static conditions with pre-load and nucleation phases described in section 2.3).

The waves generated by the nucleation are identified: P-waves and S-waves in $P^{(1)}$ and $P^{(2)}$, and the generalized Rayleigh (GR) wave at the interface. As the wave velocities are different in $P^{(1)}$ and $P^{(2)}$, the nucleation induced different displacement on opposite side of the interface, causing changes in normal stress. Two rupture fronts propagating (left and right fronts) from the nucleation can be observed (the black points are in sliding).

Figure 2.5 shows the rupture profile (a) and the cumulative sliding (b) as a function of x position on the interface.

Figure 2.7 presents the evolution of the normal and tangential contact stress and relative tangential velocity at two different points left and right from the nucleation. The relative tangential velocity is defined as:

$$\dot{u}_T = \frac{\partial(u^{(1)}(x_{C_i}) - u^{(2)}(x_{D_i}) - u_N(x_{C_i}))}{\partial t} \quad (2.8)$$

Where D_i is the contact node on $P^{(2)}$, defined according to the closest projection of the node C_i (of $P^{(1)}$) to $P^{(2)}$.

At the left of the nucleation zone, the rupture front vanishes at the x position of 8.7mm. It corresponds to a decaying supershear pulse-like rupture ($c_{RUP} \approx 1700\text{m/s}$). From cumulative sliding profile in figure 2.5(b) it can be seen that, after the sliding induced by the front arrival, the sliding stops and after a short sliding time the contact zone is self-healing (sticking again).

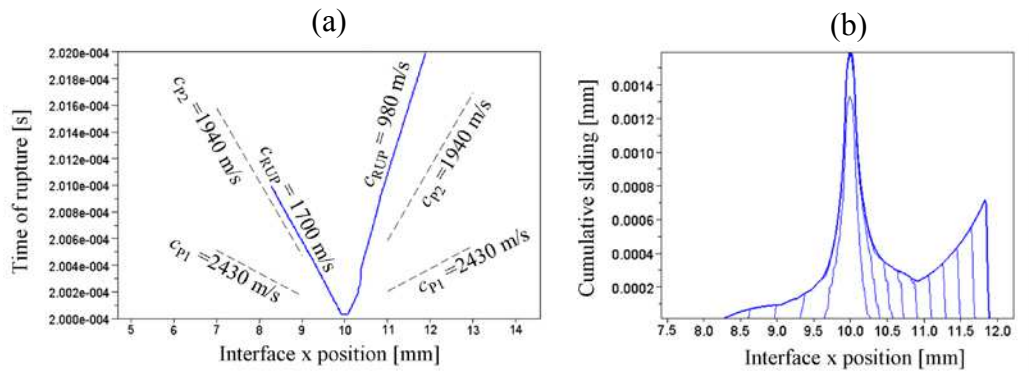


Figure 2.5 (a) Rupture profile and (b) cumulative sliding as a function of x position on the interface (representation of cumulative sliding at the interface each $2e-7\text{s}$ from $2e-4$ to $2.02e-4$) $L_{nuc} = 0.125\text{mm}$. Nucleation instant $2e-4 \text{ s}$.

Along the propagation, the sliding distance (figure 2.5(b)) and the relative sliding velocity (figure 2.7(c)) at the interface are both decreasing, causing the decaying of the rupture.

The rupture is associated with a small decrease of normal stress as it can be seen in figure 2.7(a). Figure 2.6(a) shows the nodal velocity vectors in the vicinity of the slip pulse at the time $2.008e-4\text{s}$. In figure 2.4 and 2.6 the interface zone characterized by sliding is highlighted with a darker line. The supershear rupture front, following the P wave of $P^{(2)}$, is characterized by an asymmetric Mach cone. The end of its propagation is due to the lack of energy for the interface to slide during a longer time.

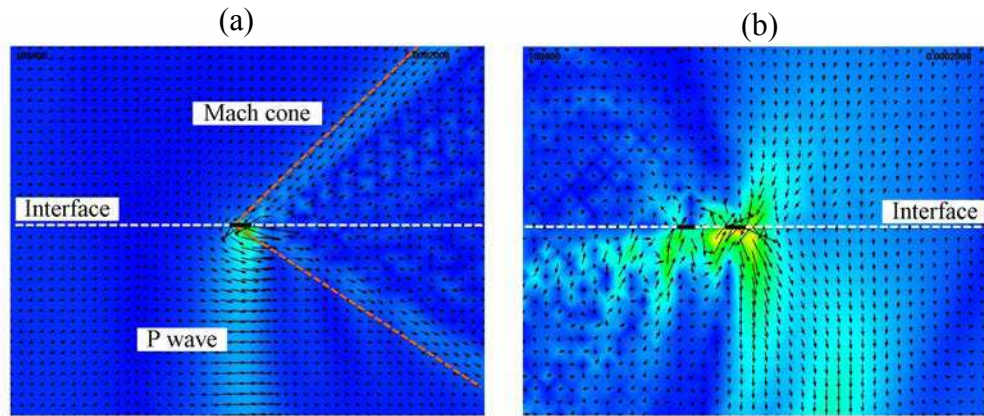


Figure 2.6 Isovalues of velocity in the vicinity of the (a) left and (b) right rupture front.

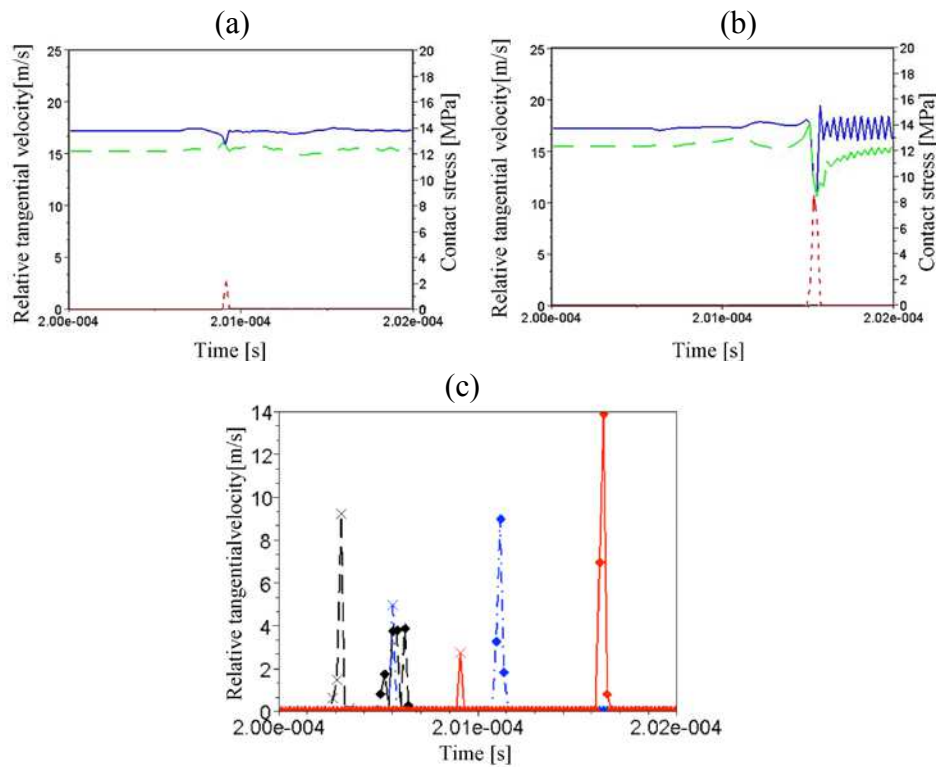


Figure 2.7 (a) and (b) Normal (—) and tangential (—) contact stress and relative tangential velocity (---) in time at (a) $x = 8.5\text{mm}$, left from the nucleation and (b) $x = 11.5\text{mm}$, right from the nucleation. (c) Relative tangential velocity in time at (---) 0.5mm (—••) 1mm and (—) 1.5mm from the nucleation zone. (×) corresponds to the left rupture and (•) to the right one.

The right-hand pulse, with respect to the nucleation zone, is a self-sustained sub-Rayleigh pulse. The velocity of the rupture front is $c_{RUP} \approx 980$ m/s (near to $c_{R2} = 950$ m/s). From figure 2.5(b) it can be seen that, as for the left one, the rupture is self healing. Because the sliding distance is increasing along the propagation, this corresponds to the propagation of a sliding pulse in self sustained manner. Figure 2.6(b) is the representation of the nodal velocity vectors in the vicinity of the slip pulse at the time 2.008×10^{-4} s. As previously, the interface zone characterized by sliding is highlighted with a darker line. At the head of the pulse, the projection on y-axis of the particle velocity is in the negative y direction and larger in the softer medium ($P^{(2)}$) than in the stiffer one $P^{(1)}$; this causes a decreasing of normal stress and facilitates the sliding. On the contrary at the end of the pulse, the particle velocity is in the positive y direction and because it is also larger in ($P^{(2)}$) than in $P^{(1)}$, the sliding zone becomes sticking, causing the self-healing of the interface [ANDR 97]. This decrease of normal stress, with respect to the left rupture, allows the rupture for be self-sustained and the energy released by the rupture contributes to have an increasing relative sliding velocity (figure 2.7(c)) and an increasing sliding length (figure 2.5(b)).

These results are consistent with those of Andrews and Ben Zion [ANDR 97]. The nucleation causes the propagation of a slip pulse at about the Rayleigh wave velocity in the direction of imposed displacement of the slower velocity medium (in the positive x direction).

2.4.2 Influence of the length of nucleation

Figure 2.8 presents the rupture profiles and the cumulative sliding for different nucleation lengths (L_{nuc}). When the nucleation length increases the strain energy released increases.

The left rupture is a self-sustained supershear pulse for nucleation length greater or equal than 0.25 mm. The velocity of left rupture front tends to the velocity of P waves in the softer material $P^{(2)}$ (c_{P2}).

The right rupture is a sub-Rayleigh pulse when nucleation length is less or equal than 0.25 mm. The additional part of strain energy released is consumed by the left rupture to become self-sustained. For a nucleation length of 0.5 mm, whereas the left rupture remains a self-sustained pulse, the right one becomes a supershear crack. The phenomenon of self-healing disappeared and as the rupture front passes by, the part of broken interface continues to slide, causing more important friction dissipation than for a pulse-like rupture [ADAM 01].

The obtained results agree with recent literature reported in section 1.3 and allow for validating the numerical model used in this work.

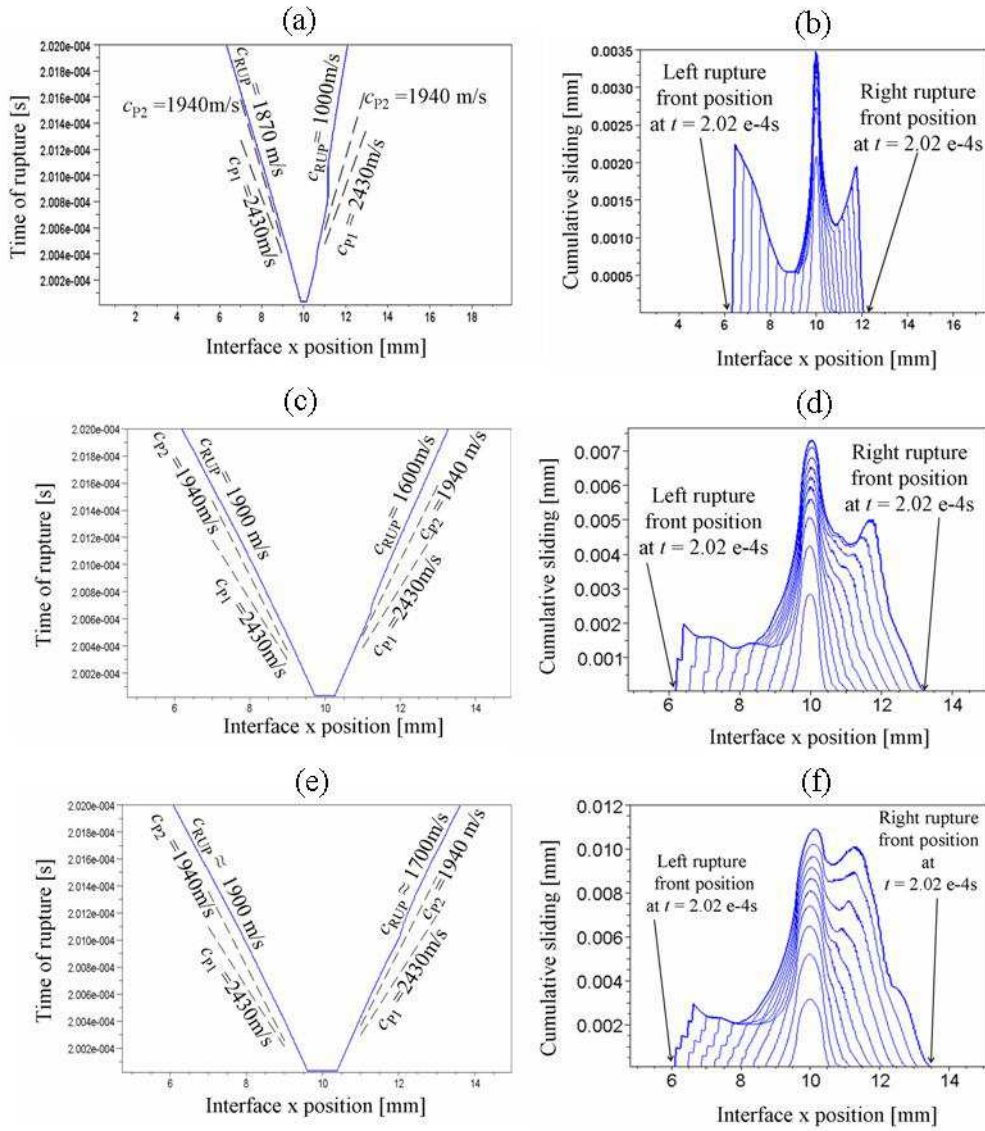


Figure 2.8 Rupture profile for (a) $L_{nuc} = 0.25$ mm, (c) $L_{nuc} = 0.50$ mm and (e) $L_{nuc} = 0.75$ mm. Cumulative sliding as a function of x position on the interface for (b) $L_{nuc} = 0.25$ mm, (d) $L_{nuc} = 0.50$ mm and (f) $L_{nuc} = 0.75$ mm (representation of cumulative sliding at the interface each $2e-7$ s from $2e-4$ to $2.02e-4$).

2.5 Rupture at contact surfaces with asperities

2.5.1 Introduction of roughness

To introduce the roughness the two profiles in contact have been modified assigning them undulations to reproduce the asperities of a surface. The two bodies are pressed together by the same global force applied in the previous simulations. Sinusoidal profiles have been considered; this allows for simplifying the analysis and keeping the focus on the relationship between the propagating waves in the bodies and the distribution of the asperities over the surfaces, which is function of the sinusoid length. For each sinusoid length, matching sinusoids with different spatial phases and amplitudes, four paths have been selected to be introduced at the interface; they are summarized in table 2.3.

(a)

Model	Symbol
1. Smooth surfaces	
2. Roughness in phase	
3. Roughness with π spatial phase difference	
4. Roughness only on a surface	

(b)

- $L_{nuc} = 0.0125$ mm
- ◆ $L_{nuc} = 0.0625$ mm
- $L_{nuc} = 0.125$ mm

λ [mm] \ A [mm]	0.00125	0.005	0.01
0.075	●	● ◆ ■	
0.6			● ◆ ■

Table 2.3. Types of roughness: (a) Roughness patterns, schematic symbols of the profile on the two surfaces in contact; (b) Roughness parameters of the simulations, L_{nuc} is the nucleation length.

The 1st case, smooth surfaces, has already been discussed in section 2.4. In the 2nd case the sinusoidal profiles over the two contact surfaces are in phase; in the 3rd case they have a spatial phase difference of π radians and in the 4th case there is roughness only over one of the two surfaces. Every roughness profile is characterized by the amplitude A and the spatial wavelength λ . For every pattern of table 2.3(a), simulations with different values of A and λ and with different length of nucleation have been carried out (table 2.3(b)). The material properties are the same used in section 3.

2.5.2 Effect of roughness on wave propagation

2.5.2.1 Coupled/uncoupled wave propagation

Figure 2.9 represents the isovelocities (mm/s) for two different values of the roughness with the pattern 3 (in table 2.3(a)) and length of nucleation of 0.0125 mm (where $L_{nuc}^* = L_{nuc}/\Delta x = 1$, the size of 1 mesh element side), at $6.8e-7$ s after the nucleation. The contact points highlighted in black are in sliding and in grey are in adherence.

In the figure 2.9(a) it can be seen that the P-waves, S-waves, the head waves (P-S conversion) [DUNH 04] and the Rayleigh waves radiate away from the rupture, in independent (uncoupled) way along the two materials; they propagate symmetrically with respect to the vertical axis, meaning that there is no coupling between the waves propagating through the two bodies in contact. The rupture at the contact interface occurs (right and left to the nucleation zone) when the first wave reaches the asperities in contact so that there is a supershear rupture front (Fig. 2.11(a) and 2.11(b)) with velocity at about the longitudinal velocity of the stiffer material (Table 2.2).

On the contrary in figure 2.9(b), for a smaller length of the sinusoidal roughness, the waves propagating through the two bodies are coupled, similarly to the case without roughness. The rupture profile on the left is different from the rupture profile on the right (Figure 2.14), due to the same mechanism discussed in section 2.4, consisting in the generation of dynamic changes of normal stresses that depends on the slip gradient, material properties and direction of rupture propagation.

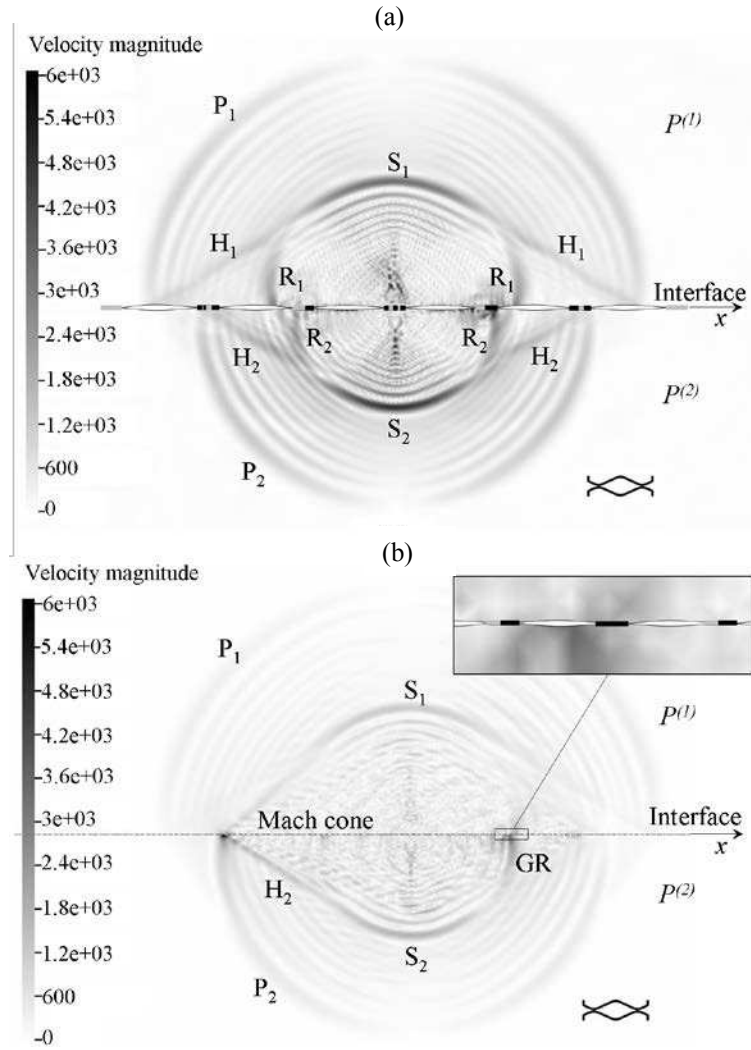


Figure 2.9 Velocity isovalues [mm/s] (on the zone of fine mesh of figure 2.2) at 6.8×10^{-7} s after the nucleation, length of nucleation 0.0125 mm, roughness with π spatial phase difference. (a) $\lambda = 0.6$ mm, $A = 0.01$ mm. (b) $\lambda = 0.075$ mm, $A = 0.00125$ mm, in the inset a magnification of 10x. P longitudinal wave, S shear wave, H head wave (P - S conversion), R Rayleigh wave. GR generalized Rayleigh wave. Snapshot size 4.5x3 mm. The contact points highlighted in black are in sliding and in grey are in adherence (rupture propagation in static conditions with pre-load and nucleation phases described in section 2.3).

To understand the uncoupling/coupling behaviour between the waves on the two bodies in contact, it can be observed (fig. 2.10(a)) that in the first case, when the head wave front of the $P^{(1)}$ body reaches the first contact zone (about 2.7×10^{-7} s) the head wave front of the $P^{(2)}$ body is still back, on the zone without contact.

In such configuration the two fronts can not interact according to the mechanism described in the section 3.1. Thus, it is important to account for the width of the wave front, which is function of the stress and velocity fields in the vicinity of the crack tip, with respect to the spatial wavelength of the roughness. When they are of the same order of magnitude (fig 2.10(b)) both the head waves and the following Rayleigh waves, can interact each other; in fact, especially at the beginning of the propagation, there are contact zones in which the wave fronts are simultaneously present, although shifted.

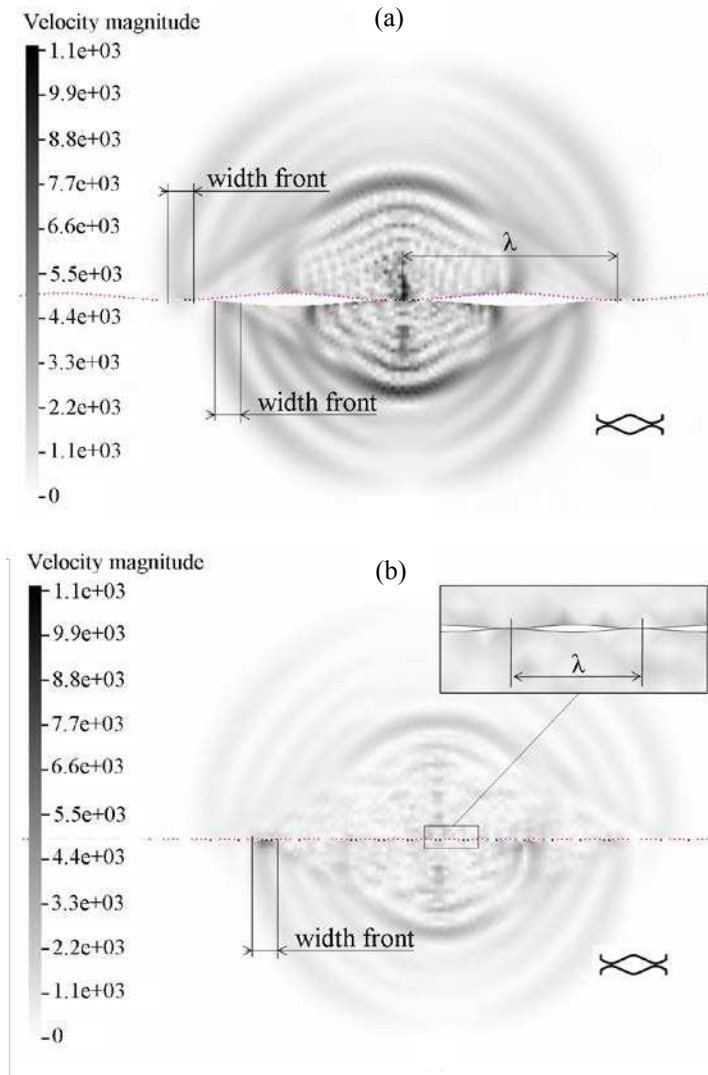


Figure 2.10 Velocity isovalues [mm/s] 2.7×10^{-7} s after the nucleation, length of nucleation 0.0125mm, roughness with π phase difference. (a) $\lambda=0.6$ mm, $A=0.01$ mm. (b) $\lambda=0.075$ mm, $A=0.00125$ mm, in the inset a magnification of 5x. Snapshot size 1.8x1.3 mm.

2.5.2.2 Stress distribution and rupture profiles

It isn't obvious to define the type of the rupture exactly, due to roughness. In a more general approach, it is known that the crack mode is favoured by relative high and smooth initial background stress and low or no coupling of slip to changes of normal stress (the mechanism described in section 2.4.1); while the pulse mode is favoured by opposite conditions [SHI 06]. As the rupture front moves, it continuously generates waves which are proportional to the local stress intensity factor and the instantaneous velocity of the rupture front [SHI 06]. The presence of roughness, i.e. zones where the asperity are in contact and zones where there isn't contact, brings to a heterogeneous shear and normal stress distribution, even inside the contact area, and causes a more complex rupture process.

Figure 2.11 shows the rupture profile relative to the case of figure 2.9(a); figure 2.12 shows the relative cumulative sliding profile, non-dimensionalized with respect to roughness wavelength λ , for the same case. Keeping the attention, for example, on the first zone of contact at the right of the nucleation zone, when the first front of rupture (the longitudinal wave of the stiffer body) reaches the summit in contact, only the external points slide, while the central points, which have a lower local ratio between tangential and normal stress, do not slide (Figure 2.11(a) and Figure 2.12 at $x \sim 10.5$ mm).

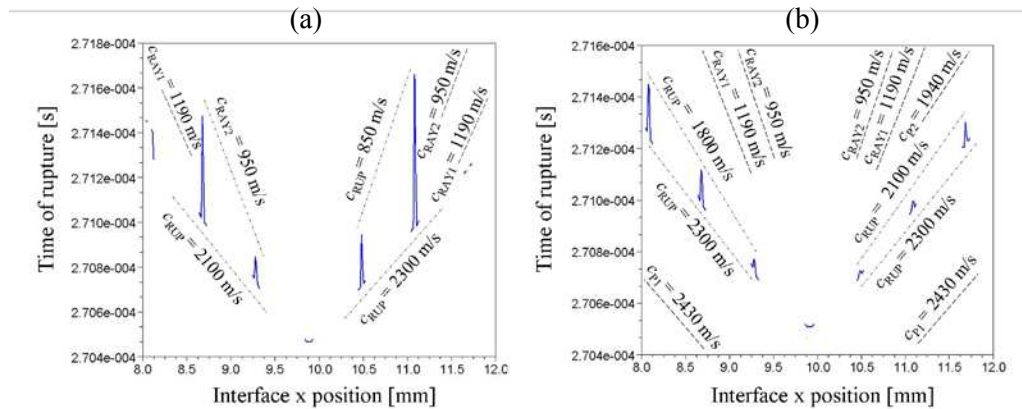


Figure 2.11 Roughness with π phase difference, $\lambda=0.6$ mm, $A=0.01$ mm (ref. Fig.2.9(a)). (a) Rupture Profile (time of rupture) with $L_{nuc} = 0.0125$ mm. (b) Rupture Profile with $L_{nuc} = 0.1$ mm. Nucleation instant $2,704e-4$ s.

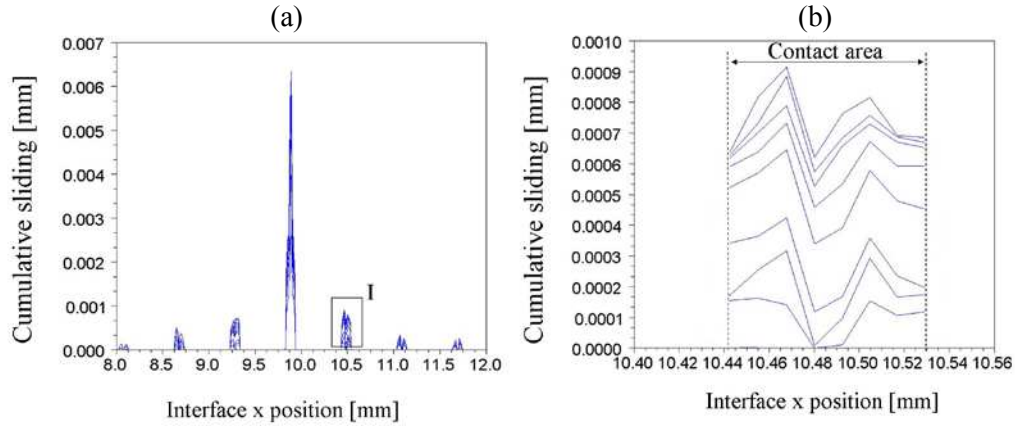


Figure 2.12 Cumulative sliding profile, roughness with π spatial phase difference, $\lambda=0.6$ mm, $A=0.01$ mm, length of nucleation 0.0125mm, (ref. fig 2.9(a)). (a) Global profile. (b) Magnification of the rectangle I. The profiles are given every $0.12e-7$ seconds.

So the first rupture front skips the central part of asperity [DAS 77], because the energy is not sufficient for causing the sliding of the nodes where the tangential stress is lower. However, this effect is a redistribution [RUBI 07] of the stress inside the asperities. In particular this fact predisposes such points to slide more easily. The second wave that arrives on the asperity is the longitudinal wave of the softer body; the energy of this wave too is not sufficient to cause a global sliding on the asperities, even if a further change of the stress distribution is caused.

Finally the nodes at this zone slip when the third wave, the Rayleigh wave of the upper body, arrives. This behaviour explains the feature of the rupture profile in figure 2.11(a), where two different velocity of propagation can be identified by connecting the external and internal points of the asperities. For examples on the right, for the external points of every asperity there is a rupture front with velocity of 2300 m/s, while for the internal points $c_{RUP}=850$ m/s.

When the nucleation length is increased, the released energy is increased too; then, for causing the slipping of all the nodes of the asperity, the first and the second wave fronts are sufficient; this can be seen in the figure 2.11(b), which refers to the same model but with a longer nucleation length, $L_{nuc} = 0.1$ mm ($L_{nuc}^* = L_{nuc}/\Delta x = 8$). It can be seen the reduction of the slip delay of the central respect the external points of the asperities, i.e. closer velocity of the rupture fronts. As before, by connecting the points of the graphic, it is possible to identify the propagation velocities of the waves.

Fig. 2.13 shows the rupture profile for the case in figure 2.9(b); in this case, while the rupture of the first (two or three) asperities close to the nucleation zone takes place entirely with the arrival of the first wave, the rupture of the

asperities away from the nucleation zone is differentiated: the left part of every asperity, where the ratio between tangential and normal stress is close to 1, slide with the arrival of the first wave, while the right part of the contact slide later, with the arrival of the other wave fronts, because of the initial lower ratio between tangential and normal stress. In figure 2.13 the propagation velocities are also reported. So at the right of the nucleation zone two rupture fronts can be observed: the first interests the left part of every asperity ($c_{RUP}=2300$ m/s) and the second the right one ($c_{RUP}=1600$ m/s). At the left of the nucleation zone there are also two different rupture fronts for the left ($c_{RUP}=1940$ m/s) and the right ($c_{RUP}=1800$ m/s) part of the asperity, but after $2.708e-4$ s the rupture of the whole asperity take places with the slower front.

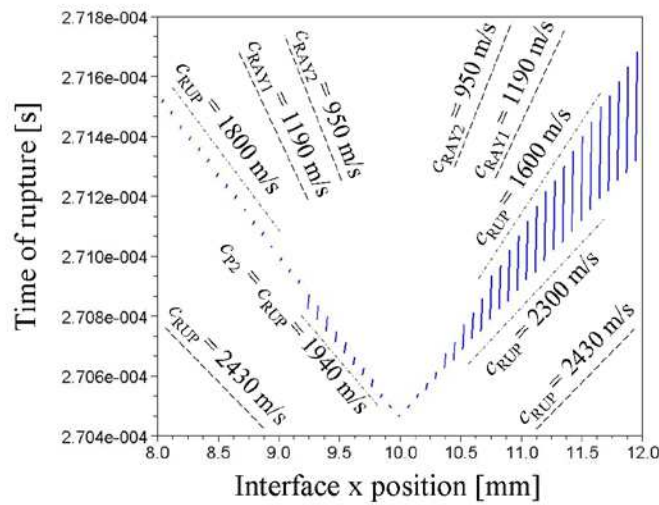


Figure 2.13 Roughness with π phase difference, $\lambda=0.075$ mm, $A= 0.00125$ mm, length of nucleation 0.0125 mm (ref. Fig.2.9(b)).

2.5.3 Effect of the roughness pattern

Further numerical experiments carried out with the patterns 4 of table 2.3(a), characterized by roughness only on a surface, showed similar behaviour to the patterns 3 (Figure 2.14(b)). Instead, the second pattern, with roughness in phase, showed rupture profiles, cumulative sliding graphics and coupling behaviour (Fig. 2.14(a)) similar to the results obtained without roughness (section 3), except for the presence of the heterogeneity on the initial stress distribution. It has to be noted that the energy released causes a sliding less than 5% of the spa-

tial wavelength λ of the asperity, so that there are not jumps of an asperity in the trough of the near asperity.

The variability of the stress involves that a different amount of energy is released from the areas in sliding along the rupture; Figure 2.14(b) shows that the zones characterized by larger energy behave like new nucleation zones, as it can be seen from the new waves radiated from the broken asperities; this can be interpreted as an example of multi nucleation spots or multiple shocks [DAS 77].

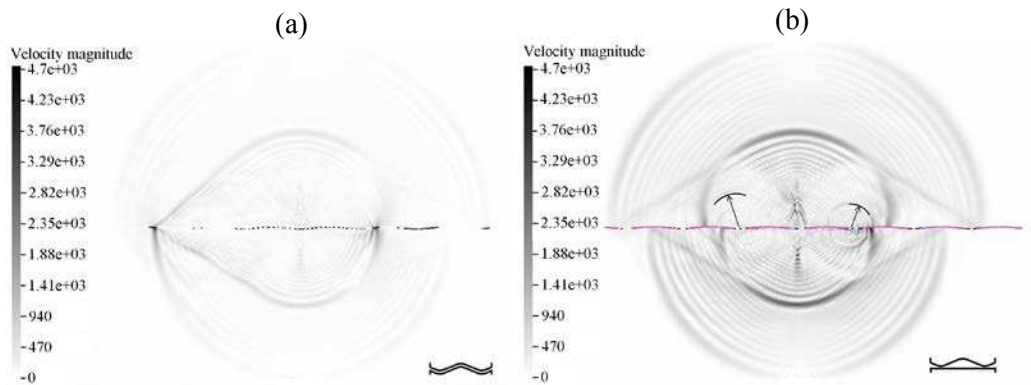


Figure 2.14 Velocity isovalues [mm/s] $8.2e-7$ s after the nucleation, length of nucleation 0.0125mm , $\lambda=0.6\text{ mm}$, $A= 0.01\text{ mm}$. (a) Roughness in phase (b) Roughness only on a surface difference. Snapshot size $5 \times 3.5\text{ mm}$. The points highlighted in black are in sliding.

2.6 Conclusions

The dynamic rupture on a smooth interface between dissimilar materials has been investigated. The results obtained are consistent with the results found in literature [ANDR 97] for smooth interfaces, allowing for a validation of the numerical model. The nucleation causes the propagation of a slip pulse at generalized Rayleigh wave speed in the direction of sliding of the slowest velocity medium. The nucleation length is showed to be a main parameter of influence of the rupture dynamics. Increasing the nucleation length causes the energy released for rupture to increase, and the rupture to change its velocity and type (pulse-like or crack-like). The roughness has been then introduced at the contact surfaces; the consequent heterogeneous stress distribution causes a more complex rupture process:

- Depending on the relative dimension between the roughness wavelength and the width of the wave fronts, two different behaviours can be observed: i) a coupling between the wave propagating into the two bodies, which causes the developing of two asymmetric rupture fronts in the opposite directions respect to the nucleation zone; ii) a decoupling of the wave propagation inside the two materials, characterized by an independent wave propagation and symmetry respect to the nucleation zone.

- In the second case the rupture profiles highlight a differentiated rupture inside the asperities; a first wave, when passing through the asperities, forces a part of the contact zone to slide and provide a redistribution of the local stress at the remaining part. Afterwards, a successive wave front can cause the sliding of others parts of the contact zone. Thus there are different rupture fronts at different velocities for different zones of the asperities. The velocities of the rupture fronts depend on the energy released at the nucleation.

- The analysis has been carried out on a sinusoidal roughness for different patterns, depending on the spatial phase between the sinusoids of the two surfaces in contact. The amount of the slip is, for all the simulations, much smaller than the roughness wavelength.

Results highlight similar behaviour when the roughness causes sharp variations on the contact stress distribution, while, for a continuous contact (spatial phase difference equal to zero) between the surfaces, the behaviour is similar to the case of flat contact surfaces.

The presented results allow for asserting that the roughness at the interface plays a key role on the rupture propagation. A detailed parametrical analysis as a function of the roughness characteristics need to be carried out to relate them with the features of the resulting rupture. In particular a further study will be carried out to investigate a general criteria for having coupled or uncoupled wave propagation.

3 Wave propagation during sliding initiation

Introduction

This section presents the results of the numerical simulations of the sliding onset between two bodies. While the previous chapter dealt with rupture dynamics when the two bodies in contact are at rest in this chapter the onset of the relative sliding is presented. Recent literature deals with either established sliding contacts, focusing on the instable vibrations of the system (see section 1.2), or rupture (an initially sticking zone of the frictional interface that becomes in sliding state) propagation in a static contact interface (see section 1.3); the initiation of the sliding process has been rarely investigated (see for example [RUBI 04][RUBI 07][BRAU 09]).

The analysis is here focused on very a short time to the purpose of studying the phenomena involved in the sliding initiation, the switch from adherence to sliding, rather than the sliding steady state. In addition the high value of rupture speeds [DIBA 10a] and the relative small dimensions of the model require a quite small integration time step and large computational efforts to identify changes in the propagating wave field.

During sliding initiation the rupture is triggered at localized zones of the interface where first the local tangential stress reaches the critical value imposed by the friction law. These events, being confined local slips, will be referred in the following as “micro-slips”. Conversely the slip will be referred as macro-slip when it interests a large part of the interface. Although this classification reminds the terms “slip” and “sliding” used in [RUBI 04], it is important to specify that in this work “micro-slip” would mean a more restricted zone of slip (approaching at the limit the concept of single nucleated rupture) and “macro-slip” does not mean necessary the sliding of the entire interface. Each micro-slip behaves as a single nucleated rupture ([DIBA 10a] and reference therein) and activates propagation of different type of waves along the interface and inside the bodies (longitudinal waves, shear waves, surface waves). The macro-slip activates waves of greater magnitude that can make slide a large part of the interface; they can reach the boundaries of the system where they are reflected triggering the global dynamics of the system [IBRA 94][AKAY 02]. Vice-versa the interaction between the waves (direct and reflected/stationary waves) affects the evolution of the slip along the interface and, in a sort of closed loop, setting up a relationship between local and global dynamics.

This chapter wants to approach the initiation of the sliding and to investigate how the micro-slips at the interface (precursors acting as distributed ruptures at the contact surface) trigger the macro-slip between the two bodies in contact. The understanding of the micro-slips and macro-slip mechanism is a necessary step toward their reproduction and control, which could allow for either controlling the global friction coefficient or reducing the induced vibrations and their damaging effects.

How demonstrated in [ADAM 95] and [RANJ 01] and illustrated in the section 1.2, in the case of bimaterial interface the dynamic changes in normal stress increase with the propagation distance due to a continuous transfer of energy to shorter wavelengths (Adams instability). This can bring to ill-posedness and grid size dependence of the problem [COCH 00]. To consider this problem, different types of simulations have been carried out, with and without regularisation laws [PRAK 93][COCH 00]; in fact using the words of Ben- Zion [BEN 01] “...regularized calculations may be used to perform a clean parameter-space study in a regime that is not fully realistic, while non-regularized calculations may explore realistic behaviour but they contain a mixture of real and numerical artefacts. Perhaps an appropriate approach is to employ both types of calculations in a careful and balanced way.”. The analysis has been performed using this "balanced way", with the purpose of obtaining common features of the behaviours of the system and so, more likely, of the behaviour of the real underneath physical phenomena, avoiding the suppression of essential features that the regularization of the contact law might cause.

Even if the simulations can be partially affected by numerical artefacts, the results presented in this work have been extrapolated and validated by parameter space analysis and by limiting the maximum simulation time; moreover, the results obtained on rupture dynamics with smooth contact surfaces agree with the results in the literature, allowing for validating the simulation of short time periods presented into the paper.

The chapter is organized as follows: first the numerical model and the relative assumptions are described; then the sliding initiation is investigated following different steps: i) analysis of the global contact forces; ii) analysis of the role of the precursors; iii) analysis of the wave propagation; iv) approach to the relationship between local and global dynamics. Subsequently a comparison with the results of experimental works in the literature is presented. Finally the conclusions are carried out.

3.2 Description of the model

The 2D (plain strain deformation) model consists of two different isotropic elastic finite media separated by a frictional interface at $y=0$ (Figure 1). The two bodies are pressed together by a global normal force (per depth unit) N applied on the lower external surface on $P^{(l)}$, which is then subjected to a constant horizontal velocity V until to produce slipping over the frictional interface (Figure. 1). In such a way the slip is parallel to the direction of the rupture propagation, namely in mode II [DIBA 10a]. Hereinafter the subscript 1 denote the material below the interface, and 2 the material above, which is the more compliant one (Figure 1). Table 1 shows the material properties used for the simulations; the degree of material contrast $1+\gamma=c_{S1}/c_{S2}$ [SHI 06] is in the range of existence of the generalized Rayleigh wave (GR) (see Introduction). The choice of the materials is due to their versatility and suitable characteristics with the perspective of realizing a future experimental set-up. In fact, acting on the cooling rate of the Epoxy resin, its Young modulus can be varied allowing for material pairs with different degree of material contrast γ .

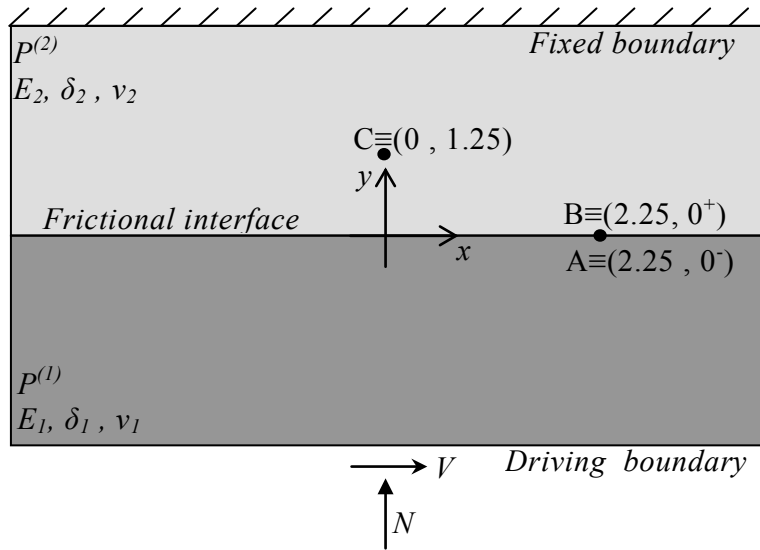


Figure 3.1 Geometry of the 2-D bi-material model. Two bodies of 3×10 mm. The mesh consists of quadrilateral elements. The dimension Δx_1 of the element of the lower body is in constant ratio r with the dimension of the element of the upper body Δx_2 : $r = \Delta x_1 / \Delta x_2 = 2.3$. This difference aids to assure a good implementation of the contact algorithm avoiding possible numerical noise due to the a symmetric mesh. N compressive force, V translation velocity. Point $A \in P^{(1)}$ and points $B, C \in P^{(2)}$.

In addition the polycarbonate exhibits strong birefringence in both the elastic and plastic regimes and a high level of transparency so that it is used photoelastic (and photoplastic) applications as in the investigation of the rupture growth.

	<i>Medium n°1 (Polycarbonate)</i>	<i>Medium n°2 (Epoxy resin)</i>
<i>Dimensions</i>		
Length L [mm]	10	10
Width W [mm]	3	3
<i>Common properties</i>		
Young modulus E [GPa]	3.9	2.5
Density ρ [Kg/m ³]	1202	1300
Poisson ratio ν	0.38	0.33
Longitudinal wave speed c_P [m/s]	2108	1973
Shear wave speed c_S [m/s]	1293	1188
Rayleigh wave speed c_R [m/s]	1180	1085
Material contrast γ		0.09
<i>Specific properties</i>		
Compressive Force N [N]		10
Initial normal stress $\sigma_0 = N/L$ [MPa]		1
Horizontal velocity V [mm/s]		10
Damping coefficient α [s ⁻¹]		40
Damping coefficient β [s]		0.45 e-6
Coulomb friction coefficient μ		1

Table 3.1 : Input data of the bodies in contact. The common properties are the same for all the simulations performed in this work. The specific properties refer to the parametrical simulation presented in the next section.

During the sliding initiation, when micro-slips happen locally, even if the rest of the contact is in adhesion (eq. 6), a large part of it has reached a high level of shear contact stress. Therefore, every single rupture episode propagates in a very high energy contest. In addition the high level of the shear stress produces, during the rupture, more rapid changes in the local slip velocity, approaching impulsive phenomena. From a numerical point of view this implies high-frequency and high-amplitude numerical oscillations, due also to the effect of the Adams instability (see introduction). The friction laws used at the interface are the classic Coulomb law and a simplified Prakash-Clifton friction law, described in the section 2.1. The use of regularized laws can reduce or eliminate

the numerical oscillations due to the Adams instability but it may suppress as well features at high frequencies of the physical phenomenon; therefore, in this work simultaneous simulations, either with and without regularization, have been carried out to identify the common features that are referable unequivocally at the physics of the problem. Moreover the bimaterial effect increases with the propagation distance and this analysis is limited both in space and in time, reducing the deleterious effects on the reliability of the results. Simulations with different mesh sizes have been performed to assure the convergence. Three mesh sizes have been tested: "large" ($\Delta x_2=50 \mu m$), "medium" ($\Delta x_2=25 \mu m$) and "fine" ($\Delta x_2=12.5 \mu m$) until convergence of the results.

The numerical model used here to study the rupture propagation during sliding initiation has been validated as well by the reproduction of rupture dynamics in static contacts [DIBA 10a].

3.3 Sliding initiation

3.3.1 Study of the global contact forces

This section presents the results obtained with the model in figure 1 using the classic Amontons-Coulomb friction law at the interface and with friction coefficient equal to 1. The simulation parameters are reported in table 1. Figure 3.2 shows the time evolution of the sum of the forces at the interface (in x and y direction), normalized to the compressive force N .

Because the aim of this section is the analysis of the local phenomena related to the sliding between the two bodies in contact, the damping coefficient α has been opportunely increased at the begin of the simulation, when the normal contact force and the tangential preload are applied. In fact a low value of α would cause large low frequency oscillations, due to the system vibrational response to the loading phase of the contact between the two bodies; in this case, a long simulation time would be required before the damping of the system vibrations. Increasing α reduces the oscillations coming from the preloading phase, allowing to reach a steady state before the initiation of the sliding at the contact interface. Then, the value of α is brought back to the wished value for simulating the sliding initiation. Otherwise, as showed in the next chapter, where its effect has been opportunely investigated, the damping coefficient α affects only the low frequencies (system dynamic response) of the phenomenon.

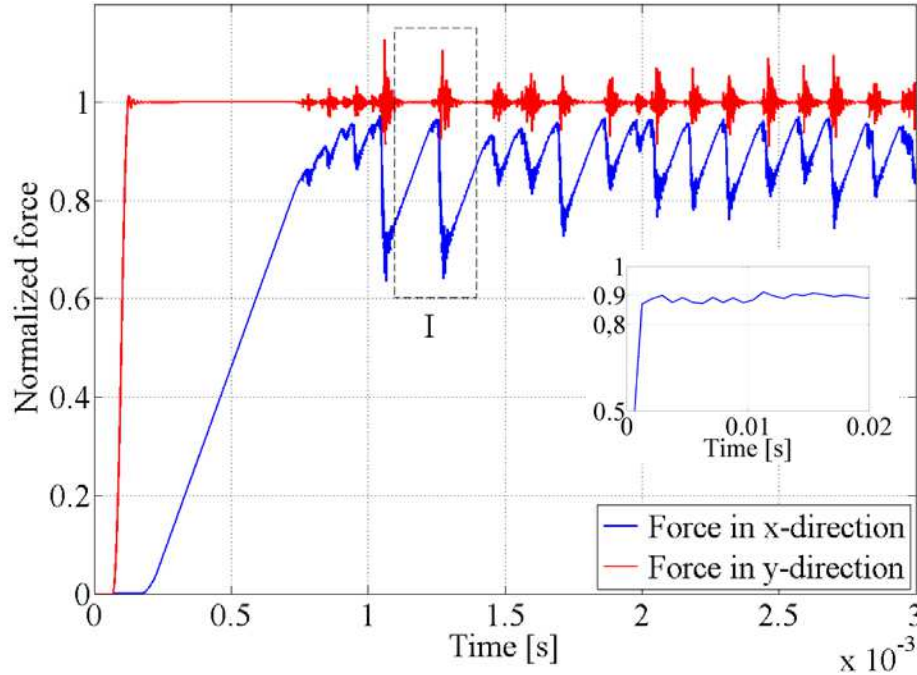


Figure 3.2 Evolution of the global contact forces (normalized to the compressive force N) vs. time. Inset shows the mean value (every $1e-3s$) of the tangential force over a longer time interval. The simulation parameters are presented in table 3.1.

The analysis is focused on very short time ($< 3e-3$ s). In fact, due to the high value of rupture speeds [DIBA 10a] and the relative small dimensions of the model, restricted time is needed to identify changes in the propagating wave field. However also long term data have been recorded and examined (see inset in figure 3.2). It can be observed that, after a first linear growth, the tangential force presents irregular fluctuations, i.e. a series of ramps each followed by a sudden drop. In the simulated time interval the pattern of the force reaches a “stationary” behaviour (analyzing the forces over a longer time, it can be seen that the mean value of the tangential force, inset in figure 3.2, has no significant variations) showing the same repetitive sequence: increase of the stored elastic energy (i.e. the growth of the force ramp) followed by a macro-slip between the contact surfaces (i.e. the drop of the tangential force). This effect is due to the presence of zones at the contact interface where the shear contact force reaches locally the critical value dictated by the friction law and switch in sliding state. Like asserted in the introduction it will be referred to micro-slip or macro-slip depending on the extension of the zone in sliding with respect to the whole interface. As explained hereinafter the micro-slips are related to the smooth

changes in the slope of the force ramps that can be observed in the Figure 3.2 [DIBA 10b] or in Figure 3.3a. On the other hand macro-slip causes the drops at the end of the ramps, when a large part of elastic energy of the media is released.

The presence of micro-slips during the growth of the ramp of the tangential force is a "dynamic" phenomenon characterized by a continuous exchange between micro-zones in adherence that switch in sliding and micro-zones in sliding that return in sticking state. Either if each micro-slip theoretically behaves like a single nucleated rupture in static conditions [DIBA 10a], in the case of rupture during sliding initiation the micro-slip events and the related wave propagations at the interface lead to a highly nonuniform stress distribution [RUBI 07]; therefore the features of the rupture depend strongly on the stress fields at the interface where it passes and on the other waves that it crosses. The rupture changes its characteristics while in progress, for example switching from pulse-like to crack-like, decreasing rapidly or continuing itself only as a pure wave without causing local slip, or, finally, splitting in two new ruptures (see below). Generally these waves have short distance of propagation due to the limited extension of the micro-slip. When the energy released by the micro-slips is large enough, it can sustain detectable wave propagation away from the contact; these phenomena are known by the name of "precursors" (precursor of the macro-slip), mainly in geophysics, and have been observed experimentally (see for example [RUBI 07][ZIGO 11]) and numerically [BRAUN 09]. Precursors are intrinsically characterized by the fact that they occur at tangential global force well below the critical value expected by the friction law ($\mu |N|$ for the Coulomb law).

3.3.2 Wave propagation analysis

Focusing the attention on a single force ramp, Figure 3.3(a) shows a magnification (rotated) of the Figure 3.2 between 1.05×10^{-3} s and 1.35×10^{-3} s (dashed rectangle I in Figure 3.2); in figure 3.3(b) and 3.3(c) the correspondent contact status of the interface (adherence, sliding or detached) respectively in percentage or along the interface is represented during the same time interval. This graphic is representative of what happens at the interface during each single ramp shown in Figure 3.2.

Referring again to figure 3.3, at 1.1×10^{-3} s, after the force drop relative to the previous ramp, all the contact nodes return in sticking state (Figure 3.3(b) and 3.3(c)); even if there are still waves that cross the bodies and the interface, how can be noted by the oscillations in the force (Figure 3.3(a)), their magnitude cannot trigger the sliding of contact nodes.

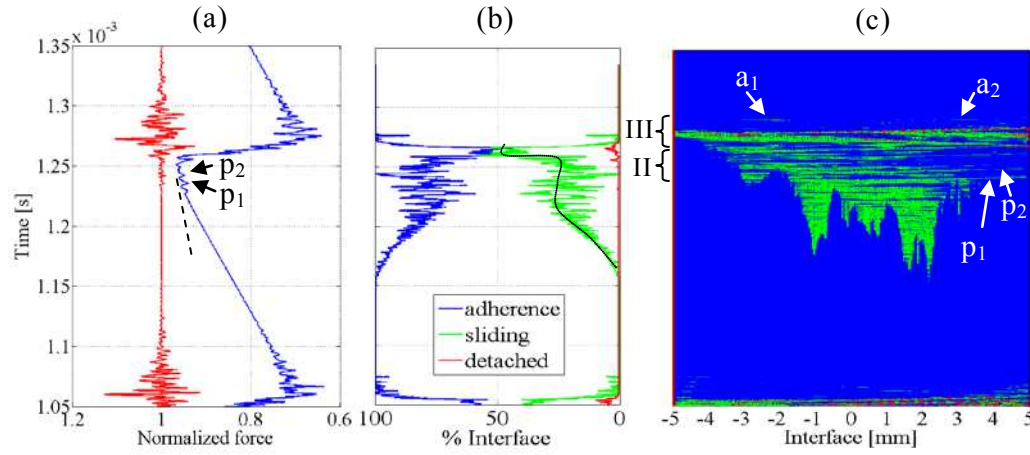


Figure 3.3 (a) Sum of the contact forces between $1.05e-3$ s $1.35e-3$ s, (interval I of figure 3.2), blue=force in x-direction, red=force in y-direction; (b) Status of the interface during the same time interval, in percentage; (c) Status of the contact zones, along the interface, during the same time interval: green spot=sliding; red spot=detachment; blue spot=adherence. Interval II= $(1.228e-3 \text{ s} \div 1.242e-3 \text{ s})$, Interval III= $(1.253e-3 \text{ s} \div 1.275e-3 \text{ s})$.

Then, at $1.15e-3$ s, isolated micro-slips start to occur in different zones of the interface, but the released energy of each of them is very small and the wave propagation is limited to the regions closest to each micro-slip. In this phase the micro-slips are so enclosed in some zones of the interface and form the sort of dendrites that can be observed in figure 3.3(c). For increasing time, due to the energy provided continuously by the displacement of the lower body, the micro-slips grow in width and coalesce each other (several "dendrites" coalesce in figure 3.3(c)) so that there is a variation of the average percentage of the nodes in sliding (dotted line in figure 3.3(b)) and, consequently, an analogue change in the mean slope of the tangential force. When number of micro-slip is considerable, the slope change is appreciable in the graphic of the global tangential force (dashed line in figure 3.3(a)) [DIBA 10b]. The behaviour of the rupture propagation recovered in this first phase agree with the propagation of the "slow front" registered experimentally in [ODED 11].

The part of the interface in sliding increases with time and continuously sticking zones switch in sliding and zones in sliding get back in sticking state, how can be seen in figure 3.3(b). Then, when a sufficient number of micro-slips switches in sliding at the nearly same time they can release enough energy to sustain an important wave propagation, to which is associated a rupture front: these precursors are characterized by slip fronts that traverse part of the interface (e.g. green lines p_1 and p_2 in figure 3.3(c) representing two supershear ruptures propagating toward the right,) and cause small drops of the tangential force (corresponding drops p_1 and p_2 in figure 3.3(a)). Precursors propagating in the

opposite sense (toward the left) at about the Generalized Rayleigh speed can be observed too. With the increase of time and increasing number of precursors are triggered and their distance of propagation increases, similarly to what observed experimentally in [RUBI 07], until they reach the boundaries. This phenomenon is more evident in figure 3.4 that presents a magnification of the interval II in figure 3.3(b). In this figure additional information are presented by the seismic profile: at every time step a plot gives the trend of the sliding velocity of the nodes at the overhanging side of the interface, so that the curves plotted at different time steps allow for identifying how the waves propagate in time at the contact interface. Figure 4 provide a clear representation of the dynamic complexity at the interface. Because of the series of micro-slips (i.e. multiple nucleations) there is a stream of waves of different type and propagation velocity that cross back and forth the interface, some decaying (arrow n° 4) because of damping, other reaching and reflecting at the boundaries and interfering each other. For example a supershear rupture propagating toward the opposite to the slip direction of the more compliant solid (arrow n° 1, speed 1800 m/s around the $\sqrt{2}c_s$) can be detected; when it reaches the right boundary two waves rise up from the reflection, one is supershear (arrow n° 3, speed 1825 m/s) and the second one is a generalized Rayleigh wave GR (arrow n° 2, speed 950 m/s).

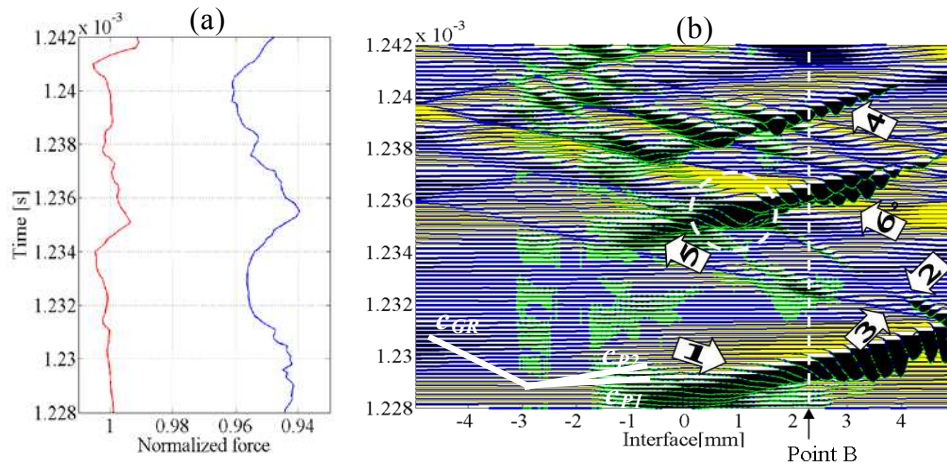


Figure 3.4 (a) Contact forces between $1.228 \times 10^{-3} \text{ s}$ and $1.242 \times 10^{-3} \text{ s}$, (interval II of figure 3.3), blue=force in x-direction, red=force in y-direction. (b) Seismic velocity profile and status of the contact nodes of the upper body (body n° 2 in figure 3.1) during the same interval: the green points on the lines mean sliding, blue points mean adherence, red points mean detachment; the amplitude of the curves represent the magnitude of the horizontal velocity of the point; the nodes at the contour of black zones are moving toward the x-negative direction, on the contrary nodes at the contour of yellow zone are moving in the x-positive direction; at the bottom on the left, as reference, are indicated the longitudinal wave speeds.

In a early time from the reflection, only the GR waves causes rupture, how can be seen from the points in sliding state (green points on the curves); on the other hand the supershear wave crosses the interface without causing sliding, according to the “bimaterial effect” on supershear and subsonic ruptures described in the introduction.

It can be noted also how the wave n° 5 and n°2 cross together (dot white circle) with a constructive interference and how, after that, the supershear wave splits in two other waves (arrow n°6 in figure 3.4(b)).

The GR wave, as well as the majority of the ruptures examined until here, have pulse-like feature similar to what obtained from other type of numerical simulations in literature [BEHR 11]; this can be noted in figure 3.4(b) where, after the passage of the most part of the rupture fronts, the interface returns in sticking (bleu points). There is not enough energy for having crack-like ruptures which would cause a major sliding of the interface.

3.3.3 From local to global dynamics

Figure 3.5 shows the isovelocities in the two bodies at 1.25×10^{-3} s seconds (ref. Fig 3.3); it can be noted that there are two supershear ruptures propagating toward the right (W1 and W2), with their characteristic Mach cone formed by the head waves. The first is going to cross the generalized Rayleigh wave (GR) which propagates toward the left, while the second is reaching the boundary (see Introduction). From the different angles of the cones it can be deduced that the rupture have different velocity of propagation ($W1 \approx 1900$ m/s, $W2 \approx 1800$ m/s). In the figure also other waves (RW) can be noted, which are the waves reflected by the boundaries.

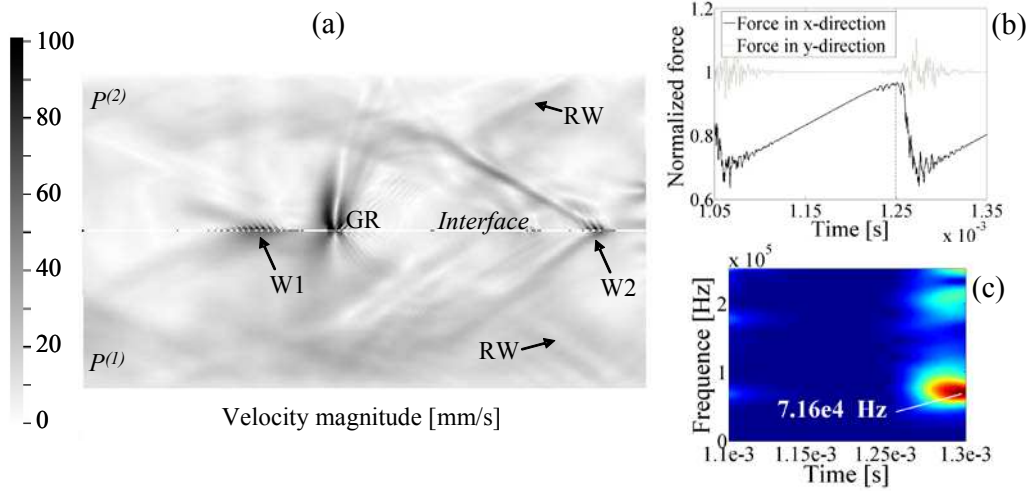


Figure 3.5 (a) Isovelocities at 1.25×10^{-3} s. The black nodes at the interface are in sliding; (b) Contact forces between 1.05×10^{-3} s 1.35×10^{-3} s, (interval I of figure 2); (c) Spectrogram, at the same time interval, of the tangential force (Hamming window 1×10^{-4} s).

When the waves that origin at the interface reach the boundaries with enough energy, waves that cross all the interface rise up from their reflection; causing extensive rupture and preceding the passage to the main slip event, the above-called macro-slip. During the macro-slip (drop force in figure 3.5(b)) the energy released activates rupture and waves propagation of greater magnitude that reach the boundaries of the system and, being here reflected, excite the dynamics of the whole system. Figure 3.5(c) shows the spectrogram of the tangential contact force for the same time interval of figure 3.3(a).

It can be noted how at the end of the macro-slip, the first vibration mode of the system at a frequency of about 7.16×10^4 Hz is strongly excited. This frequency falls between the two values of the first eigenfrequency of the system (composed by the two bodies in contact) corresponding to different status at the interface: complete sliding and adherence. Indeed calculations provide a fre-

quency $6.7e4$ Hz for the complete sliding condition and $7.6e4$ Hz for the complete adherence condition.

Once the mode excited, oscillations of the contact force can be observed after the dropt; these oscillations are due to the deformation of the system that is vibrating at its eigenfrequencies, affecting as well the stress distribution at the contact interface.

As observed the interaction between local and global dynamic is a complex phenomenon that assumes a "recursive" character: the waves, generated at the interface, propagate inside the bodies exciting the system vibration; vice versa the system modes affect the status of the interface and consequently the manner in which the waves are generated; in addition the change in the status of the contact nodes modifies the dynamics of the systems (eigenfrequencies and eigenvectors), complicating further the analysis .

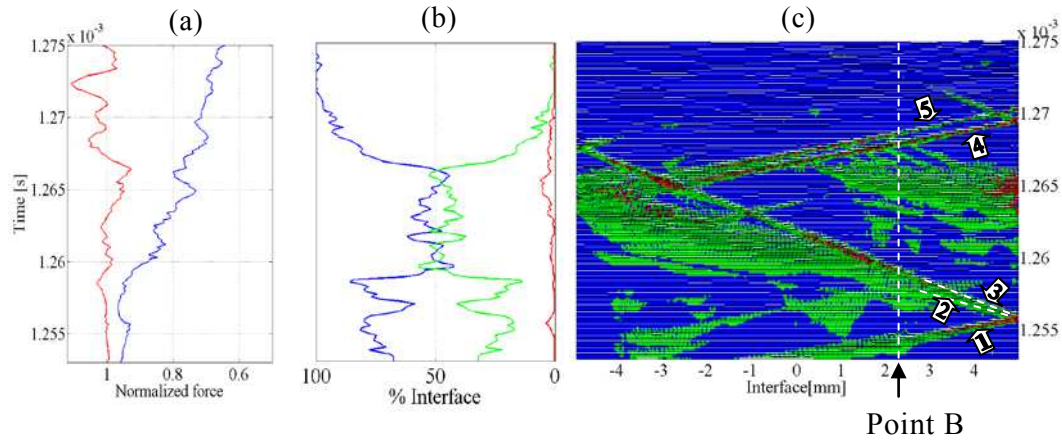


Figure 3.6 (a) Contact forces between $1.253e-3$ s $1.275e-3$ s, macro-slip (interval III of figure 3.3) blue=force in x-direction, red=force in y-direction; (b)-(c) Status of the interface and seismic profile during the same interval. Green=sliding; red=detachment; blue=adherence.

To get more insight on the macro-slip phase figure 3.6 presents the status of the interface and the seismic profile where, for the sake of clarity, the status and the amplitude of the wave have been conveniently scaled; in fact the local velocities in this phase are an order of magnitude (10^3 mm/s) greater than those in figure 3.4 (10^2 mm/s). It can be observed that although a large part of the interface undergoes in sliding in a crack-like manner, rupture propagation with pulse-like characteristic are still detected. At about $1.255e-3$ s a supershear (1800 m/s) pulse-rupture (1) propagating towards the right reaches the boundary and is reflected. By the reflection two different waves are generated: a supershear wave (2) that behaves as a crack-like front and crosses all the interface melting with the pre-existing slip field independently originated before by the coalescence of micro-slips, and a sub-Rayleigh pulse-like front rupture (3) (860 m/s) that

crosses the entire interface. After the passage of this latter front the interface becomes again in adherence (Figure 3.6(b)) due to his self-healing feature explained in section 2.4.1. The crack-type feature of the supershear wave (2) allows for the sudden increase of the percentage of sliding zones. Local detachment zones can be observed too. From the reflection of the supershear "enlarged" front with the left boundary two other ((4)(5)) supershear ruptures are triggered propagating towards the right.

After the macro-slip other isolated ruptures, named "aftershocks" [LIU 11], can be observed (a_1 and a_2 in figure 3.3(c)) and are interspersed by zone of total adherence of the interface.

Looking at the same phenomena described until here from a different point of view, figure 3.7(a) shows the x-velocities of the node A of the interface (ref. figure 3.1), belonging to the lower body and of the node B belonging to the upper body.

The signals refer to the same time interval of figure 3.4(a), where is also indicated the position of the node B; the velocities show the passage of the waves numbered from 1 to 5 in figure 4-b.

It can be observed that, in according to the positions of the two nodes, the two signals are opposite in sign and the difference in their magnitude is due to the different stiffness of the two materials. The figure also shows the sliding status (star markers on the curve of node B) of the contact node during time; the velocity variations generated by the precursors decay rapidly after each passage of the wave. Figure 3.7(b) shows the normal and tangential contact stresses during the same time interval. Figure 3.8 refers to the macro-slip phase (Figure 3.6); the passage of the rupture fronts is highlighted by the impulsive increase of the slip velocity, the continuous sliding status and the consequent decrease of the local tangential stress.

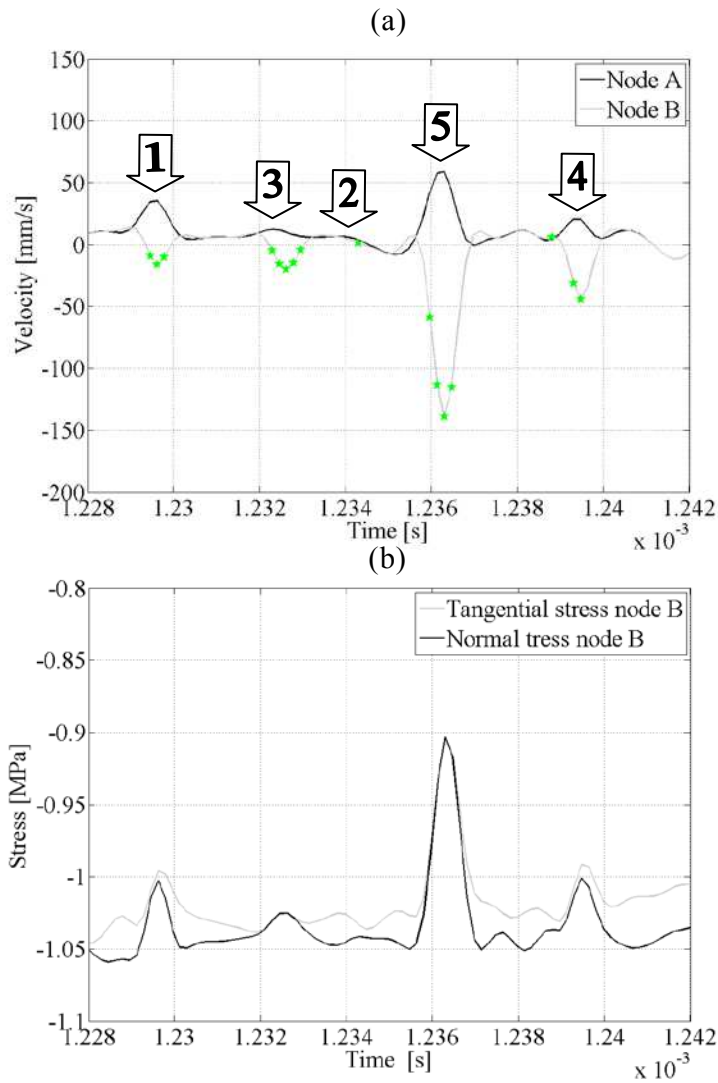


Figure 3.7 (a) x -velocities of the node A (belonging to body number 1, black line) and of the node B (belonging to body number 2, grey line) of figure 3.1 during the same time interval of figure 3.4, the star markers mean that the node is sliding; (b) Tangential and normal stress of the node B.

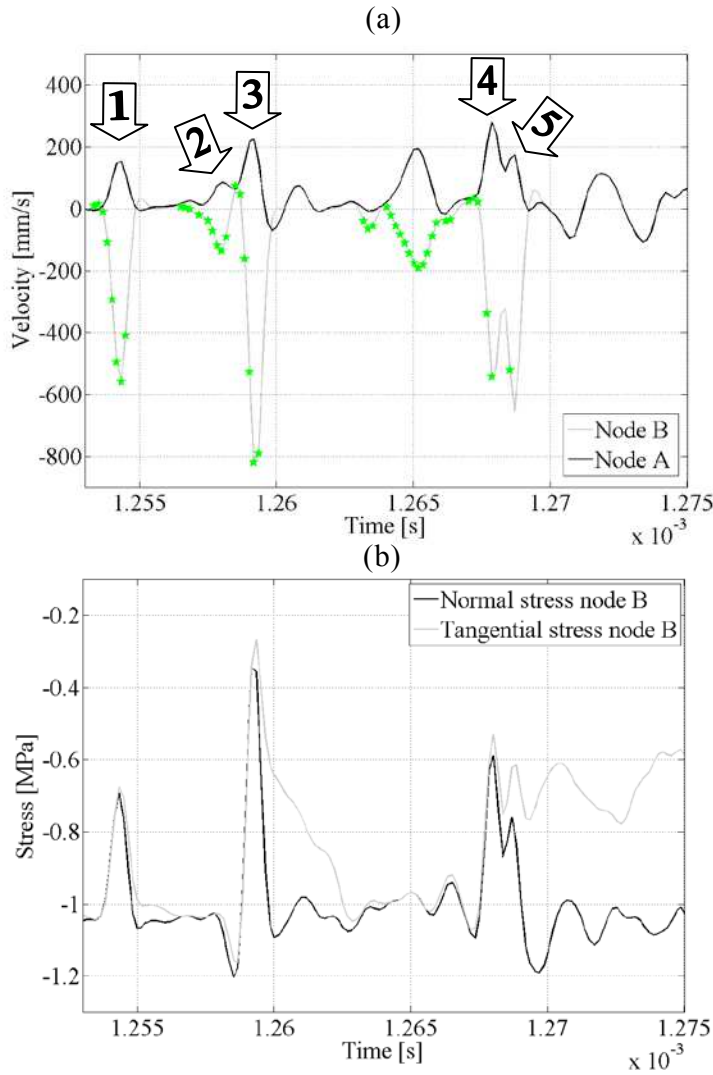


Figure 3.8 (a) x -velocities of the node A (belonging to body number 1, black line) and of the node B (belonging to body number 2, grey line) of figure 3.1 during the same time interval of figure 3.6, the star markers mean that the node is sliding; (b) Tangential and normal stress of the node B.

Figure 3.9 finally shows the evolution of the x -coordinate of the node A (at the top) and the relative signal of the x -acceleration (at the bottom) in the time interval between $0.65\text{e-}3\text{s}$ and $1.33\text{e-}3\text{s}$. These plots allow for easily identifying the series of macro-slips by the abrupt increase of the x -displacement and the large oscillation of the accelerations. The dashed line in figure 8 can be named “long-term motion”, in according to similar behaviours registered in experimental geophysics measurement [ROGE 03], or as the line of “continuous sliding”, as it is addressed in the next chapter.

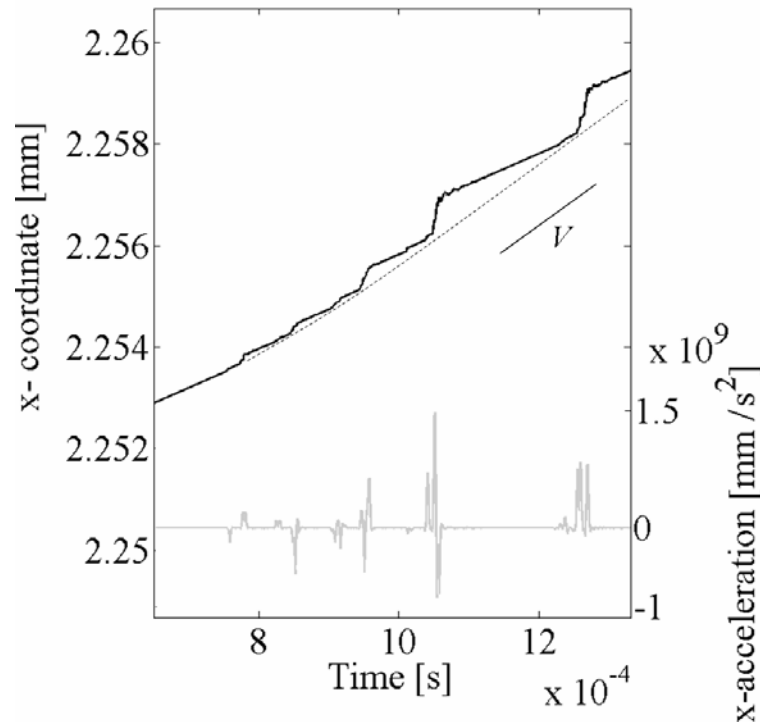


Figure 3.9 At the top: evolution of the x -coordinate (continuous black line) of the node A during a longer interval of time ($0.65e-3s$ and $1.33e-3s$, see figure 3.2) and “long term” motion (dashed line), at the upper-right angle is also indicated the direction correspondent to the translation velocity $V=10\text{ mm/s}$ (figure 3.1); At the bottom: correspondent variation of the x -acceleration (grey line).

The oscillations of the accelerations showed at the bottom of figure 8 are triggered by superficial ruptures and the consequent propagating waves that excite the system vibration, allowing the interaction between local contact dynamics and global dynamics (vibrational response) of the system.

3.4 Comparison with experimental works

Comparison with experimental works requires always careful attention, because of the intrinsic and inevitable differences between what is simulate and what happen in real conditions. This is due either to many effects voluntary omitted to simplify the numerical (or theoretical) problem as well to many effects that could not be opportunely accounted for in the model, but which are unavoidable in an experimental set-up. In addition for the subject treated in this

thesis there is not a so extensive production of experimental papers; consequently an identical experimental work to compare with the presented numerical simulations misses. The experimental reproduction of this work is, in fact, one of the perspectives prefigured for the future. However some general remarks can be asserted by a first comparison with experimental works present into the literature.

Very interesting in this sense are the two works of Rubinstein et al. [RUBI 04] [RUBI 07] already cited in section 1.2.2, and both focused on the onset of the frictional sliding and the work of Oded and Fineberg [ODED 11]. In [RUBI 07] the authors performed experimental tests with two identical blocks of PMMA (polymethyl-methacrylate) separated by a rough interface. At the onset of the sliding and before the main slip event, they observed drops in the friction force and related them to a series of discrete precursor events (as in section 3.3.2). The precursors are initiated at the sample trailing edge where the global shear force is applied, in this thesis the precursor are initiated at the centre or centre-left side of the interface and this is in agreement to the slight anti-symmetry introduced in the shear stress at the interface by the normal pre-load.

During the experiments the distance of propagation of the precursors increases until they trigger the transition to a extended sliding (macro-slip) [RUBI 07]. In this transition three different rupture fronts play a key role: sub-Rayleigh, intersonic and the so called “slow front” (with speed an order of magnitude lower than the others) [RUBI 04]. It is interesting to note that, as mentioned before, beside the sub-Rayleigh and supershear fronts, which clearly characterize the phenomena studied in the previous sections, also the slow front ([ODED 11]) can be related with the growth and the coalescence of micro-slips. In addition the speed of growth of the dendrites in figure 3.3(c) examined in section 3.3.2 is of the same order of magnitude.

Another remarkable consideration is related to the effect of the wave propagation as systematic cause of non-uniformity (of the stress) at the interface as observed in section 3.3.1.

Similar behaviour of the global contact forces has been as well measured experimentally in [VOIS 07] and [ZIGO 11]. In these works, for particular test conditions, can be also observed changes in the slope of the ramp force before the macro-slip similar to the ones registered in the simulation presented in this paper

All this considerations provided by the experimental work are consistent with what observed in the analysis showed in this chapter: in particular they agree in the key role of the precursors and, more in general, of the wave propagation at the interface in triggering the macro-slip and in affecting the macroscopic behaviour of the system, that is what is measured at the remote boundaries.

3.5 Conclusions

The presented chapter deals with the analysis of the onset of the sliding between two deformable bodies separated by a frictional interface.

First the evolution along the time of the sum of the contact forces as a function of the phenomena occurring at the interface has been investigated. It has been shown how the different phases in the evolution of the tangential force are related to a specific local dynamics at the interface between the two bodies. During the force ramps, i.e. the growth of the tangential force, elastic energy is cumulated in the system. Isolated micro-slips start to occur in different points of the interface and every single micro-slip behaves like a nucleated rupture, i.e. as a source of propagating waves; nevertheless the released energy is small and slip propagation is limited at the neighbourhood of the micro-slip nucleation zone, while the waves decay rapidly because of the damping. Thus, in this phase, the micro-slips are confined in restricted zones of the interface and they dissipate a low part of the elastic energy, before the occurring of the macro-slip phase. Due to the energy continuously provided by the displacement of the lower body the micro-slips grow in width and coalesce each other; every time that a series of micro-slips coalesce together, there is a variation of the average percentage of the zone in sliding causing an analogue change in the mean slope of the global tangential force. In this phase the part of the interface in sliding increases and contact points switch in sliding and sticking state continuously, in a sort of dynamic equilibrium. When a sufficient number of micro-slips switches in sliding at the nearly same time, they release enough energy to sustain a detectable wave propagation, to which is associated a rupture front, named precursor, which occurs at values of the force well below the critical value expected from the friction law. A precursor causes an abrupt small variation of the tangential global force and a consistent amount of propagating waves.

During the sliding initiation the micro-slip events and the related wave propagations at the interface lead to a highly nonuniform stress distribution, so that the features of the rupture depend strongly on the stress fields at the interface and the interaction with other propagating waves.

During the macro-slips, i.e. the drop of the force at the end of the ramp, the energy released activates ruptures and waves propagation of greater magnitude that, reaching and reflecting at the boundaries, excite the dynamics of the system that start vibrating at its eigenfrequencies. Thus, the wave generation at the contact (local dynamics) excite the system dynamics; vice versa, the system vibration affects the wave propagation and rupture nucleation at the contact.

4 Parameter space analysis

Introduction

In this chapter a parametric space analysis is performed on the system investigated in the previous chapter. The aim is to investigate the role of the key parameters in the wave generation and propagation at the interface; how they affect the transition between micro-slips and macro-slip; the origin of stick-slip like behaviour and continuous sliding; and, finally, the coupling between the local and global dynamics, showing how the macroscopic friction behaviour of the system is strongly related to the local rupture dynamics at the contact.

All the values, marked by an asterisk, are normalised to the correspondent values used in the simulation discussed in the previous section; in particular indicating by a superscript the parameters used in the sample simulation examined in chapter 3 (α' , β' , β_2' , N' , V'), the parameters of the current simulations (α , β , β_2 , N and V) are adimensionalized in the following manner: $\alpha^* = \alpha / \alpha'$, $\beta^* = \beta / \beta'$, where α and β are respectively the mass matrix damping coefficient and the stiffness matrix damping coefficient (see expression 2.2 in section 2.2 and table 3.1); $\beta_2^* = \beta_2 / \beta_2'$ where β_2 is the numerical damping coefficient of the integration method (expression 2.3 in section 2.2); $N^* = N / N'$ where N is the normal pre-load (Figure 3.1) and $V^* = V / V'$ where V is the translation velocity (Figure 3.1).

4.2 Effect of material damping

This section deals with the influence of the parameters regulating the material damping of the system. Damping is introduced in the model as proportional: α is the mass matrix coefficient and affects mainly the low frequencies; β is the stiffness matrix coefficient and affects mainly the high frequencies.

Figure 4.1 shows the behaviour of the global tangential force for different values of the damping coefficients.

Figure 4.1(a) shows that α , which damps the low frequencies, does not affect significantly the global behavior (the ramps and the following drops) of the force; on the contrary it affects the oscillations of the system after each macro-slip, which are related to the dynamic response of the system. When increasing the value of α , the vibrational response of the system and, thus, the energy stored by the system vibrations is dissipated, reducing the oscillations of the contact force. Thus, the value of the α coefficient does not affect directly the

generation and propagation of waves at the contact (local dynamics), but it affects the vibration energy of the system (global dynamics) as a consequence of the macro-slip events that excite its dynamics; the α coefficient is has a key role in the storing of vibration energy of the structure, which is transferred from the contact to the structure itself.

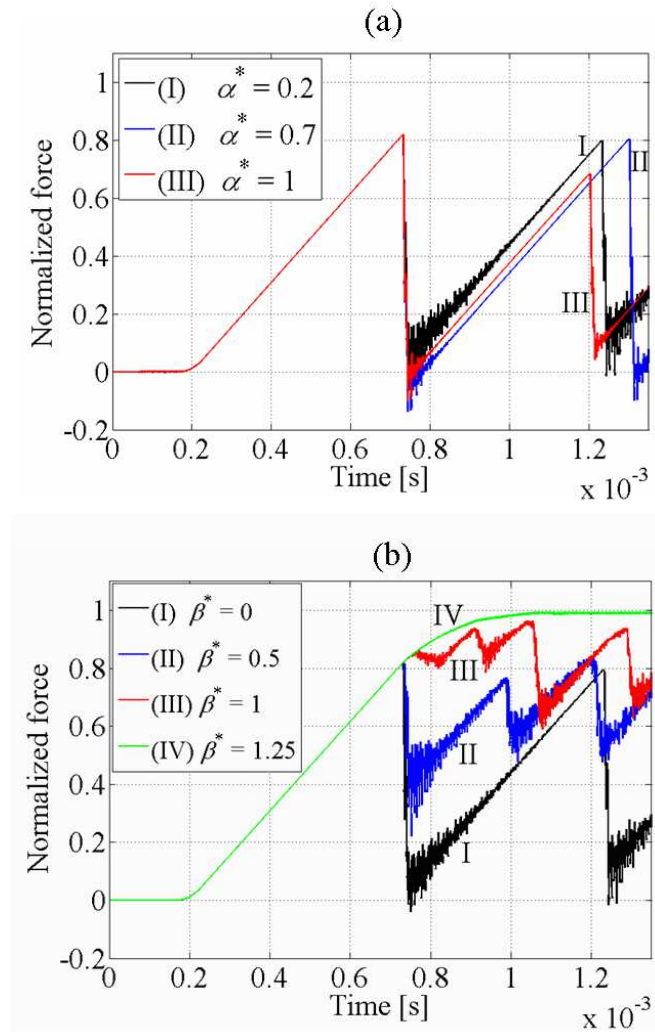


Figure 4.1. Tangential contact force of contact in x-direction in function of: (a) Mass matrix damping coefficient α ($\beta^*=0$, $\beta_2^*=1$, $N^*=1$); (b) Stiffness matrix damping coefficient β ($\alpha^*=0.2$, $\beta_2^*=1$, $N^*=1$). The parameters not indicated have the same value of table 3.1.

The curves shown in figure 4.1(b) refer to the variation of the value of the damping coefficient β , which, on the contrary, affects the high frequencies and thus the wave propagation at the contact. As the β coefficient increases, the force change drastically its pattern going towards a reduction of the macro-slip

drops up to the borderline case where there are no more drops in the tangential force, which reaches asymptotically the limit value $\mu|N|$. Contextually there is a change on the profile of each force ramp: the larger is the value of β , the more the curve tends to change gradually its slope before the macro-slip event, and the final macro-slip tends to be less abrupt. This is due to the fact that an increased damping leads to extinguish the high frequency oscillations and thus the micro-slip propagation, avoiding the triggering of the energy release due to the macro-slip event; on the contrary, if β is low the first micro-slips (ruptures) that arise are not damped and they have enough energy to trigger the macro-slip suddenly. The more β increases the more the micro-slips are extinguished and several of them need to arise before being able to trigger the macro-slip; the elastic energy tends to be drained slowly by them so that the macro-slip is less abrupt. Section 4.8 shows the analysis of the local phenomena in detail. The amount of micro-slips necessary for triggering the macro-slip event can be related to the length of the "slow front" measured experimentally by [ODED 11], before the macro-sliding. If, finally, the β coefficient have a sufficient high value, all the elastic energy is drained by damping the waves generated by the micro-slips and the force follows the curve IV in figure 4.1(b), which characterizes a "continuous sliding" between the two solids, without drops of the global tangential force or impulsive excitation of the system dynamics. Thus the β coefficient, affecting the local phenomena (micro-slips) that occurs at the contact interface, has a key role in the transition of the macroscopic frictional behavior of the system, passing from stick-slip like behavior to continuous sliding.

4.3 Effect of numerical damping

As discussed in the first chapter, handling numerical simulations that deal with friction brings itself a series of wariness to adopt to obtain robust results; thus, it is useful to investigate the influence of parameters that are strongly related to the numerical elaboration.

To this aim figure 4.2 presents the results dealing with the influence of the coefficient β_2 , used in the code for the numerical forward Euler method of integration, and of the time of regularization of the contact law.

As can be noted in the figures 4.2 and 4.3 the β_2 and β coefficients have the same effect; in fact, starting from $\beta_2^*=1$ (that means $\beta_2=0.5$, i.e. the central difference method), when the coefficient increases the curves tend to reach the condition of "continuous sliding" (IV).

This is due to the introduction of numerical damping, which affects mainly the high frequencies, with the increasing of the β_2 coefficient.

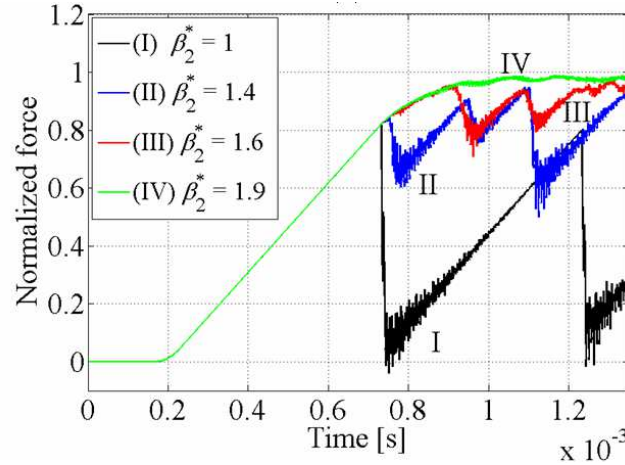


Figure 4.2. Tangential contact force in x -direction in function of the numerical coefficient β_2 of the integration method ($\alpha^*=0.2$, $\beta^*=0$, $N^*=1$); The parameters not indicated have the same value of table 3.1.

Thus, when simulating contact problems, a particular attention has to be placed on the using of such a parameter: even if it can help the convergence of the results, it can affect as well the physical phenomena at the origin of the contact behaviour.

4.4 Effect of the regularisation parameter

Figure 4.3 presents the effect of different values of the regularization time of the contact law.

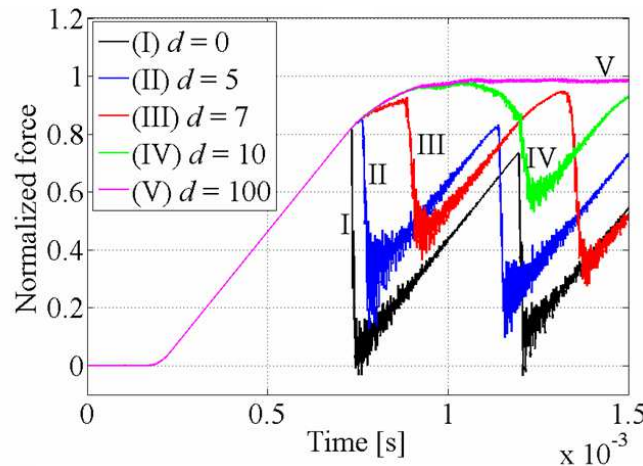


Figure 4.3. Tangential contact force in x -direction in function of the different values of the time of regularisation \hat{t} (see section 2.2) $d=\hat{t}/\Delta t$ ($\alpha^*=0.2$, $\beta^*=0$, $\beta_2^*=1$, $N^*=1$). The parameters not indicated have the same value of table 3.1.

The regularization time, defined in expression 2.7 in section 2.2, sets the delay of the variation of the tangential frictional stress with respect to changes of the normal stress; the parameter d represent a normalized parameter of the regularization time respect to the integration time step that has been set in the explicit code to perform the simulation presented in the previous section ($\Delta t = 0.334 \times 10^{-8}$ s). The effect of increasing d is a cutting of the high frequency contents associated to the heaviside pattern of the classical Coulomb friction law; consequently this parameter affects as well the high frequency content of the contact dynamics (wave propagation), introducing a sort of damping at the contact surface; the effect is similar to the effect of the variation of β . For these reasons, the previous chapter presented results obtained with no regularization of the contact law and with β_2 equal to 0.5, in order to avoid the suppression of physical phenomena at high frequencies by numerical artefacts.

4.5 Effect of the pre-load

Figure 4.4 shows the effect of different values of the pre-load N (Figure 3.1). When the normal force increases, the amplitude of the force drops and the time period between each macro-slip increases; this is due to the larger amount of the elastic energy stored into the system before the energy is released by the macro-slip phases.

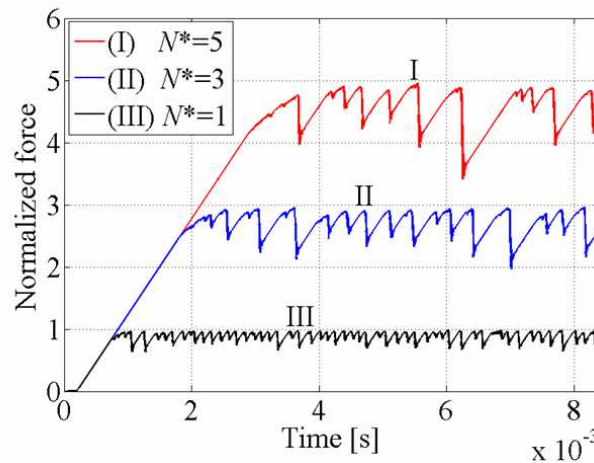


Figure 4.4 Tangential contact force in x -direction in function of the pre-load $N^* = N/N_0$ ($\alpha^* = 1$, $\beta^* = 1$, $\beta_2^* = 1$). The parameters not indicated have the same value of table 3.1.

As the pre-load increases the detachment zones during the macro-slip (red zones in 4.9(a)) reduce, but the rupture propagation speeds during the slip

events are not affected, because they depend on the ratio between the stress fields [ANDR 76].

4.6 Effect of the friction coefficient

In figure 4.5 is showed how different values of the friction coefficient μ affect the pattern of the force. When the friction coefficient decreases, the period of the ramps decreases and proportionally decreases also the force drop amplitude; this is related to the reduction of the deformation energy stored in the system. If the friction coefficient is enough low, the transition between the stick-slip like behaviour and continuous sliding can be observed. In fact, even if the β damping coefficient is unchanged, at each micro-slip a lower amount of energy has to be dissipated, allowing again for a progressive draining of the energy.

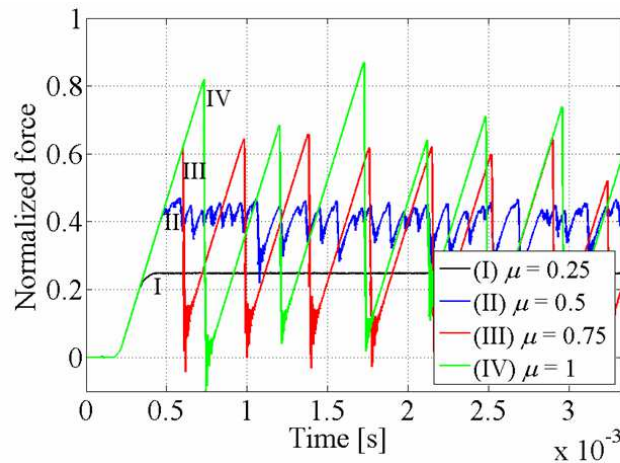


Figure 4.5 Tangential contact force in x -direction in function of the Coulomb coefficient of friction ($\alpha^*=1$, $\beta^*=0$, $\beta_2^*=1$, $N^*=1$). The parameters not indicated have the same value of table 3.1.

4.7 Effect of the translation velocity

Figure 4.6 shows the diagrams of the contact forces for different values of the translation velocity V (see figure 3.1), respectively lower and higher than the velocity $V' = 10$ mm/s used in the sample simulation studied in the previous section.

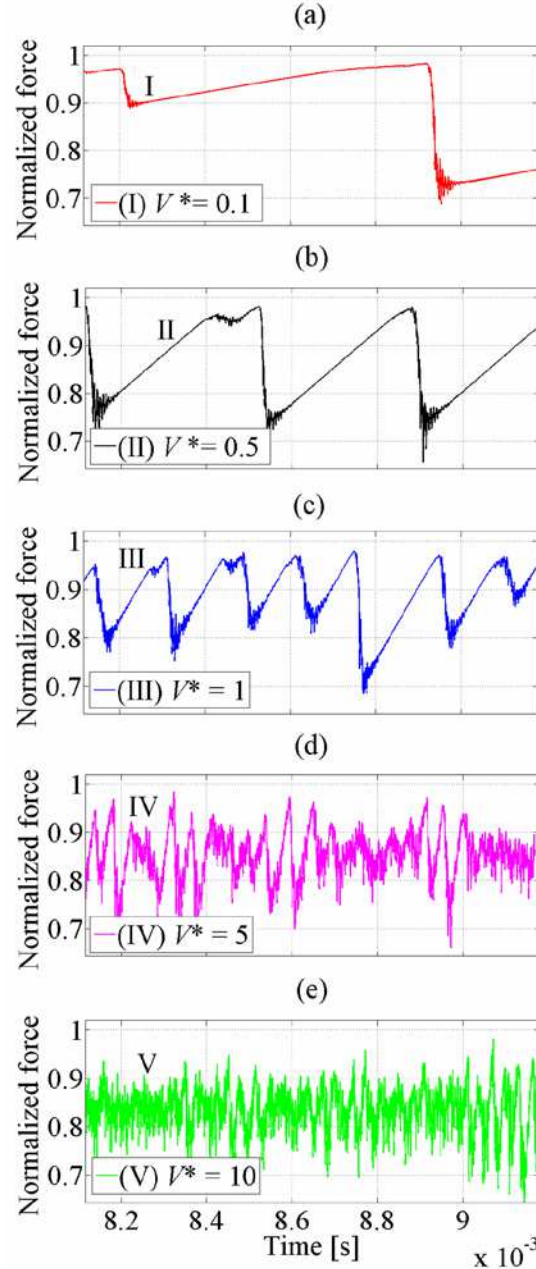


Figure 4.6 Tangential contact force for different values of the translational velocity V normalized respect to the velocity V' of the sample simulation of section 3 ($V' = 10$ mm/s): (a) $V^* = 0.1$; (b) $V^* = 0.5$; (c) $V^* = 1 = V'$; (d) $V^* = 5$; (e) $V^* = 10$. All the graphics have the same x-scale and y-scale.

It can be seen that the ramp/drop pattern of the tangential force shortens with the increase of the translational velocity; it is interesting to note that the drop of the macro-slip seems not to be influenced significantly by the velocity, in contrast to what observed in some experimental works [URBA 04]. In fact, although the force drop period varies along the time (figure 4.6), its amplitude seems not to be so affected (almost for the range of velocities examined); this is due to the fact that the dynamic phenomena at the interface, i.e. the ruptures propagation speed (order 10^5 mm/s), are in any case faster than the translational velocity V . This explains also the fact that the slope (negative) of the macro-slip remains almost the same.

However, when the velocity of translation increases there is a more energetic vibration field; in fact, for the same value of α , there is no time between two subsequent macro-slips to damp the system vibrations. Thus the system is continuously excited and it vibrates at its eigenfrequencies.

These vibrations, through their "bouncing" effect at the interface plays the same role of the vibrations externally applied at the contact system [POPO 10]; they can bring to a reduction of the global friction force as can be deduced by figure 4.7, where the mean value of the tangential contact force is plotted for different values of the translational velocity.

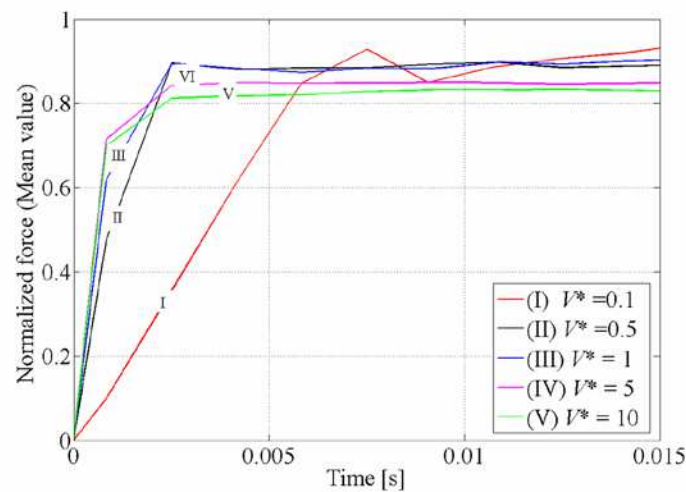


Figure 4.7 Mean value of the tangential contact force for different values of the translational velocity V^* (see also the caption of figure 4.6).

4.8 Analysis of the local dynamics

It is interesting to investigate the change of the wave propagation field at the interface during the macro-slip phase as a function of the damping coefficient β . It has been shown in figure 4.1.b that when increasing β the drop of the macro-slip reduces and it tends to be less abrupt, because the energy is previously dissipated by several micro-slips. Figure 4.8 shows on the left different patterns of the tangential force during macro-slip and, on the right, shows the contact status at the interface for the time interval corresponding to a single macro-slip. It can be noted as, passing from a more abrupt drop to a softer one (increasing β) the wave field changes drastically. In the first case (figure 4.8(a),(b)), for β equal to 0, the phenomenon is governed mainly by a supershear rupture, originated at the interface from a nucleation zone around -1 mm and propagating toward the right; the rupture has a crack-like front that brings all the interface in sliding and detachment, all the elastic energy is released suddenly and a large part of the contact nodes detaches during the energy release. From the nucleation zone also a sub-Rayleigh rupture front originates and propagates towards the left. It is reflected by the left boundary, triggering a second supershear rupture crack-like front. The macro-slip event is triggered suddenly by the first ruptures (micro-slips). Nevertheless, just before the macro-slip event, it is possible to recover again the phase of growth of the micro-slips with the consequent enlargement of the sliding “dendrite” (as in the section 3.3.2) up to approximately 1.203e-3s (figure 4.8(b)), when the switch to more rapid dynamics occurs (sub-Rayleigh front toward the left and supershear front toward the right). This phase can be assimilated to the growth of the “slow front” described in [ODED 11]; in figure 2.c of this experimental work can be observed the same qualitatively transition from “slow” to “fast” phase; the speeds characterizing the two phases have, respectively, the same order of magnitude observed in figure 4.8(b). As β increases (figure 4.8(c),(d)) the front of the supershear right-oriented rupture reduces its energy (previously dissipated by the micro-slips) and passes from a crack-like feature to “self-healing crack”-like [GERD 01a], reducing the width front; in addition the rupture tends to split (in the time) in a larger number of ruptures. For a larger value of β (figure 4.8(e),(f)) the width of the rupture fronts shrink even more as a pulse-like, the elastic energy released by every supershear rupture reduces and can be observed a GR front emerging from the reflection (case study of section 3). In figure 4.8(g),(h) it can be observed how the macro-slip tends to split to a larger number of rupture fronts both in the right and the left directions, behaving like a series of subsequent micro-slip phenomena; the ruptures move on an interface that is already partially sliding, due to coalescence of isolated micro-slip. In the asymptotic condition of continuous sliding, which can be reached for example

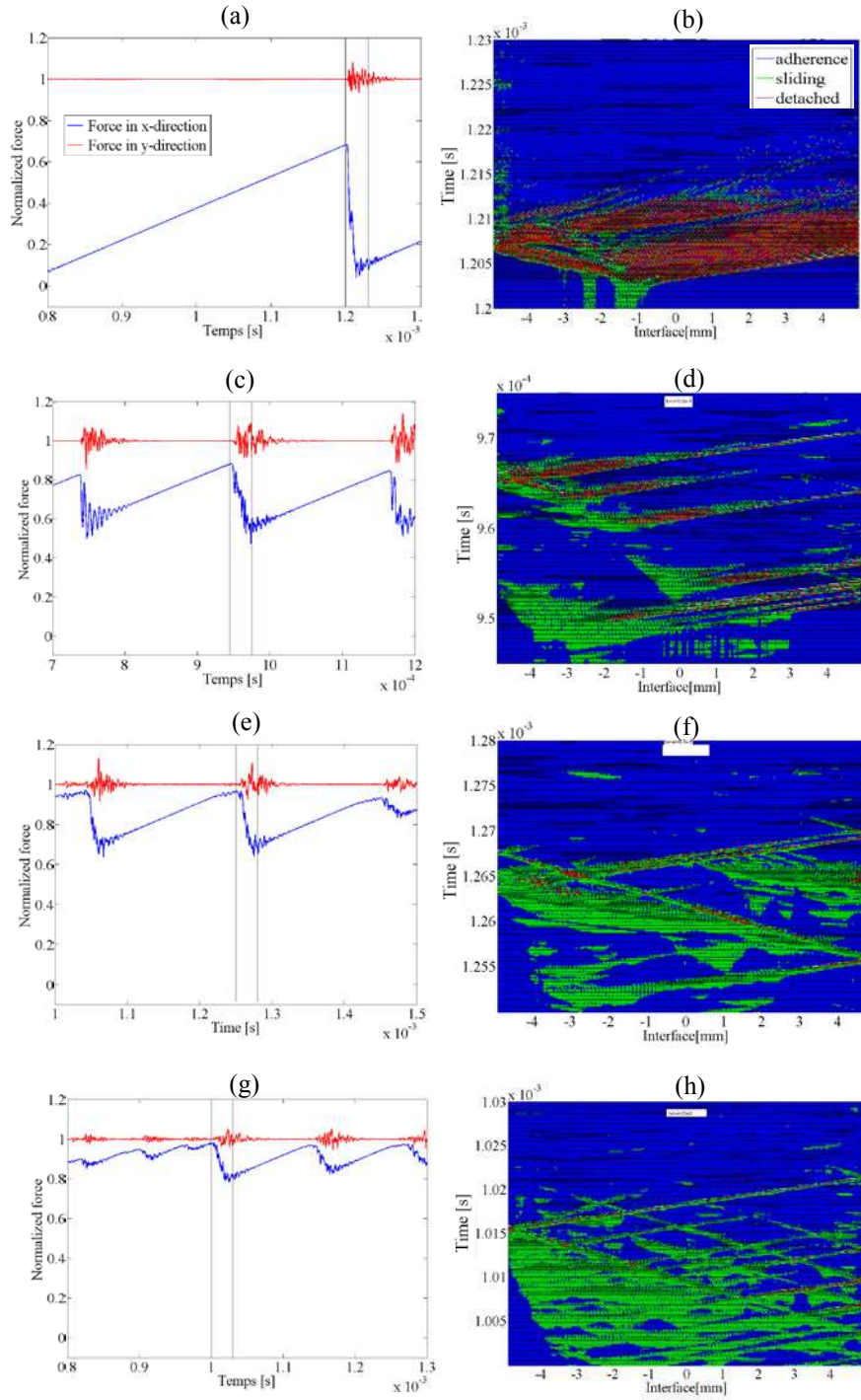


Figure 4.8. Typical macro-slip in the tangential force and relative status at the interface for different value of damping coefficient β . a-b, $\beta^*=0$; c-d, $\beta^*=0.6$; e-f, $\beta^*=1$; g-h, $\beta^*=1.12$; red=force in y-direction, blue=force in x-direction. The parameters not indicated have the same value of table 3.1.

for high values of β (Figure 4.1(b) curve IV), the global sliding of the surface is provided by the random distribution of micro-slips nucleating along the entire interface with a distribute wave generation and propagation field.

The velocity of propagation of the ruptures seems not to be affected by the different patterns of the macro-slip maintaining their values around 950 m/s for the sub-Rayleigh left oriented ones and 1800 m/s for the supershear right oriented ones. These values are in accordance to the theoretical studies on the pulse-like rupture velocity of propagation in the slip direction of the more compliant solid (GR wave [WEER 63]) and in the opposite direction [supershear wave WEER 02], in the case of dissimilar materials. The presented graphics are related to the variation of β ; however the same considerations apply every time there is this type of change in the macro-slip patterns, allowing for linking the macroscopic behaviour of the system (stick-slip, continuous sliding, induced vibrations, etc.) to the local phenomena (local rupture dynamics) occurring at the interface.

4.9 Comparison with experimental works

In this section a further comparison with experimental works in literature is presented in addition to considerations made in the previous section. The different pattern of the frictional force studied in section 4.8 can be related to the different stages of the friction experiment presented in [ZIGO 11] and reported in figure 1.5. The figure 1.5(b), classified by the authors as unstable regime, shares many similar features with the results in figure 4.9(a). In fact, in the experiments, the jumps of the slider produce short duration and high amplitude acoustic signals, and no TLS is recorded. Even if it would be difficult to link directly the TLS with the precursors, however they can be related with micro-slip events that happens before the main slip. In this sense the description of the phenomena of figure 4.8(a) agrees with the one of figure 1.5(b): there are no relevant localized slip phenomena before the main slip event and the first few macro-slips have enough energy to trigger the macro-slip.

Looking at the figure 1.5(c), it presents the results of experiments where the sample has accumulated displacement. In this condition the slider still obeys a stick-slip behaviour but is creeping before and after the jumps [ZIGO 11]; the slope of the force changes (it reduces) and the associated acoustic emission presents two type of signal: a tremor like signal with long duration and low amplitude and a strong impulsive event, which is the signature of the jump. This behaviour is significantly the same of figure 4.8(e), 4.8(f) or of the curve III and IV of figure 4.1(b) 4.2(a)(b), which is due to the presence of relevant micro-slip/precursor

events before the macro-slip. Finally in figure 1.5(d) the stable regime, characterized by smooth oscillations during which the TLS are identical to those recorded before the main slip event in figure 1.5(c), is represented. This can be a further confirmation that continuous sliding observed in some simulations (curve IV of figure 4.1(b) and 4.2(a)(b)) is a limit case where the sliding is assured by the succession of micro-slips, as those found before the macro-slips.

Analogue consideration can be carried out by the comparison with results from [VOIS 07], reported in figure 4.9. In particular, a similar pattern of the tangential force (ramps and drops) during the macro-slip is obtained, although in this case the signal of the force is not enough defined to appreciate changes in the slope of the force.

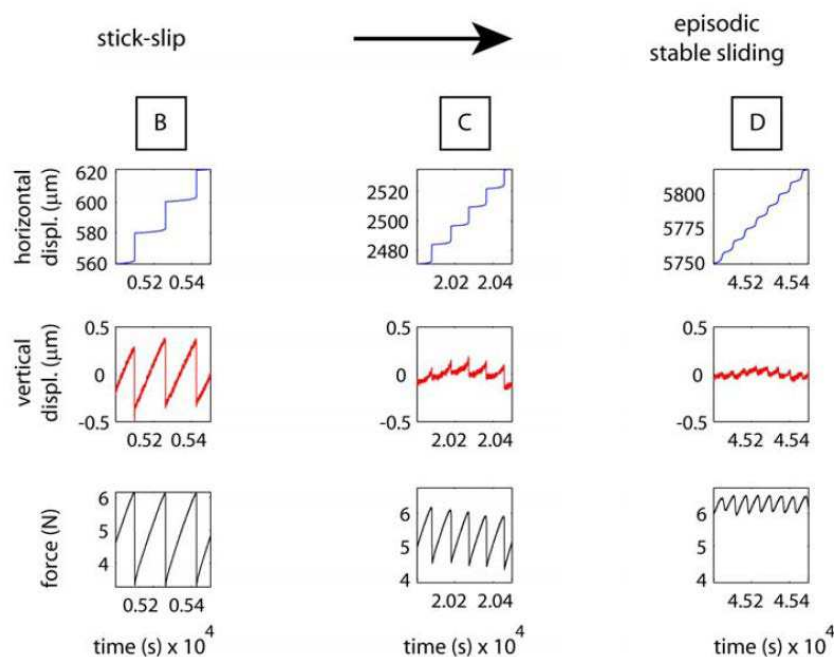


Figure 4.9 Change in frictional behaviour of a salt/glass friction experiment from [VOIS 07]; B) the beginning of the experiment; C) the mid-run of the experiment, with a cumulated slip of 2500 μm . D) the end of the experiment, with a cumulated displacement of about 6000 μm .

Finally by the comparison with [RUBI 04][RUBI 07] and [ODED 11], interesting conclusions have been drawn about the similarity between the different phases of the onset of the frictional sliding measured experimentally in those papers (slow front/ precursors/sliding) and the ones investigated in this work (growth of the micro-slips/ precursors/macro-slip), both in the order of magnitude of the rup-

ture speeds and in the same qualitatively behaviour in the shift from a phase to the subsequent one.

The agreement between the numerical results, presented in this thesis, and the few available experimental works in literature allows for a first validation of the obtained results and encourages forward a deeper numerical investigation. Nevertheless an experimental work, dedicated to the validation of the numerical results, is one of the main perspectives of this project.

4.10 Conclusions

A parameter space analysis has been carried out. The effect of the damping coefficients, friction coefficient μ , system pre-load and numerical simulation coefficients has been investigated. The results allow for highlighting the interaction between the macroscopic sliding behaviour of the system (stick-slip, continuous sliding) and the induced vibrations (global dynamics) to the local dynamics at the contact.

The α damping coefficient affects the low frequency vibrations of the system and thus the vibration energy due to the system dynamic response to the local excitation at the contact; the friction coefficient μ controls the deformation energy stored in the system before each macro-slip and affects the amount of energy of each micro-slip; β and d , when increased, have a dissipative effect of the micro-slip propagation, reducing the slope of the ramps and the amplitude of the force drops up to completely eliminate the discontinuous trend of the force and reaching the state of continuous sliding. This effect is due to the progressive dissipation of the elastic energy by a random distribution of subsequent micro-slips all around the whole contact surface, rather than by the sudden apparition of the macro-slip energy release. The energy of the wave fields generated by the distributed micro-slips is dissipated progressively by the material (damping coefficients) or contact (regularization time) damping.

The presented analysis showed the effect of each parameter, when the others are maintained constant. Obviously, the final behaviour of the system is function of the interaction of the phenomena affected by each parameter. For instance, the presented results show that when the friction coefficient decrease, a continuous sliding can be reached with lower values of the β damping coefficient; as well, when increasing the translational velocity, a larger energy per time is introduced into the system, and a larger α damping coefficient is needed to damp the vibration of the system induced by the contact. The analysis of the rupture dynamics at the contact interface showed as the macroscopic behaviour of the system is deeply linked to the phenomena at the interface.

5 Conclusions

The presented thesis is addressed to investigate the mechanisms at the base of the wave and rupture fields at a tribological interface and his relationship with the local characteristics of the surfaces in contact as well with the macroscopic behaviour of the system (stick-slip, continuous sliding, dynamic instabilities ecc.).

A 2D finite element model, composed by two finite dimensional solids in sliding contact, has been developed for a general approach to the problem. In a first “propaedeutic” part (chapter 2) the rupture dynamics on a smooth contact interface between dissimilar materials has been investigated. The nucleation of a rupture at the centre of the interface causes the propagation of a slip pulse at generalized Rayleigh wave speed, in the direction of sliding of the more compliant solid, and a pulse-like supershear rupture, in the opposite direction. As the energy released for the rupture increases, the rupture changes its velocity and type (pulse-like or crack-like). The results obtained are consistent with the experimental and numerical results found into the literature for smooth interfaces, allowing for a validation of the numerical model.

5.1 Original contributions

5.1.1 Effect of roughness

Once the numerical model validated, the periodical roughness has been then introduced at the contact surfaces; the consequent heterogeneous stress distribution causes a more complex rupture process. The analysis shows that, depending on the relative dimension between the roughness wavelength and the width of the wave fronts, two different behaviours can be observed:

- i) a coupling between the wave propagating into the two bodies, which causes the developing of two asymmetric rupture fronts in the opposite directions respect to the nucleation zone, as in the case of smooth interface;
- ii) a decoupling of the wave propagation inside the two bodies, characterized by an independent wave propagation, symmetric respect to the nucleation zone.

The rupture profiles highlight a differentiated rupture inside the asperities. There are different rupture fronts at different velocities for different zones of the asperities; the velocities of the rupture fronts are function of the energy released at the nucleation. The analysis, carried out with a sinusoidal roughness with different patterns, highlights similar behaviour when the roughness causes sharp variations on the contact stress distribution; while, for a continuous stress distribution (spatial phase difference equal to zero) between the surfaces, the behaviour is similar to the case of flat contact surfaces.

The results show how the roughness, and more precisely the degree of non-uniform stress distribution introduced at the interface by the roughness, plays a key role on the rupture propagation.

5.1.2 Sliding initiation: relationship between global and local phenomena

After the analysis of the rupture propagation in preloaded static contacts, the onset of sliding between the two deformable bodies has been investigated.

First, the evolution along the time of the sum of the contact forces (global behaviour) as a function of the phenomena occurring at the interface (local dynamics) has been investigated. It has been shown how the different phases in the evolution of the tangential force are related to a specific local dynamics (micro-slip, precursors, macro-slip) at the interface between the two bodies.

During the force ramps, i.e. the growth of the tangential force, the elastic energy is cumulated into the system (whose magnitude is proportional to the friction coefficient). The elastic energy is due to the relative displacement between two bodies contact and its spatial distribution is function of the bodies geometry and boundary conditions. Isolated micro-slips start occurring at different zones of the interface and every single micro-slip behaves like a nucleated rupture; nevertheless the released energy is small and the slip propagation is limited at the neighbourhood of the micro-slip nucleation zone, while the waves decay rapidly because of the damping. Thus, in this phase, the micro-slips are confined in restricted zones of the interface and they dissipate a low part of the elastic energy, before the occurring of the macro-slip phase.

Due to the energy continuously provided by the relative displacement of the bodies the micro-slips grow in width and coalesce each other; every time that a series of micro-slips coalesce together, there is a variation of the average percentage of the zone in sliding causing an analogue change in the mean slope of the global tangential force. In this phase the part of the interface in sliding increases and contact points switch in sliding and sticking state continuously, in a

sort of dynamic equilibrium. When a sufficient number of micro-slips switches in sliding, they release enough energy to sustain a detectable wave propagation, to which is associated a rupture front, which is named precursor in geophysics (in the sense of precursor of the main slip event); it occurs at values of the tangential force well below the critical value expected from the friction law. At the precursors are associated abrupt small variations of the tangential global force and a consistent amount of propagating waves.

During the sliding initiation the micro-slip events and the related wave propagations at the interface lead to a highly nonuniform stress distribution, so that the features of each rupture depend strongly on the stress fields at the interface and the interaction with other propagating waves.

Once the energy released by the ruptures allows for triggering a crack-like propagation front, the macro-slip between the two solids in contact occurs, with a consequent release of energy; the global tangential force drop and a consistent excitation of the system dynamics occurs.

5.1.3 Parametrical analysis: from stick-slip to continuous sliding

A parameter space analysis has been carried out to evaluate the effect of different parameters as the damping coefficients, the local friction coefficient, the system pre-load and the numerical simulation coefficients. The results allow for highlighting the interaction between the macroscopic sliding behaviour of the systems, the induced vibrations and the rupture dynamics at the contact.

It has been highlighted that:

- i. the α coefficient affects the relative low frequency vibrations of the system and thus the vibration energy due to the system dynamic response to the local excitation at the contact;
- ii. the friction coefficient μ controls the deformation energy stored in the system before each macro-slip and it affects the amount of energy released by each micro-slip;
- iii. the β damping coefficient and the contact law regularization time (d) have a dissipative effect of the micro-slip propagation, reducing the slope of the force ramps and the amplitude of the force drops, up to completely eliminate the discontinuous trend of the force and reaching the state of continuous sliding. The analysis of the local propagation wave field at the contact surface highlighted that this effect is due to the progressive dissipation of the elastic energy by a random distribution of subsequent micro-slips all around the whole contact surface, rather than by the sudden apparition of the macro-slip energy release. The energy of the wave fields generated

by the distributed micro-slips is dissipated progressively by the material (material damping β) or contact (regularization time) damping.

The presented analysis showed the effect of each parameter, when the others are maintained constant. Obviously, the final behaviour of the system is function of the interaction of the phenomena affected by each parameter. Nevertheless, the parametrical analysis allows highlighting the relationship between the macroscopic behaviour of the system (stick-slip, sliding, etc.) with the local phenomena and the main effects of each parameter. The influence on the transfer of energy between local and global dynamics of the system has been approached as well.

The numerical results presented in this thesis have been compared with experimental works presented in literature, showing a good agreement and allowing a better interpretation of the involved phenomena.

The works object of this thesis allowed for investigating the coupling between local rupture dynamics wave generation and propagation, global dynamics and macroscopic frictional behaviour between two bodies in contact. The presented parametrical analysis gives the basis for understanding of the effect of the system parameters on the local rupture phenomena and, consequently on the macroscopic behaviour of the system.

5.2 Perspectives

Concerning the future works, two main tracks of investigation can be identified: i) a further numerical analysis is needed to get more insides on the local phenomena and their coupling with the system dynamics; ii) an experimental investigation is needed for validating and applying the obtained numerical results.

5.2.1 Further numerical analysis

Further simulations are needed to get more insides on the rupture front propagation at the contact interface; in detail:

i) Quantify, in function of different parameters, the release of energy needed to trigger precursors and macro-slips. In particular its ratio with the deformation energy stored in the system can give some interesting information for predicting, or avoiding, macro-slip events.

ii) Investigate further the condition of occurrence of a pulse-like propagation. One of the main conclusions of this thesis is around the necessity, in order to avoid the macro-slip and the consequent stick-slip behaviour of the system, of changing the crack-like features of the main slip events toward several pulse-like fronts; up to obtaining a continue series of micro-slips with short propagation distance. In effect, in literature, several papers deal with the investigation of pulse-like or crack-like conditions, mostly belonging to the geophysics fields. The presented results agree with the literature, as observed in the previous chapters where, in addition, the effect of key parameters (β, d) has been presented. The different influence of these factors as a function of the biomaterial effect has to be investigated.

As mentioned above, the results from the parametrical analysis give some important insides of the effect of each single parameter on the local and global behaviour of the solids in contact. A further investigation is needed to highlight the mutual interaction between system and contact parameters. The effects of further key parameters, like surface roughness, need to be investigated

A detailed parametrical analysis of the sliding initiation as a function of the roughness needs to be carried out. In particular an investigation of the effect of the roughness on the excitation of the system dynamics, trough the wave generated at the contact, is needed to get more insides on friction induced vibrations.

A further investigation is needed to analyze the effect of external wave fields on the friction behaviour; i.e. how, by introducing artificial wave fields it is possible to modify the global behaviour of the system (global friction coefficient, stick-slip or continuous sliding). The results discussed in this thesis show that the non-uniform distribution of the contact stresses affects the rupture propagation; a non-uniform stress distribution can be obtained through propagating artificial wave fields.

5.2.2 Experimental analysis

An experimental investigation is needed to reproduce and further validate the numerical results; the material properties used for the simulations have been chosen for employing resin epoxy and polycarbonates as bodies in contact.

Reproducing the sliding between two bodies and measuring global information, like the global contact forces and accelerations at different points of the system, will allow for a comparison with the numerical simulations. Recovering the wave field distribution in time results more difficult experimentally; photo-elastic and acoustic techniques will be investigated.

An experimental parametrical analysis will allow for validating the numerical one and get some insight more on the effect of the key parameters (preload, translation velocity, materials, etc.).

Finally, an experimental test bench will allow for introducing artificial wave fields on the contact and investigate their effect on the macroscopic friction coefficient and on the transition between stick-slip behaviour and continuous sliding.

6 References

- [ADAM 95] Adams G.G., "Self-excited oscillations of two elastic half-spaces sliding with constant coefficient of friction", *J. appl. Mech.*, **62**, 867–872 (1995).
- [ADAM 98] Adams G.G., "Steady sliding of two elastic half-spaces with friction reduction due to interface stick-slip", *J. appl. Mech.*, **65**, 470–475 (1998).
- [ADAM 99] Adams G.G., "Dynamic motion of two elastic half-spaces in relative sliding without slipping", *ASME Journal of Tribology*, **121**, 455–461 (1999).
- [ADAM 01] Adams G.G., "An intersonic slip pulse at a frictional interface between dissimilar materials", *ASME Journal of Applied Mechanics*, **68**, 81–86 (2001).
- [AKAY 02] Akay A., "Acoustic of friction", *J. acoust. Soc. Am.*, **11** (4), 1525-1548 (2002).
- [AKAY 00] Akay A., Wickert J., Xu Z., "Investigation of Mode lock-in and friction interface", *Final Report, department of mechanical engineering*, Carnegie Mellon University, Pittsburgh, 2000.
- [AMON 699] Amontons G. "De la résistance causée dans le machines", *Mem. Acad. R. Sci.*, 206-226 (1699).
- [AMPU 08] Ampuero J.P., Ben-Zion Y., "Cracks, pulses and macroscopic asymmetry of dynamic rupture on a bimaterial interface with velocity-weakening friction", *Geophysical Journal International*, **173**, 674-692 (2008).
- [ANDR 76] Andrews D.J., "Rupture velocity of plane strain shear cracks", *Journal of Geophysical Research*, **81** (32), 5679-5687 (1976).

- [ANDR 97] Andrews D.J., Ben-Zion Y., "Wrinkle-like slip pulse on a fault between different materials", *Journal of geophysical Research*, 102 (10), 553-571 (1997).
- [BAIL 02] Baillet L., Sassi T., "Finite Element method with Lagrange multipliers for contact problems with friction", *Comptes rendus mecanique*, 334, 917-922 (2002).
- [BAIL 05a] Baillet L., Sassi T., "Mixed finite element formulation in large deformation frictional contact problem", *Revue Européenne des Eléments Finis*, 14 (2-3), 287-304 (2005).
- [BAIL 05b] Baillet L., Link V., D'Errico S., Laulagnet B., Berthier Y., "Finite element simulation of dynamic instabilities in frictional sliding contact", *Journal of Tribology*, **127**, 652-658 (2005).
- [BEHR 11] Behrendt J., Weiss C., Hoffmann N.P., "A numerical study on stick-slip motion of a brake pad in steady sliding", *Journal of Sound and Vibration*, **330**, 636-651 (2011).
- [BEN 01] Ben-Zion Y., "Dynamic ruptures in recent models of earthquake faults", *J. Mech. Phys. Solids* **49**, 2209-2244 (2001).
- [BEN 02] Ben-Zion Y., Huang Y., "Dynamic rupture on a interface between a compliant fault zone layer and a stiffer surrounding solid", *Journal of Geophysical research*, **107**, 2242 (2002).
- [BENG 97] Bengisu M.T., AKAY A., "Relation of dry-friction to surface roughness". *ASME J Tribol.*, **119**, 18-25 (1997).
- [BERT 95] Berthier Y., "Maurice Godet's third body", *22nd Leeds-Lyon Symposium on Tribology*, 2209-2244 (1995).
- [BERT 01] Berthier Y., In "Background on friction and wear", *Handbook of materials behaviour models*, Lemaître Academic Press, 676-99 (2001).
- [BOWD 50] Bowden F. P., Tabor D., "Friction and lubrication of solid. Part 1", *Clarendon Press*, Oxford (1950).

- [BOWD 54] Bowden F.P., Tabor D., "Friction and lubrication of solid. Part 2", *Clarendon Press*, Oxford (1954).
- [BRAU 09] Braun O. M., Barel I., Urbakh M., "Dynamics of Transition from static to kinetic Friction", *Physical Review Letters*, **103**, 194301 (2009).
- [BRIE 06] Brietzke G.B., Ben-Zion Y, "Examining tendencies of in-plane rupture to migrate to material interfaces," *Geophys. J. Int.* **167**, 807–819 (2006).
- [BURR 79] Burridge R., Conn G., Freund L.B, "The Stability of a Rapid Mode II Shear Crack With Finite Cohesive Traction", *Journal of Geophysical Research*, **84**, 2210-2222 (1979).
- [CAPO 11] Capozza R., Rubinstein S.M., Barel I., Urbach M., Finemberg J., "Stabilizing stick-slip friction" *Physical Review Letters*, **107**, 024301 (2011).
- [CARP 91] Carpenter N.J., Taylor R.L., Kantona M.G., "Lagrange constraints for transient finite element surface contact", *International Journal of Numerical Methods of Engineering*, **32**, 103-128 (1991).
- [COCH 00] Cochard A., Rice J.R., "Fault rupture between dissimilar materials: Ill-posedness, regularization and slip-pulse response", *Journal of Geophysical Research*, **105**, 25 891 (2000).
- [COMN 77] Comninou M., Dundurs J., "Elastic interface waves involving separation", *ASME Journal of Applied Mechanics*, **44**, 222-226 (1977).
- [COMN 78a] Comninou M., Dundurs J., "Elastic interface waves and sliding between two solids", *ASME Journal of Applied Mechanics*, **45**, 325-330 (1978).
- [COMN 78b] Comninou M., Dundurs J., "Can two solids slide without slipping", *International Journal of Solids and Structures*, **14**, 251-260 (1978).

- [COMN 82] Comninou M., Barber J.R., Dundurs J., "Disturbance at a frictional interface caused by a plane elastic pulse", *ASME Journal of Applied Mechanics*, **49**, 361-366 (1982).
- [COUL '785] Coulomb C.A., "Theorie de machines simples", *Memoire de Mathematique et de Physique de l'Academie Royale*, Paris, 161-342 (1785).
- [DAS 77] Das S, Aki K., "Fault plane with barriers: a versatile earthquake model", *Journal of Geophysical Research*, **82**, 5658-5670 (1977).
- [DAS 83] Das S, Kostrov B.V., "Breaking a single asperity", *Journal of Geophysical Research*, **88**, 4277-4288 (1983).
- [DIBA 10a] Di Bartolomeo M., Meziane A., Massi F., Baillet L., Fregolent A., "Dynamic rupture at a frictional interface between dissimilar materials with asperities", *Tribology International*, **43**, 1620-1630 (2010).
- [DIBA 10b] Di Bartolomeo M., Meziane A., Massi F., Baillet L., Culla A., "Dynamics of rupture at frictional interface during sliding initiation", in *Proc. X Biennial Conference on Engineering Systems Design and Analysis ESDA* (ASME Conference Proceedings vol. 2, Applied Mechanics), Istanbul, Turkey, July 12-14, 2010, 375-384 (2010).
- [DUND 79] Dundurs J., Comninou M., "Interface separation caused by a plane elastic wave of arbitrary form", *Wave Motion*, **1**, 17-23 (1979).
- [DUNH 03] Dunham E.M., Favreau P., Carlson J.M., "A supershear transition mechanism for cracks", *Science*, **299**, 1557-1559 (2003).
- [DUNH 04] Dunham E.M., Archuleta R.J. "Evidence for a supershear transient during the 2002 Denali fault earthquake", *Bulletin of seismological Society of America*, **94**, S256-S268 (2004).
- [FEST 06] Festa G., Villotte J.P., "Influence of the rupture initiation on the intersonic transition: Crack-like versus pulse-like modes", *Geophysical Research Letters*, **33**, L15320 (2006).

- [FREU 90] Freund L.B., "Dynamic fracture mechanics", *Cambridge university press*, New York (1990).
- [FREU 78] Freund L.B., "Elastic Waves involving separation", *Discussion ASME Journal of Applied Mechanics*, **45**, 226-228 (1978).
- [GERD 01a] Gerde E., Marder M., "Friction and fracture", *Nature.*, **413**, 285-288 (2001).
- [GERD 01b] Gerde E., "Fracture and Friction", PhD Dissertation, University of Texas at Austin (May 2001).
- [GEUB 01] Geubelle P.H., "Intersonic crack propagation in homogeneous media under shear-dominated loading: numerical analysis", *Journal of the Mechanics and Physics of Solids*, **49** (3), 571-587 (2001).
- [GODE 84] Godet M., "The third body approach: a mechanical view of wear", *Wear*, **100**, 3437-452 (1984).
- [GRAF 91] Graff K.F., "Wave Motion in Elastic Solids", New York Dover Publications (1991).
- [GRIG 72] Grigorova S.R., "Eliminating self-induced vibrations due to friction", *Sov. Phys.-Dokl.*, **17**, 60-61 (1972).
- [IBRA 94] Ibrahim R.A., "Friction-induced vibration, chatter, squeal and chaos", *Appl. Mech. Rev.*, **47** (7), Part I 209-226, Part II 227-253 (1994).
- [LEBO 03] Lebon F., "Contact problems with friction: models and simulations", *Simulation Modelling Practise and Theory*, **11**, 449-463 (2003).
- [LINC 04] Linck V., Baillet, Berthier Y., "Dry friction: Influence of local dynamic aspect on contact pressure, kinematics and friction", *Tribol. Ser.*, **43**, 545-552 (2004).
- [MADR 83] Madriaga R.M., "High Frequency Radiation from Dynamic Earthquake Fault Models", *Annales Geophysicae*, **1**, 17-23 (1983).

- [MART 90] Martins J.A.C., Oden T., Simões F.M.F., "A study of static and kinetic friction", *International Journal of Engineering Science*, **28**, 29-92 (1990).
- [MART 02] Martins J.A.C., Raous M., "Friction and Instabilities", *Springer-Verlag*, New York (2002).
- [MASS 10] Massi F., Rocchi J., Culla A., Berthier Y., "Coupling system dynamics and contact behaviour: Modelling bearings subjected to environmental induced vibrations and 'false Brinelling' degradation", *Mechanical Systems and Signal Processing*, **24** (4), 1068-1080 (2010).
- [MASS 08] Massi F., Saulot A., Baillet L., Berthier Y., "Couplage entre « dynamique du mécanisme » et « dynamique locale du contact associé »", *20ème journées francophones de tribologie - tribologie et développement durable*, France (2008).
- [MEZ 07] Meziane A., D'Errico S., Baillet L., Laulagnet B., "Instabilities generated by friction in a pad-disc system during the braking process", *Tribology International*, **40**, 1127-1136 (2007).
- [MILL 38] Mills H.R. "Brake squeak", *Technical report 9000B, Institution of Automobile Engineers*, PA, (1978).
- [MILL 79] Miller R.K., Tran H.T., "Reflection, refraction and absorption of elastic waves at a frictional interface: SH motion", *ASME Journal of Applied Mechanics*, **46**, 625-631 (1979).
- [MILL 81] Miller R.K., Tran H.T., "Reflection, refraction and absorption of elastic waves at a frictional interface: P and SV motion", *ASME Journal of Applied Mechanics*, **48**, 155-161 (1981).
- [MURT 75] Murty G.S., "Wave propagation at an unbounded interface between two elastic half-spaces", *J. Acoust. Soc. Am.*, **58** (5), 1094-1095 (1975).
- [NORT 72] North M.R., "Disc brake squeal - a theoretical mode", *Technical Report 1972/5, Motor Industry Research Association*, Warwickshire, England, 1972.

- [NOSO 00] Nosonovsky M., Adams G.G., "Dilatational and shear waves induced by the frictional sliding of two elastic half-spaces", *International Journal of Engineering Science*, **39**, 1257–1269 (2000).
- [NOSO 02] Nosonovsky M., Adams G.G., "Interaction of elastic dilatational and shear waves with a frictional sliding interface", *ASME Journal of Vibration and Acoustics*, **124**, 33–39 (2002).
- [ODED 11] Oded B.D., Fineberg J., "Static Friction Coefficient Is Not a Material Constant", *Physical Review Letters*, **106**, 254301 (2011).
- [ODEN 85] Oden J.T., Martins J.A.C., "Models and computational methods for dynamic friction phenomena", *Computer Methods in Applied Mechanics and Engineering*, **52**, 527-634 (1985).
- [POPO 10] Popov V.L., Starcevic J., Filippov A.E. "Influence of ultrasonic in-plane oscillations on static and sliding friction and intrinsic length scale of dry friction processes", *Tribol. Lett.*, **39**, 25-30 (2010).
- [PRAK 93] Prakash V., Clifton R.J., "Time-Resolved Dynamic Friction Measurements in Pressure-Shear, Experimental Techniques in the Dynamics of Deformable Solids", *Applied Mechanics Div.*, vol. **165**, 33-48 (1993).
- [PRAT 10] Pratt E., Léger A., Jean M., "About a stability conjecture concerning unilateral contact with friction", *Non linear dynamics, Springer*, **59** (1-2), 73-94 (2010).
- [RABI 58] Rabinowicz E., "The intrinsic variables affecting the stick-slip process", *Proc. Phys. Soc.* , **71**, 668-675 (1958).
- [RANJ 01] Ranjith K., Rice J.R., "Slip dynamics at an interface between dissimilar materials", *J. Mech. Phys. Solids*, **49**, 341-361 (2001).
- [RAYL 900] Rayleigh Lord J.W. Strutt, "On waves propagated along the plane surface of an elastic solid", in *Scientific Papers*, Cambridge, England Vol. **2**, 441-447 (1900).

- [REN0 11] Renouf M., Massi F., Saulot A., Fillot N., "Numerical Tribology of Dry Contact", *Tribology International*, **44** (7-8), 834-844 (2011).
- [ROGE 03] Rogers G., Dragert H., "Episodic Tremor and Slip on the Cascadia Subduction Zone: The Chatter of Silent Slip", www.sciencexpress.org, /8 May 2003 / Page 2/10.1126/science.1084783.
- [RUBI 04] Rubinstein S. M., Cohen G., and Fineberg J., "Detachment fronts and the onset of dynamic friction", *Nature*, **430**, 1005-1009 (2004).
- [RUBI 07] Rubinstein S. M., Cohen G., and Fineberg J., "Dynamics of Precursors to Frictional Sliding", *Physical Review Letters*, **98**, 226103 (2007).
- [RUIN 83] Ruina A., "Slip instability and state variable friction law", *J. Geophys. Res.*, **88** (10), 359-370 (1983).
- [RUSS 03] Russo L., "The Forgotten Revolution: How Science Was Born in 300 BC and Why it Had to Be Reborn", *Springer* 2004, ISBN: 3540203966, 487 p.
- [SCHO 46] Scholte J.G., "The range of existence of Rayleigh and Stoneley waves", *Mon. Not. R. Astron. Soc., Geophys. Suppl.*, **5**, 120-126 (1947).
- [SKAR 92] Skåre T., Ståhl J.E., "Static and dynamic friction processes under the influence of external vibrations", *Wear*, **154**, 177-191 (1992).
- [SPUR 61] Spurr R.T. "A theory of brake squeal", *Proceedings of the Automobile Division, Institution of Mechanical Engineers 1961-1962*, **1**, 33-52 (1961).
- [STON 24] Stoneley R., "Elastic waves at the surface of separation of two solids" in *Proc. R. Soc. London Ser. A*, **106**, 416-428 (1924).
- [SHEN 07] Sheng G., "Friction-induced vibrations and sound: principles and applications", CRC Press, Boca Raton (2008).

- [SHI 06] Shi Z., Ben-Zion Y., "Dynamic rupture on a bimaterial interface governed by slip-weakening friction", *Geophys. J. Int.*, **165**, 469-484 (2006).
- [SHI 08] Shi Z., Ben-Zion Y., Needleman A., "Properties of dynamic rupture and energy partition in a solid with a frictional interface", *Journal of the Mechanics and Physics of Solids*, **56**, 5-24 (2008).
- [URBA 04] Urbakh M., Klafter J., Gourdon D., Israelachvili J., "The nonlinear nature of friction", *Nature*, **430**, 525-528 (2004).
- [VARO 04] Varotsos P., "Fracture and Friction: a review", *Acta Geophysica Polonica*, **52** (2), 105-142 (2004).
- [VICT 67] Victorov I.A., "Rayleigh and Lamb Waves: Physical theory and applications", Plenum Press, New York (1967).
- [VOIS 07] Voisin C., Renard F., Grasso J.R., "Long term friction: From stick-slip to stable sliding", **34** L013301 (2007).
- [WEER 63] Weertman J., "Dislocations moving uniformly on the interface between isotropic media of different elastic properties", *Journal of Mech. Phys. Solids*, **11**, 197-204 (1963).
- [WEER 80] Weertman J., "Unstable slippage across a fault separates elastic media of different elastic constant", *J. Geophys. Res.* **85**, 1455-1461 (1980).
- [WEER 02] Weertman J., "Subsonic type earthquake dislocation moving at approximately $\sqrt{2}$ × shear wave velocity on interface between half spaces of slightly different elastic constants", *Geophys. Res. Lett.*, **29**(10) (2002),doi:10.1029/2001GL013916.
- [XIA 04] Xia K., Rosakis A.J., Kanamori H., "Laboratory Earthquakes: The Sub-Rayleigh to Supershear Rupture Transition", *Science Magazine*, **303**, 1859-1861 (2004).
- [ZIGO 11] Zigone D., Voisin C., Larose E., Renard F., Campillo M., "Slip acceleration generates seismic tremors like signals in friction experiments", *Geophysical Research Letters* **38**, L01315 (2011) doi: 10.1029/2010GL045603.

FOLIO ADMINISTRATIFTHESE SOUTENUE DEVANT L'INSTITUT NATIONAL DES SCIENCES
APPLIQUEES DE LYON

NOM : DI BARTOLOMEO Prénoms : Mariano	DATE de SOUTENANCE 19 décembre 2011
TITRE : WAVE GENERATION AND PROPAGATION AT TRIBOLOGICAL INTERFACES Thèse en cotutelle entre l'Université de Rome « La Sapienza » et l'INSA de Lyon	
NATURE : Doctorat Ecole doctorale :MEGA Spécialité :Mécanique	Numéro d'ordre :
Code B.I.U. – Lyon : T 50/210/19 / et bis	CLASSE :
<p>RESUME : La génération et la propagation d'ondes aux interfaces de contact est un problème fondamental en mécanique car il a une incidence directe sur un grand nombre de systèmes mécanismes qui sont constitués aussi bien de zones de contact statiques ou en glissement relatif. Il est à l'origine des vibrations induites par le frottement, des instabilités acoustiques, de l'endommagement des surfaces, de l'usure et de la rupture par fatigue.</p> <p>L'objectif de ce travail est d'approfondir la connaissance sur la génération et la propagation des ondes à travers l'interface et leur relation avec les caractéristiques locales de la surface de contact et avec la dynamique globale du système, afin de contrôler leurs effets sur le frottement, contrôler les instabilités et réduire les phénomènes d'usure.</p> <p>Les résultats mettent en avant le rôle-clé des micro-slips et des précurseurs (propagations d'ondes détectables qui ont lieu pour des valeurs de la force tangentielle globale inférieures à la valeur prévue par la loi de frottement) dans l'amorçage du macro-slip entre les deux corps. En fonction de leur distribution et de leur intensité, l'évolution des forces de contact change en passant d'un comportement de type stick-slip à un glissement continu. La dynamique locale au contact (propagation des ondes et ruptures) a été reliée au comportement global du système (stick-slip, glissement continu, vibrations induites); l'effet des paramètres du contact et du système sur le transfert d'énergie vibrationnelle entre le contact glissant et le système a également été examinée: en fonction de leurs valeurs, on peut avoir différentes modalités d'excitation du système (par une distribution de micro-slips ou par des macro-slips) et différents processus de propagation et dissipation d'énergie (en passant par la réponse dynamique des corps en contact).</p>	
MOTS CLES : Frottement sec - Propagation d'onde – Rupture dynamique – Analyse numérique - Instabilités frottement - Rugosité – Précurseur – Bi-matériaux	
Laboratoire(s) de recherches : Laboratoires de Mécanique des Contacts et des Solides (LaMCoS), INSA de Lyon Dipartimento Ingegneria Meccanica e Aerospaziale (DIMA), La Sapienza Université de Rome	
Directeurs de thèse : Y. BERTHIER A. FREGOLENT Directeur de recherche (CNRS) (INSA de Lyon) Professeur (La Sapienza Université de Rome)	
Président du jury : Composition du jury : Yves BERTHIER (LaMCoS, INSA de Lyon) Francesco MASSI (LaMCoS, INSA de Lyon) Annalisa FREGOLENT (DIMA, Univ. "La Sapienza") Antonio CULLA (DIMA, Univ. de Rome "La Sapienza") Laurent BAILLET (ISTerre, Université J. Fourier, Grenoble) Adnan AKAY (ME, Bilkent University, Ankara) Frédéric LEBON (LMA, Université de Provence, Marseille)	